TESIS DE LA UNIVERSIDAD DE ZARAGOZA

2013

122

Gorka García Sáinz

Estudio experimental de la co-gasificación de fangos de EDAR y carbón con aire en lecho fluidizado

Departamento
Ingeniería Química y Tecnologías del Medio Ambiente

Director/es
Ábrego Garrués, Javier
Sánchez Cebrián, José Luis

http://zaguan.unizar.es/collection/Tesis

ISSN 2254-7606

Prensas de la Universidad
Universidad Zaragoza

Universidad Zaragoza
1542

Tesis Doctoral

ESTUDIO EXPERIMENTAL DE LA CO-GASIFICACIÓN DE FANGOS DE EDAR Y CARBÓN CON AIRE EN LECHO FLUIDIZADO

Autor

Gorka García Sáinz

Director/es

Ábrego Garrués, Javier
Sánchez Cebrián, José Luis

UNIVERSIDAD DE ZARAGOZA

Ingeniería Química y Tecnologías del Medio Ambiente

2013

Repositorio de la Universidad de Zaragoza – Zaguan http://zaguan.unizar.es

TESIS DOCTORAL

Universidad de Zaragoza

Departamento de Ingeniería Química y Tecnologías del Medio Ambiente

Estudio experimental de la co-gasificación de fangos de EDAR y carbón con aire en lecho fluidizado

Septiembre de 2013

Gorka García Sáinz

TESIS DOCTORAL

Universidad de Zaragoza

Departamento de Ingeniería Química y Tecnologías del Medio Ambiente

Estudio experimental de la co-gasificación de fangos de EDAR y carbón con aire en lecho fluidizado

Memoria que presenta para optar al Grado de Doctor en Ingeniería Química

Gorka García Sáinz

Zaragoza, Septiembre de 2013

La presente Tesis Doctoral, que lleva por título "Estudio experimental de la co-gasificación de fangos de EDAR y carbón con aire en lecho fluidizado", realizada por D. Gorka García Sainz y dirigida por los doctores D. Javier Ábrego Garrués y D. José Luis Sánchez Cebrián se presenta como compendio de las siguientes publicaciones:

I. G. García, J. Arauzo, A. Gonzalo, J.L. Sánchez, J. Ábrego, *Influence of feedstock composition in fluidised bed co-gasification of mixtures of lignite, bituminous coal and sewage sludge*, Chem. Eng. J., 222 (2013) 345–352.

II. G. García, E. Cascarosa, J. Ábrego, A. Gonzalo, J.L. Sánchez, *Use of different residues for high temperature desulphurisation of gasification gas*, Chem. Eng. J., 174 (2011) 644-651.

III. G. García, A. Monzón, F. Bimbela, J.L. Sánchez, J. Ábrego, *Desulfurization and catalytic gas cleaning in fluidized bed co-gasification of sewage sludge-coal blends*, Energy Fuels, en prensa (2013). DOI: 10.1021/ef400259g

IV. G. García, E. Campos, I. Fonts, J.L. Sánchez, J. Herguido, *Gas Catalytic Upgrading In A Two Zone Fluidized Bed Reactor Coupled To A Co-Gasification Plant*, Energy Fuels, en prensa (2013). DOI: 10.1021/ef400227z

Lo que se hace constar en cumplimiento del Reglamento sobre Tesis Doctorales de la Universidad de Zaragoza (artículo 17, apartado a), aprobado según el acuerdo de 17 de diciembre de 2008 del Consejo de Gobierno de la Universidad

D. Javier Ábrego Garrués, Profesor Ayudante Doctor, y

D. José Luis Sánchez Cebrián, Profesor Titular de Universidad,

ambos pertenecientes al Departamento de Ingeniería Química y Tecnologías del Medio Ambiente, y al Grupo de Procesos Termoquímicos del Instituto Universitario de Investigación en Ingeniería de Aragón (I3A) de la Universidad de Zaragoza

CERTIFICAN

Que la presente memoria titulada

Estudio experimental de la co-gasificación de fangos de EDAR y carbón con aire en lecho fluidizado

ha sido realizada bajo nuestra dirección en el Departamento de Ingeniería Química y Tecnologías del Medio Ambiente por D. Gorka García Sáinz, autorizando su presentación como compendio de publicaciones.

Y para que así conste, firmamos este certificado en Zaragoza, a 1 de Mayo de 2013.

Fdo. Prof. Dr. Javier Ábrego Garrués Fdo. Prof. Dr. José Luis Sánchez Cebrián

Índice de la Memoria

1. Introducción general

La investigación del Grupo de Procesos Termoquímicos (GPT), perteneciente al Instituto Universitario de Investigación en Ingeniería de Aragón (I3A) y al departamento de Ingeniería Química y Tecnologías del Medio Ambiente de la Universidad de Zaragoza, se desarrolla en diversas líneas, como son los procesos de pirólisis y gasificación de biomasa y otros materiales carbonosos, la producción de biodiésel, la eliminación de contaminantes en gases de combustión, y la producción de hidrógeno mediante craqueo catalítico y el reformado en fase acuosa de corrientes residuales. Esta Tesis Doctoral se encuadra dentro de la primera línea, que es, de hecho, la más antigua de las que aborda el GPT.

En concreto, esta Tesis Doctoral surge a raíz del proyecto europeo "Coal Catalytic Co-Gasification in an Innovative Rotary Kiln Gasifier" (COCACORK), financiado por la "Research Fund for Coal and Steel" de la Comisión Europea y que se desarrolló durante los años 2005 al 2008. En este proyecto de investigación participaron el Centro Sviluppo Materiali (Italia), el Instituto Nacional de Engenharia, Tecnologia e Inovação (actualmente LNEG - Laboratório Nacional de Energia e Geologia, Portugal), Sotacarbo (Italia), Enel (Italia), Universidad de Nottingham (Gran Bretaña), Ansaldo Richerce (Italia), y el GPT por la Universidad de Zaragoza.

En el citado proyecto se estudiaron diversos procesos para la co-gasificación de biomasa y carbón, en concreto existía interés en realizar el proceso de gasificación con una mezcla de carbones, uno de ellos de baja calidad y distintas biomasas. En el trabajo realizado por el GPT se seleccionó un lignito procedente de Teruel (Aragón), un carbón bituminoso (hulla) importado de Sudáfrica, y fango de EDAR, material este último con el que el GPT lleva trabajando específicamente en los procesos de gasificación y pirólisis desde 1999 aproximadamente [1–12].

El formato elegido para presentar esta Tesis ha sido el de compendio de las publicaciones que a continuación se listan. En la presente Memoria, cumpliendo con la normativa vigente de la Universidad de Zaragoza, se presenta de forma resumida el trabajo realizado así como las conclusiones más relevantes alcanzadas en la co-gasificación de fango de EDAR y carbón y la limpieza del gas obtenidos.

Se han publicado los siguientes artículos en revistas indexadas:

I. G. García, J. Arauzo, A. Gonzalo, J.L. Sánchez, J. Ábrego, *Influence of feedstock composition in fluidised bed co-gasification of mixtures of lignite, bituminous coal and sewage sludge*, Chem. Eng. J., 222 (2013) 345–352.

II. G. García, E. Cascarosa, J. Ábrego, A. Gonzalo, J.L. Sánchez, *Use of different residues for high temperature desulphurisation of gasification gas*, Chem. Eng. J., 174 (2011) 644-651.

III. G. García, A. Monzón, F. Bimbela, J.L. Sánchez, J. Ábrego, *Desulfurization and catalytic gas cleaning in fluidized bed co-gasification of sewage sludge-coal blends*, Energy Fuels, aceptado y publicado en web (18 de abril de 2013). **DOI:** 10.1021/ef400259g

IV. G. García, E. Campos, I. Fonts, J.L. Sánchez, J. Herguido, *Gas Catalytic Upgrading In A Two Zone Fluidized Bed Reactor Coupled To A Co-Gasification Plant*, Energy Fuels, aceptado y publicado en web (18 de abril de 2013). DOI: 10.1021/ef400227z

Los artículos publicados presentan una clara unidad temática, el estudio de la co-gasificación de gas y carbón y la mejora del gas producido.

En primer lugar se estudió una variable que raramente se encuentra descrita en la bibliografía específica de gasificación, que es la influencia que ejerce, sobre la distribución y composición de los productos, la composición que se alimenta al

gasificador. En este caso el estudio está justificado porque tanto el lodo de EDAR como los carbones que se alimentan tienen un elevado contenido en cenizas, que pueden tener un efecto catalítico en el propio gasificador donde se introducen [11]. Este estudio constituyó el objeto del artículo I (Influence of feedstock composition in fluidised bed co-gasification of mixtures of lignite, bituminous coal and sewage sludge, publicado en la revista Chemical Engineering Journal), donde el efecto de la composición de la alimentación se estudió mediante un diseño experimental de mezclas, analizándose los resultados estadísticamente mediante Análisis de Varianza (ANOVA).

El gas que se obtiene en la gasificación contiene diversos contaminantes de distinta naturaleza [12]. Para algunos de ellos, como las partículas, existe tecnología industrialmente conocida y fiable para su eliminación. Sin embargo, la presencia de otros compuestos -como son los alquitranes, hidrocarburos condensables que se forman durante la etapa de descomposición térmica o pirólisis de los materiales carbonosos- exige el desarrollo de nuevos sistemas de limpieza, dado que a escala industrial, y hasta la fecha, su eliminación no se ha resuelto de manera satisfactoria. Es por ello que una buena parte de la investigación que se realiza actualmente en el proceso de gasificación se centra en la eliminación de estos compuestos del gas que se produce [13–15]. En el caso de la co-gasificación de lodos y los carbones seleccionados en este trabajo, se encuentra una dificultad adicional, la presencia de cantidades significativas de azufre en su composición, que conlleva la formación de gases sulfurados, siendo el sulfuro de hidrógeno, H_2S, el más importante [16]. La presencia de este gas implica que los catalizadores más ampliamente usados para el craqueo de hidrocarburos, basados en Ni, no pueden usarse directamente, dado que el H_2S es un veneno que desactiva el Ni por formación de NiS de forma muy rápida e irreversible [17].

Es por lo expuesto en el párrafo anterior que se planteó un estudio de la desulfuración del gas a elevada temperatura, para que se pudiera aplicar con el gas tal y como se obtiene en el gasificador. Este aspecto viene condicionado por la presencia de alquitranes, que condensan a temperaturas inferiores a 300-400 ºC, causando graves problemas en tuberías y filtros, por ejemplo [15]. Además, el tratamiento del gas en caliente tiene la ventaja de mejorar la eficiencia energética del proceso, dado que no se pierde energía del gas asociada a su calor sensible. Este estudio se realizó con gas sintético, que simula el gas producido en la co-gasificación de carbón y lodo. En esta parte de la Tesis Doctoral se usaron como materiales desulfurantes las propias cenizas y char obtenidas de los tres materiales a gasificar (lodo, hulla y lignito). Para comparar los resultados obtenidos con estos materiales, se usó dolomita calcinada, que es un material comercial de bajo precio, previamente estudiada por diversos autores en la desulfuración de gases de distinto origen, entre ellos el procedente de la gasificación de biomasa y carbón [18–21]. El trabajo realizado fue publicado en el artículo II (Use of different residues for high temperature desulphurisation of gasification gas, publicado en la revista Chemical Engineering Journal).

Si en los primeros trabajos publicados dentro de esta Tesis Doctoral se fijaron la composición de la alimentación más adecuada y las condiciones para eliminar el H_2S que se produce en la gasificación, lo siguientes trabajos abordan la limpieza del gas y mejora de sus características, con el objetivo de reducir el alquitrán presente, lo que permitiría el uso del gas para la producción de electricidad en un motor de combustión interna o una turbina.

La primera estrategia que se estudió fue más convencional, estudiando la limpieza catalítica del gas usando un catalizador comercial que, por su tamaño de partícula, debe ser usado en lecho fijo. Así en este trabajo, que se corresponde en el artículo III (Desulfurization and catalytic gas cleaning in fluidized bed co-gasification of sewage

sludge-coal blends, publicado en la revista Energy and Fuels) se estudió el efecto de la temperatura del lecho catalítico en la calidad del gas obtenido.

Por último, se planteó el uso de un reactor novedoso [22], desarrollado por el Grupo de Investigación de Catálisis, Separaciones Moleculares e Ingeniería del Reactor (CREG), perteneciente también al Departamento de Ingeniería Química y Tecnologías del Medio Ambiente de la Universidad de Zaragoza, que no ha sido usado previamente para la limpieza y mejora del gas de gasificación. Se trata del Reactor de Lecho Fluidizado de Dos Zonas (RLFDZ o TZFBR en inglés), reactor que permite integrar en un solo equipo el reformado del gas y la regeneración del catalizador ante la desactivación por deposición de coque. En este trabajo, que se corresponde con el artículo IV (Gas Catalytic Upgrading In A Two Zone Fluidized Bed Reactor Coupled To A Co-Gasification Plant, publicado en la revista Energy and Fuels), se estudió el efecto de la concentración de oxígeno alimentada en la zona de regeneración del reactor sobre el rendimiento y la calidad de los productos obtenidos.

2. Resumen

2.1. Objetivos

Como se ha comentado en el Apartado 1 de esta Memoria, el estudio que ha llevado a la realización de esta Tesis Doctoral surge del proyecto "Coal Catalytic Co-Gasification in an Innovative Rotary Kiln Gasifier" (COCACORK), que tenía como objetivo el estudio y mejora del aprovechamiento de carbón y biomasa mediante gasificación.

La gasificación de biomasa puede permitir la producción de energía mediante fuentes localmente disponibles, disminuyendo la dependencia energética de algunos países, como es el caso de España. El uso de carbón local también puede ser económica y estratégicamente beneficioso, aunque en algunos países, el carbón del que se dispone es de baja calidad, en concreto por la presencia de compuestos como el azufre que supone una contaminación atmosférica en caso de emitirse con los humos de la combustión. Este es también el caso de España, donde algunos de los carbones que se pueden extraer tienen un elevado contenido en azufre que los hace no aptos para su combustión en centrales térmicas de carbón, o al menos impone la necesidad de alimentarlos mezclados con otro carbón de mejores características.

En este escenario, se planteó como objetivo general el estudio de la co-gasificación de fango de EDAR en un reactor de lecho fluidizado y usando aire como agente gasificante, dando especial importancia a la limpieza del gas y mejora de sus características. Como objetivos parciales se establecieron los siguientes:

- Estudio de las condiciones de operación e influencia sobre los productos obtenidos.
- Estudio de la eliminación del H_2S del gas de gasificación

- Estudio de la limpieza de alquitranes del gas.

2.2. Antecedentes

La gasificación es el proceso termoquímico por el cual un sustrato carbonoso se transforma mediante una oxidación parcial en un gas combustible que contiene, entre otros compuestos, hidrógeno, monóxido de carbono, metano, dióxido de carbono, y nitrógeno, así como diversas impurezas o contaminantes. La conversión a un gas combustible permite su uso en aplicaciones distintas a la combustión convencional para generar calor o vapor para un ciclo Rankine: el gas puede llevarse a combustión en motores de combustión interna o turbinas para producción de electricidad o cogeneración simultánea de electricidad y calor, o usarse para la síntesis de productos de mayor valor añadido, como metanol u otros alcoholes, o hidrocarburos con características del diésel, la gasolina o ceras, mediante la síntesis Fischer-Tropsch.

La gasificación de biomasa se contempla actualmente como una tecnología que puede contribuir a disminuir la dependencia de los combustibles fósiles y ampliar el espectro de opciones para la producción de energía, aumentando el peso que la biomasa tiene dentro de las energías primarias que actualmente se utilizan. Dentro de la amplitud de tipos distintos de biomasa que se encuentran, el Grupo de Investigación de Procesos Termoquímicos se encuentra trabajando activamente en la aplicación de los procesos de pirólisis y gasificación de fango de EDAR.

El fango de EDAR se obtiene como resultado del proceso de tratamiento biológico de aguas residuales, y es un residuo cuya generación ha aumentado considerablemente debido a la aplicación de una legislación medioambiental cada vez más estricta [23].

La co-gasificación, que consiste en alimentar una mezcla de sustratos al reactor de gasificación, presenta una serie de ventajas, como es por una parte el aumento de

escala, ya que cuando se trata de biomasa, la disponibilidad de la misma es un aspecto crítico a la hora de escalar el proceso, y por tanto de su viabilidad económica. En el caso de usar carbón, esto implica que la disponibilidad de biomasa no es un aspecto tan crucial. Por otra parte, los procesos de gasificación de carbón a gran escala han despertado históricamente un mayor interés que los de biomasa o residuos, por lo que la co-gasificación con fango a escala industrial se beneficiaría del mayor desarrollo de la tecnología de gasificación de carbón, a la vez que permitiría el aprovechamiento energético de un residuo que se produce en cantidades ingentes y cuyo destino final es problemático.

Uno de los aspectos clave del proceso de gasificación es la formación de alquitranes, compuestos orgánicos condensables que se forman durante la gasificación mediante una serie de reacciones complejas y fuertemente dependientes de las condiciones de operación. Conforme la temperatura de reacción se incrementa, se va produciendo un "esquema de formación de alquitranes" [24], mostrado en la Figura 1.

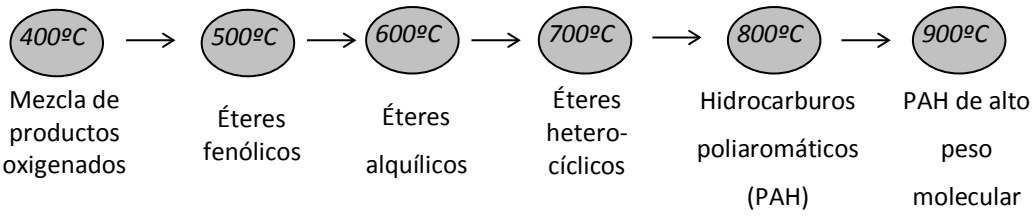

Figura 1. Esquema de formación de alquitranes.

Además de la temperatura, la presión y el tiempo de residencia también influyen en el tipo de alquitrán obtenido. En la Tabla 1 se muestra una clasificación más detallada.

Existen distintas estrategias para eliminar estos compuestos del gas, que se pueden dividir en sistemas que buscan separar el alquitrán del gas, mediante lavado o filtrado, o sistemas basados en la destrucción o craqueo de los alquitranes. La ventaja obvia de estos últimos es que no se genera una corriente que debe ser tratada a posteriori.

Además, el craqueo de alquitranes permite enriquecer el gas de gasificación, ya que se forman hidrocarburos más ligeros, a la vez que aumenta la eficiencia de conversión de la materia prima gasificada.

Tabla 1. Clasificación y propiedades de los alquitranes según Li y Suzuki [24].

Clase	Nombre	Propiedades	Compuestos representativos
1	Indetectables por Cromatografía de Gases (CG)	Muy pesados, incapaces de ser detectados por CG.	Se determinan por diferencia con el resto de los alquitranes detectables.
2	Aromáticos heterocíclicos	Contienen heteroátomos, altamente solubles en agua	Piridina, fenol, cresoles, quinolina, isoquinolina, dibenzofenol
3	Aromáticos ligeros (un anillo)	No suponen ningún problema en cuanto a su condensabilidad y solubilidad.	Tolueno, etilbenceno, xilenos, estireno
4	PAHs ligeros (2-3 anillos)	Condensan a bajas temperaturas incluso a concentraciones muy bajas.	Indeno, naftaleno, metilnaftaleno, fluoreno, antraceno.
5	PAHs pesados (4-7 anillos)	Condensan a altas temperaturas y bajas concentraciones.	Fluoranteno, pireno, criseno, perileno, coroneno.

En el craqueo se pueden diferenciar:

- Craqueo térmico: la ruptura se produce por medio de exposición a temperaturas elevadas (de 900 a 1200 ºC). Sin embargo es difícil conseguir un craqueo completo, y deben afrontarse problemas operacionales, inversiones económicas a veces excesivas, y aportes energéticos adicionales.

- Craqueo catalítico: implica el uso de un catalizador y facilita la selectividad a determinados gases. Es una técnica que ha despertado un amplio interés. En el siguiente apartado se tratará este método en mayor profundidad.

Las reacciones implicadas en la descomposición de los alquitranes han sido ampliamente descritas por diversos autores [25,26], siendo las principales las mostradas en la Tabla 2.

Tabla 2. Reacciones principales en el craqueo de alquitranes.

Reacción	**Ecuación estequiométrica**
Craqueo Térmico	$pC_nH_x \rightarrow qC_mH_y + rH_2$ *(m<n)*
Steam Reforming	$C_nH_m + nH_2O \rightarrow nCO + (n+m/2)H_2$
Dry Reforming	$C_nH_m + nCO_2 \rightarrow 2nCO + (m/2)H_2$
Formación de Carbono	$C_nH_m \rightarrow nC + (m/2)H_2$
	$CH_4 \rightarrow C + 2H_2$

El craqueo catalítico permite una mejor eficacia energética, dado que se opera a menor temperatura, y mayor especificidad en la composición del gas que se obtiene. Entre los catalizadores más usados, destacan los basados en óxidos de níquel, que han sido ampliamente estudiados para mejorar el gas procedente de la gasificación de biomasa [13,27].

Además, tanto el fango de EDAR como algunos carbones contienen cantidades significativas de azufre, que en el proceso de gasificación conducen a la generación de compuestos indeseados como el sulfuro de hidrógeno. Por tanto, se hace necesario plantear otra estrategia adicional para la limpieza y mejora de la calidad del gas.

La eliminación del sulfuro de hidrógeno que se forma durante la gasificación es crítica para el éxito de la tecnología de gasificación de estos materiales que se usan en la Tesis Doctoral, especialmente si se considera el alto contenido en azufre de partida de las materias primas alimentadas, como el fango de EDAR o el lignito turolense. Además de evitar problemas con la lluvia ácida [28], se puede producir corrosión en las

tuberías, turbinas y otros equipos. Además, si hay H_2S en el gas, el uso de catalizadores basados en Ni (metal clásico en el reformado de hidrocarburos) se ve seriamente limitado por el envenenamiento debido a la formación de NiS [13,17].

La eliminación del H_2S se puede realizar mediante procesos a baja temperatura, como el lavado con disoluciones acuosas, o por procesos de desulfuración a alta temperatura, que presentan la ventaja de una mayor eficiencia energética y se pueden aplicar tanto en el mismo lecho fluidizado como tras el gasificador. Los procesos a alta temperatura han sido revisados recientemente en el trabajo de Meng y cols. [29]. Aunque se han probado distintos compuestos metálicos, los compuestos con calcio son los más usados en procesos de gasificación y co-gasificación [20,30]. Entre los compuestos con calcio, la dolomita es uno de los más eficaces, alcanzado rendimientos en la desulfuración superiores al 90% [31,32].

Algunos autores han usado la dolomita para evitar la desactivación de un catalizador de Ni con resultados prometedores [28,33,34]. El principal problema asociado a este material es la facilidad con que se produce atrición en lechos fluidizados, limitando su aplicación en este tipo de reactores para procesos de gasificación y co-gasificación.

2.3. Metodología experimental

En este apartado se van a describir brevemente los materiales y los sistemas experimentales utilizados, así como los experimentos realizados.

2.3.1. Materiales utilizados

Como se ha comentado en la Introducción general, se han usado fango de EDAR (SS), hulla (B) y lignito (L) como materias primas para la gasificación. El fango de EDAR proviene de la planta de tratamiento de aguas "Madrid Sur" (Madrid, España) y fue sometido previamente a una digestión anaerobia y un secado térmico en la propia planta de tratamiento. Los dos tipos de carbón utilizados, hulla importada de Sudáfrica y lignito turolense, fueron amablemente cedidos por la central térmica de Andorra (Teruel), perteneciente a la empresa ENDESA.

En la Tabla 3 se muestran los análisis inmediato y elemental, así como los poderes caloríficos de estos materiales. Como puede observarse, los carbones utilizados tienen un contenido en cenizas de un 25 % aproximadamente, mientras que en el fango de EDAR representa casi el 50 %.

Estos materiales se han usado en todos los experimentos realizados, tanto del estudio de influencia de la composición como de limpieza del gas. Previamente, estas materias primas se molieron y tamizaron, usando la fracción con un tamaño entre 250 y 500 µm.

Tabla 3. Análisis elemental e inmediato y poder calorífico de las materias primas.

	Método de análisis	**B**	**L**	**SS**
Análisis inmediato				
Humedad (% peso)	ISO-579-1981	6.9	19.2	6.5
Ceniza (% peso)	ISO-1171-1976	14.3	26.3	41.3
Volátiles (% peso)	ISO-5623-1974	25.2	26.0	46.9
Carbono fijo (% peso)		53.6	28.5	5.4
Análisis elemental				
C (% peso)		65.3	37.6	27.8
H (% peso)		4.1	4.1	4.4
N (wt. %)		1.8	0.5	4.0
S (wt. %)		0.7	6.1	0.8
Poder calorífico				
PCS (MJ/kg)	ASTM-D-3286-96	25.4	14.6	12.0
PCI (MJ/kg)		24.3	13.3	10.9

PCS: poder calorífico superior; PCI: poder calorífico inferior.

En el estudio de desulfuración que se llevó a cabo, se usaron como materiales desulfurantes, char de fango (SSC), hulla (BC) y lignito (LC) obtenidos tras la gasificación en lecho fluidizado de los tres materiales por separado (temperatura de gasificación 850ºC, relación equivalente= 0.3), así como cenizas producidas a partir del char por calcinación en mufla siguiendo las condiciones de la norma UNE 32-004-84. En la Tabla 4 se muestra el análisis elemental del char, así como la superficie BET y el contenido en ceniza del char.

En la Tabla 5 se muestra la composición de las cenizas de fango (SSA), hulla (BA) lignito empleadas así composición de la dolomita, material cuyo comportamiento en desulfuración ha sido ampliamente estudiado y que se usó como referencia.

Tabla 4. Análisis elemental, ceniza y superficie BET del char usado.

	BC	**LC**	**SSC**
C (% peso)	46.8	25.2	13.8
H (% peso)	0.5	0.6	0.2
N (% peso)	1.4	0.2	0.7
S (% peso)	0.5	5.7	0.7
Ceniza (% peso)	43.6	67.3	83.0
BET (m^2/g)	244.7	173.8	59.1

Tabla 5. Composición (% en peso) y superficie BET de las cenizas y dolomita usadas.

	BA	**LA**	**SSA**	**Dolomita**
Al_2O_3	27.97	25.07	21.57	0.09
CaO	7.21	3.40	23.14	30.34
Fe_2O_3	2.71	28.04	8.56	0.01
K_2O	0.74	1.34	3.66	n.a.
MgO	1.33	1.07	5.93	20.63
Na_2O	0.35	0.16	1.37	n.a.
SiO_2	47.50	37.88	34.51	n.a.
TiO_2	1.49	0.73	1.25	n.a.
CO_2	n.a.	n.a.	n.a.	48.93
BET (m^2/g)	5.0	13.0	5.8	18.8

n.a.: no analizado

Para el estudio de desulfuración se usó una mezcla de gas sintético cuya composición se muestra en la Tabla 6.

Tabla 6. Composición del gas sintético usado en el estudio de desulfuración.

Componente	**% vol.**
H_2	10.0
N_2	58.6
CH_4	4.0
CO	10.0
CO_2	15.0
C_2H_4	1.5
C_2H_6	0.2
C_2H_2	0.2
H_2S	0.5

Además de estos materiales, se han utilizado dos catalizadores:

- En lecho fijo: Catalizador comercial de Ni. Se trata del catalizador SG9301 fabricado por BASF, suministrado en forma de monolitos cilíndricos de 17 mm de diámetro, 9.5 mm de altura y con 6 orificios axiales de 3 mm de diámetro. Se trata de un catalizador de Ni con lantano, soportado sobre aluminato de calcio. En la Tabla 7 se muestra la composición (suministrada por el fabricante) así como datos de la estructura porosa.

Tabla 7. Composición y estructura porosa del catalizador comercial.

Composición	
Compuesto	**% peso**
α-Al_2O_3	70-75
CaO	5-10
La_2O_3	1.5
NiO	10-15
Estructura porosa	
BET (m^2/g)	16.8
Área de microporos (m^2/g)	1.3
Volumen de microporos (cm^3/g)	$4.6 \cdot 10^{-4}$
Diámetro medio de poro (nm)	15.3

- En reactor de lecho fluidizado de dos zonas: Catalizador de Ni/γ-Al_2O_3. Este catalizador se preparó por el método de humedad incipiente usando $Ni(NO_3) \cdot 6H_2O$ (Panreac, 99% de pureza) sobre gamma alúmina (γ-Al_2O_3, Puralox NWa-155, fabricada por Sasol). El contenido en níquel se analizó por ICP-OES resultando ser de un 4.8 %. Tras la preparación se observó una ligera reducción del área superficial del soporte, de 142 a 118 m^2/g.

2.3.2. Sistemas experimentales usados

A continuación se describen brevemente los distintos sistemas experimentales utilizados así como la experimentación realizada en cada una de las partes que componen este trabajo (estudio del efecto de la composición de la alimentación, estudio de desulfuración con gas sintético y limpieza del gas en reactor secundario).

Reactor de lecho fluidizado. Este reactor se ha usado para realizar los experimentos de gasificación de toda esta Tesis. Se trata de un reactor de lecho fluidizado, diseñado y construido específicamente para este trabajo, fabricado en acero refractario AISI 310, con un diámetro interno de 40 mm en la zona donde se encuentra el lecho y 70 mm en el freeboard.

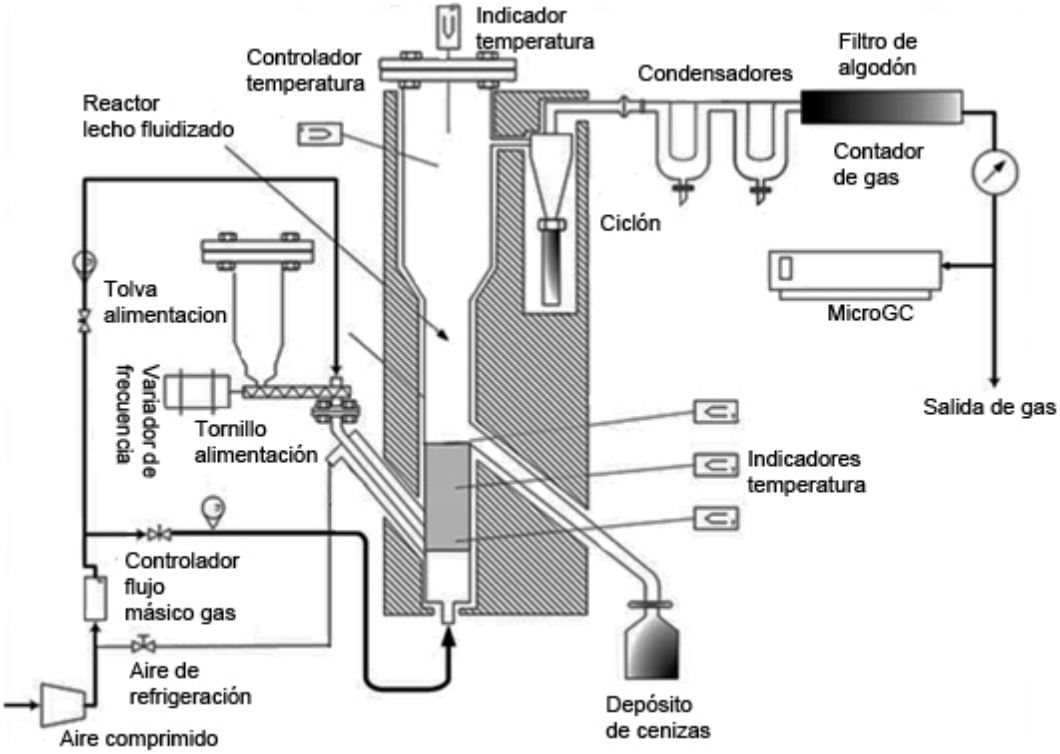

Figura 2. Reactor de lecho fluidizado

En la Figura 2 se muestra un esquema de la instalación. La altura máxima del lecho se mantiene en 310 mm sobre la placa distribuidora mediante una tubería lateral que permite la salida del char en continuo por rebose. La alimentación se introduce en continuo en el reactor, a una altura de aproximadamente 10 mm por encima de la placa distribuidora, a través de una tubería inclinada, que se enfría externamente con una corriente de aire. El flujo de aire para la gasificación se fija mediante un medidor-

controlador de flujo másico, usándose un caudal de 2.81 LN/min. El caudal de alimentación se regula mediante un variador de frecuencia conectado al motor de un tornillo sin fin. En los distintos experimentos realizados se usó una relación estequiométrica o de equivalencia del 30 % (aire alimentado respecto al necesario para la combustión completa) variando el caudal de sólido en función de su composición. La temperatura del reactor se fijó en 850ºC, al igual que la temperatura del freeboard, mediante un horno eléctrico que permite un control independiente de la temperatura de las distintas zonas. El gas que sale del reactor pasa por un ciclón y un filtro en caliente, ambos a una temperatura de 450ºC. Inicialmente en el reactor se introducen 300 g de arena con un tamaño de partícula de 250-350 μm. Los experimentos realizados han tenido una duración de 90 min una vez comenzada la alimentación, tiempo suficiente para alcanzar unas condiciones estables en el reactor y obtener una distribución y composición de los productos representativa.

A la salida del filtro en caliente, el gas se enfría mediante dos condensadores de vidrio refrigerados con hielo y pasa por un filtro de algodón que sirve para retener la niebla de alquitranes que no ha precipitado. Mediante un cromatógrafo de gases (Agilent Micro-GC 3000) se analiza el gas cada 5 min aproximadamente. Al finalizar el experimento se pesan los sólidos recogidos del lecho y ciclón, mientras los aparatos de vidrio se lavan con isopropanol. El agua condensada me mide mediante valoración Karl-Fischer y el alquitrán se calcula gravimétricamente por diferencia con el agua.

Reactor de lecho fijo para el estudio de desulfuración del gas. En la Figura 3 se muestra un esquema del sistema experimental usado. El reactor está fabricado en cuarzo, con un diámetro interno de 1.2 cm y 40 cm de altura. El sólido, alrededor de 1 g en cada experimentos, se coloca sobre fibra de vidrio, que actúa de soporte, a 18.5 cm de la parte superior del reactor, en la zona isoterma del mismo. Una vez situado el sólido, el reactor se calienta mediante un horno eléctrico hasta la temperatura final (700, 800 o 900ºC) bajo un flujo de nitrógeno. Una vez alcanzada la temperatura, se

introduce el gas a desulfurar, con un caudal de 0.05 LN/min, mediante un controlador de flujo másico, fijándose en los experimentos un tiempo espacial (WHSP, *weight hourly space time*) de 3.6 h^{-1}. La composición del gas tras el reactor se analiza con un cromatógrafo Agilent Micro-GC 3000.

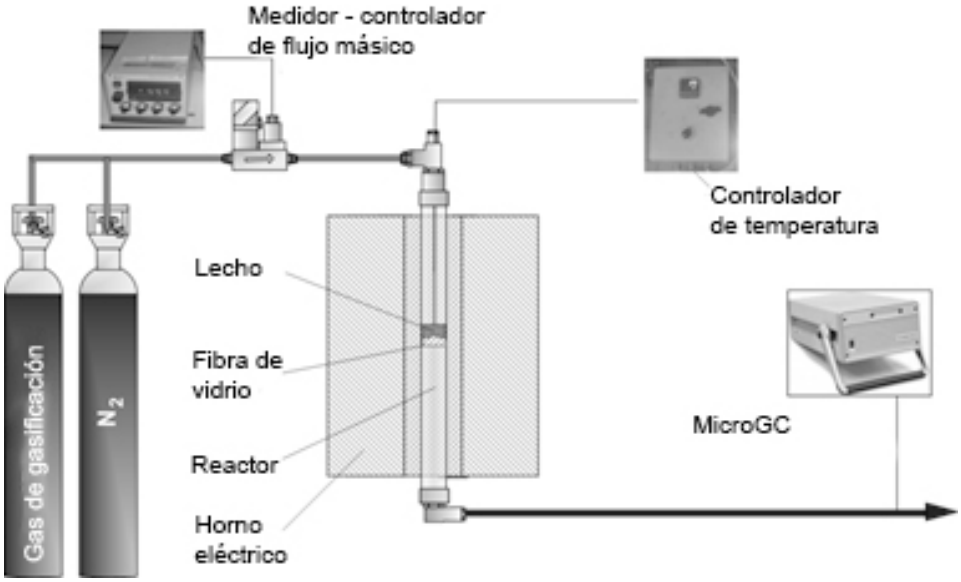

Figura 3. Reactor usado para el estudio de desulfuración

Reactor de lecho fijo usado con catalizador de Ni comercial. Este reactor se situó en serie con el de lecho fluidizado ya descrito, tal y como se muestra en la Figura 4. La conexión entre ambos reactores se hace mediante una tubería calentada externamente con una resistencia eléctrica, manteniendo su temperatura a 450ºC para evitar la condensación del alquitrán. El reactor de lecho fijo usado tiene un diámetro interno de 35.5 mm y 990 mm de longitud. Se encuentra calentado mediante un horno eléctrico con dos zonas independientes de calentamiento, lo que permite fijar temperaturas distintas en la parte superior e inferior. El gas, que entra por la parte inferior del reactor, se encuentra en primer lugar con un lecho de dolomita,

previamente calcinada (250 g de dolomita fresca, que resultan en aproximadamente 133 g tras la calcinación).

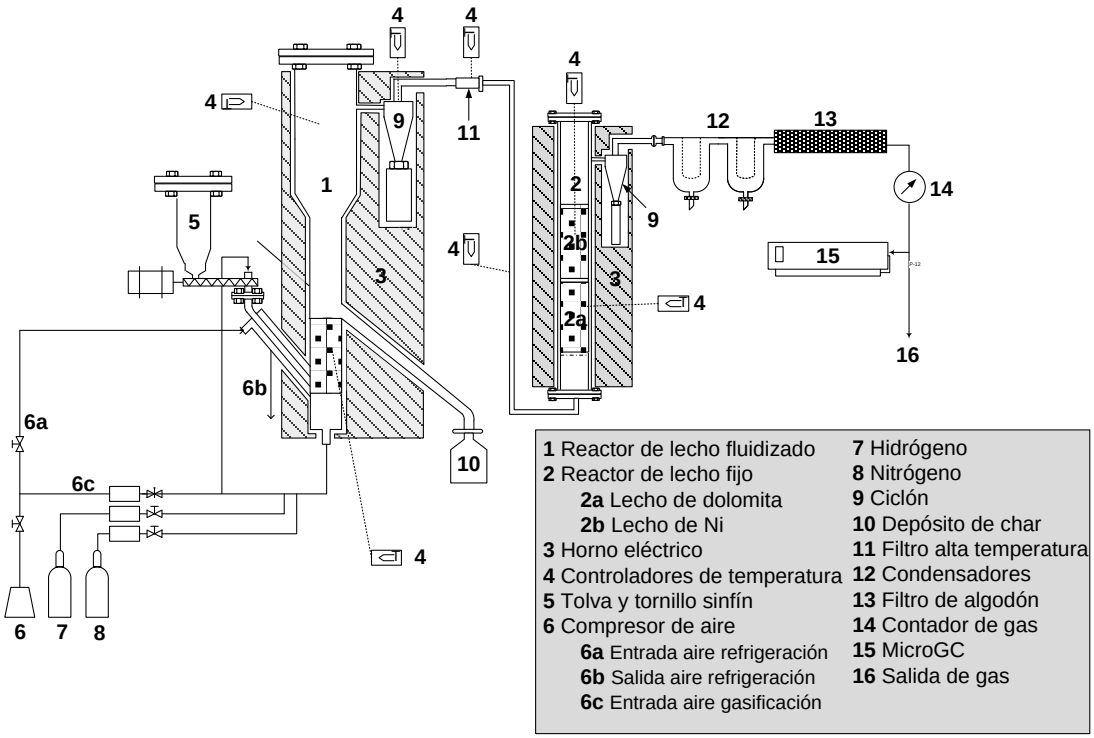

Figura 4. Sistema experimental usado en la limpieza de gas con catalizador comercial

Encima del lecho de dolomita se sitúa el catalizador de níquel (135 g), en forma de monolitos. Entre el catalizador y la dolomita se coloca fibra de cuarzo, con el fin de evitar la fluidización de la dolomita, ya que se trata de un material que se desmenuza fácilmente. Antes de cada experimentos, el catalizador de Ni se redujo a 800ºC durante dos horas, con un flujo de 2. 82 LN/min de H_2 (15 % en N_2). La temperatura de la dolomita, que se seleccionó como material desulfurante, se fijó en 800 ºC, mientras que el catalizador de Ni se usó a 800, 850 y 900ºC.

Reactor de lecho fluidizado de dos zonas. Para el estudio de limpieza del gas con el reactor de lecho fluidizado de dos zonas se usaron tanto el reactor de gasificación como el reactor de lecho fijo, en este caso únicamente con dolomita para desulfurar el gas. Tras el reactor de lecho fijo se tomó una parte del gas producido,

aproximadamente un 10 % del caudal, para su tratamiento en el reactor de dos zonas, tal y como se muestra en la Figura 5.

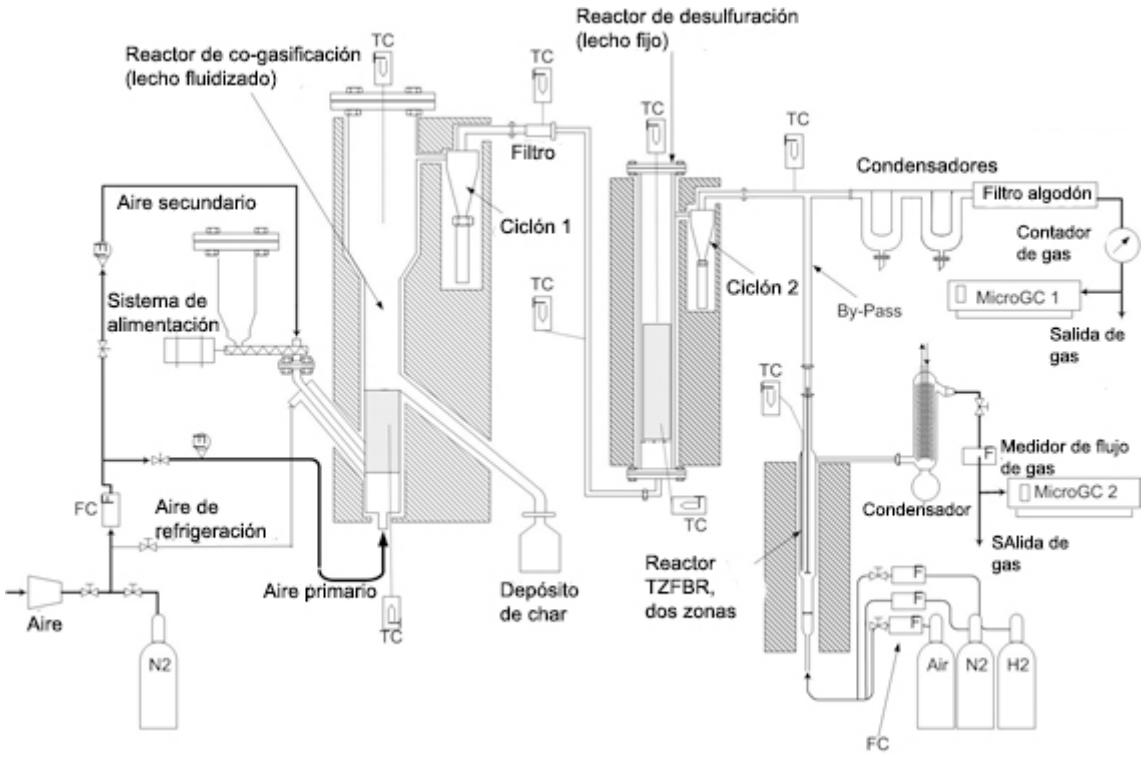

Figura 5. Sistema experimental usado en la limpieza del gas con el RLFDZ.

Tras el reactor de desulfuración donde se encuentra la dolomita, el gas se divide en dos corrientes. La mayor parte (unos 3 LN/min) pasan a un sistema de condensación y análisis, como ya se ha descrito anteriormente. El resto del gas (0.3 LN/min) se dirige al reactor de lecho fluidizado de dos zonas (RLFDZ), que se muestra en la Figura 6.

En este reactor es posible llevar a cabo las dos etapas típicas de un proceso catalítico, reacción y regeneración del catalizador. El reactor está fabricado en cuarzo, con una altura total de 510 mm. La zona de regeneración (inferior) tiene un diámetro de 18 mm, mientras que la zona de reformado tiene 28 mm de diámetro interno. El gas procedente de reactor de desulfuración entra al RLFDZ por la parte superior, a través de un tubo de cuarzo.

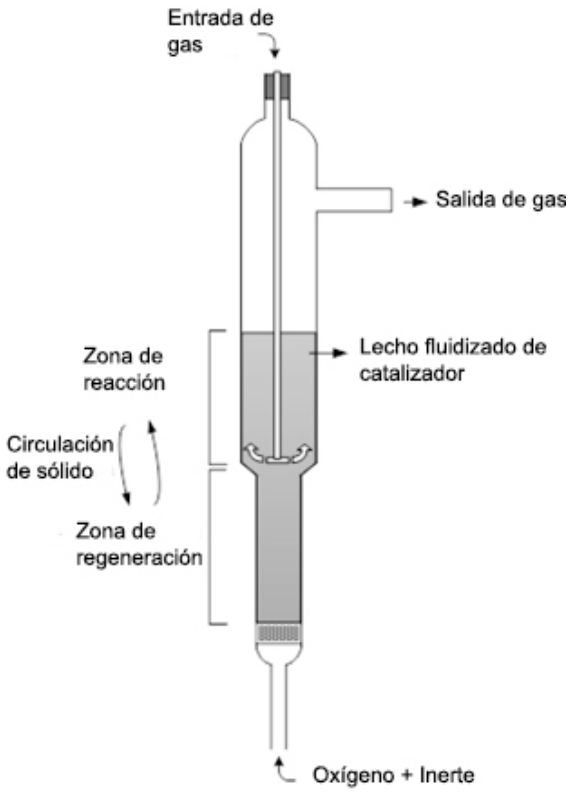

Figura 6. RLFDZ

El gas para la regeneración (O_2 y N_2 en distinta proporción) entra por la parte inferior, de modo que el movimiento del catalizador (42 g de Ni/γ-Al_2O_3) entre las dos zonas permite que realice el reformado y se regenere por combustión del coque depositado en continuo. En cada instante, aproximadamente 17 g de catalizador están en la zona de regeneración. El uso de una cantidad adecuada de O_2, permite que no se produzca combustión del gas procedente de la gasificación.

Un parámetro de especial importancia para el funcionamiento de este reactor es la relación u/u_{mf} (velocidad superficial del gas/velocidad de mínima fluidización) en las dos secciones del lecho [22]. En la experimentación llevada a cabo, se ha usado un caudal de la mezcla oxígeno/nitrógeno de regeneración de 0.3 LN/min, para obtener

una u/u_{mf} = 2.5 a la temperatura de operación. En la zona de reformado la u/u_{mf} es de 3.4, calculada teniendo en cuenta el cambio de dimensiones y el flujo de gas proveniente de la zona de regeneración junto con el caudal de gas a reformar, que como se ha comentado es de 0.3 LN/min. Hay que tener en cuenta que el uso de nitrógeno, que se eligió por simplicidad experimental, implica una dilución del gas reformado, dilución que se ha descontado en los cálculos. En el caso de una operación a escala industrial se debería usar otro compuesto, como vapor de agua, que fuera fácilmente eliminable, o usar un RLFDZ con dimensiones apropiadas para usar oxígeno puro, por ejemplo.

Antes de comenzar el experimento, se llevó a cabo la reducción del catalizador con H_2 (5%, diluido en nitrógeno) a 800ºC. La temperatura en el RLFDZ se fijó también en 800ºC mediante un horno eléctrico.

2.4. Conclusiones y trabajos futuros

En este Apartado de la Memoria se van a mostrar de forma resumida la experimentación realizada y las conclusiones más relevantes obtenidas en cada una de las partes de la que se compone este trabajo. Para mayor claridad, se ha estructurado siguiendo cada uno de los trabajos publicados, añadiendo además un apartado donde se consideran posibles trabajos de investigación que continuarían la línea de investigación que supone esta Tesis Doctoral.

2.4.1. Influencia de la composición de la alimentación

El objetivo de este estudio fue determinar cuál era el efecto de modificar la composición de una mezcla de carbón bituminoso (B), lignito (L) y fango de EDAR (SS) en los productos obtenidos en la gasificación. Estos materiales tienen un importante contenido en ceniza, en cuya composición se encuentran distintos metales, mostrados en la Tabla 5, como Al, Fe, Ca, Mg, K y Na, que pueden tener un efecto catalítico durante la gasificación [2,35–38]. Para ello se usó el reactor de lecho fluidizado descrito anteriormente, planteando para el estudio un diseño de experimentos de mezclas.

En la Figura 7 se muestra, sobre un diagrama ternario, la composición de las distintas mezclas utilizadas.

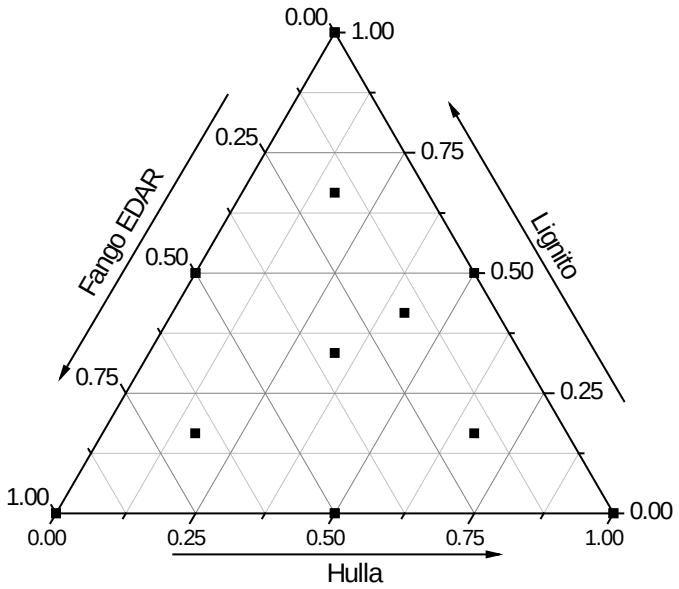

Figura 7. Mezclas usadas en el diseño experimental

En la Tabla 8 se muestran algunos de los resultados experimentales obtenidos, en concreto la concentración de alquitrán en el gas (g/m^{3}N), el % de alquitrán obtenido frente al sólido alimentado (%), el % de carbono alimentado que se convierte en gas (η_C, %), el rendimiento energético a gas (η_{energ}, %) calculado según la Ecuación 1, el poder calorífico inferior del gas seco obtenido (kJ/m^{3}N) y la producción específica de gas (Y_{gas}, m^{3}N/kg). En la Tabla 9 se muestra la composición media del gas obtenido.

$$\eta_{energ}(\%) = \frac{PCI_{gas} \cdot Y_{gas}}{PCI_{fango}} \cdot 100 \qquad \text{Ec. 1}$$

El análisis de estos resultados se realizó mediante ANOVA (análisis de varianza), que se basa en comparar la varianza experimental asociada al error (que se calcula a partir de las repeticiones que se realizan de uno o varios experimentos) con la varianza que crea, en este caso, la variación de la composición. La comparación se realiza mediante un test F de Fischer, y permite discriminar si el efecto observado es estadísticamente

significativo frente al error, con un nivel de confianza predeterminado (95% en este estudio).

Tabla 8. Resultados experimentales (1). Alquitrán, rendimiento de carbono a gas y energético, PCI del gas y producción específica de gas

Fracción masa B/L/SS	Alquitrán g/m^3N	Alquitrán %	η_C (%)	η_{energ} (%)	PCI $kJ/m^3(STP)$	Y_{gas} m^3N/kg
1/0/0	41.2/43.8	12.3/12.6	42.1/42.6	23.2/22.6	2293/2201	3.00/3.13
0/1/0	58.4/64.5	15.6/15.6	47.2/46.6	20.2/22.4	1686/2070	2.67/2.42
0/0/1	38.4/64.2	10.2/17.3	79.7/79.5	47.3/51.7	4112/3949	2.65/2.69
0.5/0.5/0	41	11.7	52	22.7	2044	2.86
0.5/0/0.5	21.9/28.7	6.1/7.7	56.0/55.0	35.0/33.2	3191/3103	2.81/2.69
0/0.5/0.5	23.0/18.2	6.0/4.9	64.6/66.7	40.8/42.7	3293/3322	2.62/2.71
0.67/0.17/0.17	28.4	8.3	48.6	24.3	2302	2.9
0.17/0.67/0.17	5.2	1.4	52.7	25	2071	2.77
0.17/0.17/0.67	38.1	10.2	64.3	40.5	3477	2.69
0.41/0.41/0.18	12.5	3.1	43.3	20.5	2090	2.46
0.33/0.33/0.33	6.4/12.9	1.6/3.5	50.1/51.3	29.7/30.5	2882/2731	2.51/2.7
	20.5/20.7	5.4/5.5	46.9/46.4	28.4/27.9	2585/2510	2.62/2.66

Tabla 9. Resultados experimentales (2). Composición media del gas (% vol.)

B/L/SS	H_2	CO	CH_4	C_2H_n	H_2S
1/0/0	5.73/5.09	9.04/8.90	1.15/1.16	0.20/0.23	0.01/0.04
0/1/0	5.44/7.50	6.01/7.84	0.80/0.60	0.09/0.10	1.00/0.82
0/0/1	8.24/7.56	8.52/8.14	3.13/3.14	1.75/1.67	0.10/0.11
0.5/0.5/0	6.23	7.73	0.92	0.11	0.2
0.5/0/0.5	8.20/8.09	9.31/9.11	1.97/1.87	0.72/0.69	0.04/0.05
0/0.5/0.5	8.87/9.04	9.26/9.53	2.23/2.00	0.74/0.72	0.41/0.42
0.67/0.17/0.17	6.41	8.25	1.13	0.29	0.07
0.17/0.67/0.17	6.55	7.46	0.86	0.2	0.31
0.17/0.17/0.67	8.81	9.32	2.15	0.99	0.14
0.41/0.41/0.18	5.9	8.07	0.89	0.2	0.11
0.33/0.33/0.33	8.10/7.55	9.24/8.87	1.54/1.45	0.49/0.47	0.13/0.32
	6.86/6.65	9.77/9.69	1.10/1.01	0.37/0.35	0.14/0.12

A partir de los efectos significativos encontrados con el ANOVA, es posible modelar empíricamente el efecto sobre las distintas variables medidas con una ecuación como la que se muestra en la Ecuación 2:

$$RV = \beta_1 \cdot W_1 + \beta_2 \cdot W_2 + \beta_3 \cdot W_3 + \beta_{12} \cdot W_1 \cdot W_2 + \beta_{13} \cdot W_1 \cdot W_3 + \beta_{23} \cdot W_2 \cdot W_3 + \beta_{123} \cdot W_1 \cdot W_2 \cdot W_3 \quad \text{Ec. 2}$$

Donde RV es cualquiera de los resultados experimentales mostrados, los coeficientes β_i representan la respuesta lineal frente a la fracción másica (W_i) de los materiales puros, los coeficientes β_{ij} son el efecto cuadrático debido al efecto sinérgico o antagónico debido a la mezcla de dos de los materiales y el coeficiente β_{123} modela el efecto cúbico debido a la mezcla de los tres materiales. Cuando un efecto no es significativo, su coeficiente no aparece en la ecuación.

En la Tabla 10 se muestran los coeficientes de regresión obtenidos tras el ANOVA, así como el valor del coeficiente de correlación R^2 y R^2 ajustado. Estos dos últimos coeficientes dan una idea de cómo se ajustan los datos experimentales al modelo empírico.

Tabla 10. Coeficientes de regresión obtenidos tras el ANOVA.

	β_B	β_L	β_{SS}	$\beta_{B\text{-}L}$	$\beta_{B\text{-}SS}$	$\beta_{L\text{-}SS}$	$\beta_{B\text{-}L\text{-}SS}$	R^2/ R^2_{adj}
Tar (g/m^{3}N)	43±8	58±7	54±7	-80±40	-90±30	-150±30	*	0.75/0.64
Tar (%)	11±2	13±2	15±2	*	-30±10	-40±10	*	0.65/0.54
η_{energ} (%)	23±1	21±1	50 ±1	-2±7*	-7±6	26±6	-130±40	0.98/0.97
η_C (%)	44±1	47±1	80±1	26±9	-23±7	11±7	-260±50	0.98/0.97
PCI (kJ/m^{3}N)	2100±90	1900±100	4100±100	*	*	*	*	0.94/0.93
Y_{gas} (m^{3}N/kg)	2.96±0.06	2.55±0.07	2.63±0.07	*	*	*	*	0.55/0.49
H_2 (%)	6.0±0.4	6.2±0.5	8.4±0.5	*	*	5±2	*	0.62/0.55
CO (%)	9.0±0.3	6.7±0.3	8.6±0.4	*	*	7±2	*	0.69/0.63
CH_4 (%)	1.1±0.1	0.6±0.1	3.2±0.1	*	-1.6±0.6	*	*	0.93/0.92
C_2H_n	0.17±0.03	0.069±0.04	1.73±0.04	*	-1.1±0.2	-0.8±0.2	*	0.99/0.98
H_2S	0.05±0.04	0.86±0.05	0.06±0.04	-1.3±0.3	*	*	*	0.93/0.92

* no significativo

Uno de los resultados más interesantes que se observan en la Tabla anterior es el efecto que tiene la mezcla de los dos carbones y fango sobre el contenido en alquitrán del gas, que se muestra de forma gráfica en la Figura 8. A partir de los coeficientes lineales del modelo, se observa como lignito y fango producen más alquitrán en el gas que la hulla cuando se gasifican alimentados puros.

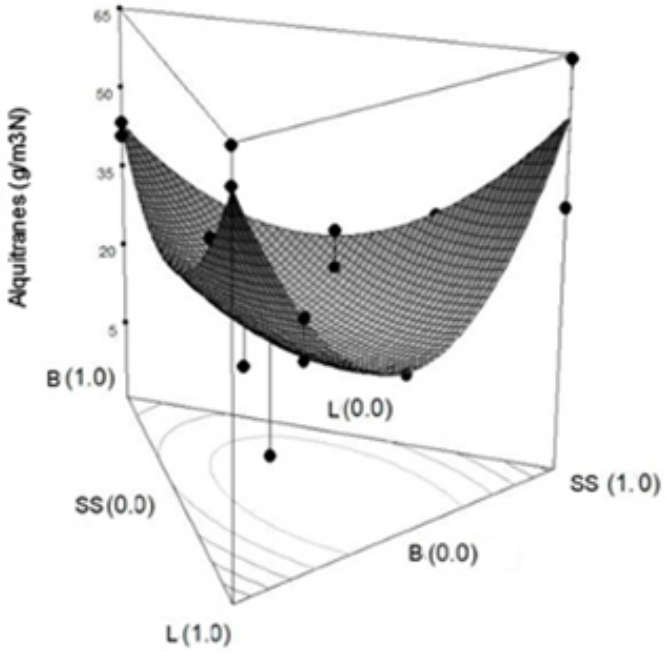

Figura 8. Influencia de la composición de la alimentación en el contenido de alquitranes en el gas.

En la Tabla 10 se observa como los tres coeficientes cuadráticos son estadísticamente significativos y tienen signo negativo, lo que indica que cualquier mezcla binaria, o ternaria, de estos materiales implica una disminución del contenido en alquitrán del gas producido. Este efecto antagónico puede deberse a la diferente composición de los inorgánicos presentes en estos materiales. Como se muestra en la Tabla 5, Al, Ca , Fe y Mg, entre otros metales, están presentes en distintas proporciones en las cenizas de

hulla, lignito y fango, metales cuyas propiedades catalíticas ha sido ampliamente estudiadas para la destrucción del alquitrán [2,35–38].

Por lo que respecta al resto de las variables experimentales medidas, se pueden observar efectos sinérgicos, estadísticamente significativos pero de poca importancia para la eficacia energética, cuando se mezclan hulla o lignito y fango, así como cuando están presentes los tres materiales. Tal y como se observa en la Figura 9, en el rendimiento de C a gas, se observa un efecto significativo para las tres mezclas binarias de materiales, aunque son poco importantes y la superficie de respuesta no se aleja apreciablemente de un plano.

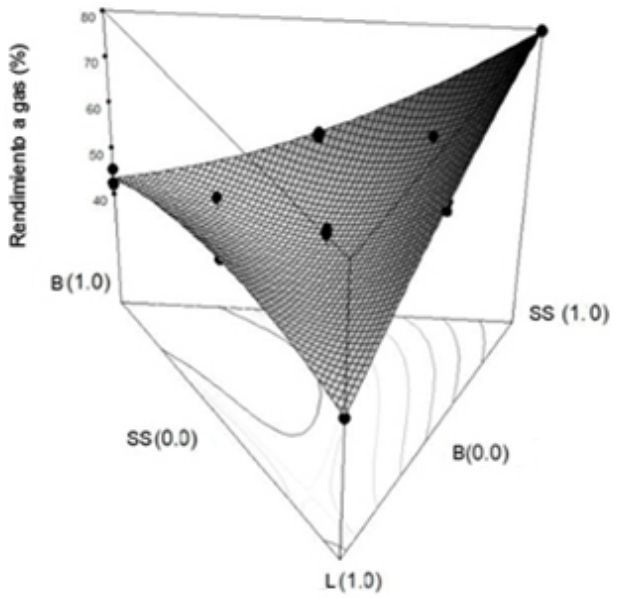

Figura 9. Influencia de la composición de la alimentación en η_C.

Para la producción de gas y el PCI del gas, no se observaron efectos de interacción entre los componentes, y las respuestas se pueden calcular combinando linealmente los valores que se obtienen para los componentes puros.

Por lo que respecta a la composición de gas, en el porcentaje en volumen medio medido de CO y H_2, hay un efecto positivo debido a la presencia simultánea de lignito y fango, lo que produce que la concentración sea máxima cuando se gasifican juntos estos dos materiales, como se observa en la Figura 10, mientras que en el resto de los componentes del gas la respuesta es lineal.

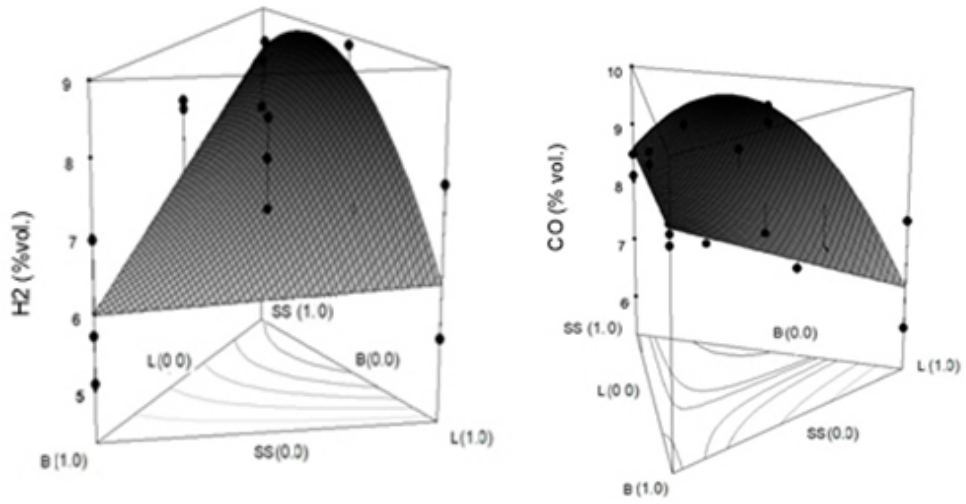

Figura 10. Influencia de la composición en el % medio de H_2 (derecha) y CO (izquierda).

Como resumen de este trabajo, se puede destacar que la co-gasificación de estos materiales tiene ventajas operacionales sobre la gasificación de cada uno de ellos por separado, ya que se obtiene un efecto antagónico en la producción de alquitrán, debido a la presencia de fango y carbón que hace que la producción del mismo sea menor de lo esperable, además la producción de hidrógeno y monóxido de carbono se ve incrementa por la presencia simultánea de lignito y fango. En el resto de parámetros analizados o bien la influencia de la mezcla de fango, lignito y hulla es muy pequeña, o bien no es estadísticamente significativa.

2.4.2. Estudio de desulfuración

En esta etapa experimental, se investigó el potencial de desulfuración del char procedente de gasificación de los tres materiales empleados en este trabajo. Los chares de lignito, hulla y fangos de EDAR se denominaron respectivamente, LC, BC y SSC. Asimismo, se comparó la capacidad de eliminación de H_2S del char con la de las cenizas de combustión de los tres materiales de partida (LA, BA y SSA, análogamente), y con la de un conocido agente desulfurante como es la dolomita calcinada [39].

La composición del gas sintético utilizado para simular la corriente de salida de un gasificador se muestra en la Tabla 6. Es preciso comentar que no se incluyó agua en la alimentación al sistema de reacción; la presencia de agua en la corriente gaseosa podría sin embargo tener una influencia apreciable en la capacidad de desulfuración de los materiales empleados [29].

Se muestra en primer lugar (Figura 11) el flujo de S calculado (mg S/min) a la salida del sistema experimental, para cada una de las tres temperaturas consideradas. Puede observarse cómo con el char de gasificación de los tres materiales testados (LC, BC y SSC) no se obtienen resultados satisfactorios; únicamente el char de lignito (LC) a 700ºC (Figura 11a) produce un gas esencialmente libre de H_2S durante algo menos de 20 minutos. En el resto de experimentos con char, el aumento de S se produce desde los primeros instantes de cada experimento.

El uso de cenizas de hulla y lignito (LA y BA, Figuras 11b, 11d y 11f) mejora sustancialmente la eliminación de H_2S en todo el rango de temperaturas, en comparación con el char de ambos materiales. Las cenizas de hulla (BA) por encima de 700ºC, o de lignito (LA) a cualquier temperatura, producen concentraciones de H_2S a la salida del sistema de menos del 0.05% en volumen. En contraste con este hecho, las cenizas de fango SSA muestran una limitada capacidad de desulfuración, siendo

únicamente capaces de producir un gas libre de H_2S durante tiempos limitados a 700 y 800ºC y presentando peores resultados que el char de fango, SSC.

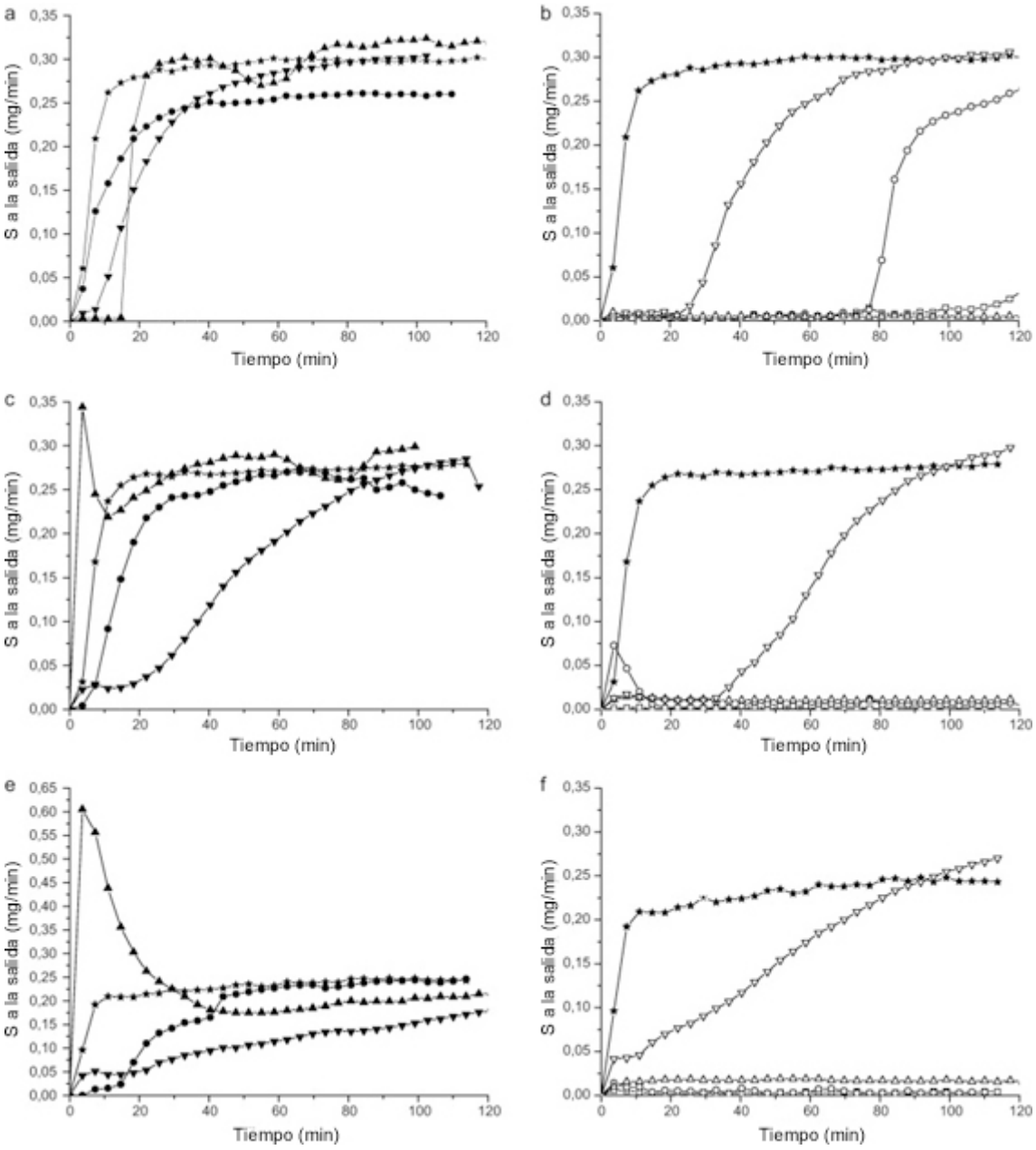

Figura 11. Caudal de S (mg S/min) a la salida de los experimentos de desulfuración, (a,b) 700ºC, (c,d) 800ºC, (e,f) 900ºC. ★ Experimentos en blanco; ● BC; ○ BA; ▲ LC; △ LA; ▼ SSC; ▽ SSA; □ dolomita calcinada.

La comparación de estos datos con los datos de referencia correspondientes a los experimentos en blanco permite el cálculo de la eficiencia de desulfuración de cada uno de los materiales a lo largo del tiempo. La Tabla 11 presenta un resumen de la eficiencia promedio (% de S capturado por el lecho) y de la capacidad de eliminación del H_2S (mg de S por gramo de material de lecho a los 100 minutos de experimento), para todos los materiales empleados en esta sección.

Como puede observarse en la Tabla 11, el char de lignito, hulla y fango empleado tiene una capacidad de desulfuración modesta, hecho ya evidenciado en la Figura 11. Resultan llamativos los valores negativos de eficiencia del char de lignito a 800 y 900ºC, lo que puede atribuirse al alto contenido original en S de este material (que puede producir liberación adicional de H_2S a altas temperaturas). Por su parte, el char de fango ofrece mejores resultados, siendo capaz de capturar algo más del 50% del S presente en la alimentación; expresado en términos de capacidad, puede retener 12.1 mg S/g de material. Este valor es similar a los encontrados en la bibliografía disponible [40,41].

Tabla 11. Eficiencia y capacidad de desulfuración de los materiales empleados.

	Eficiencia promedio de desulfuración (% de S eliminado del gas)			**Capacidad de desulfuración (tras 100 min) (mg de S por gramo of sólido)**		
T(ºC)	**700 °C**	**800 °C**	**900 °C**	**700 °C**	**800 °C**	**900 °C**
BC	17.8	15.8	23	4.7	3.1	5.1
LC	10.1	−39.7	−15.6	2.8	−1.7	−2.0
SSC	18.9	35.3	50.5	4.5	10.4	12.1
BA	72.2	97.2	97.6	23.2	24	21.3
LA	97.7	94.9	92.5	26.7	23.9	20.1
SSA	34.8	46.4	29.7	10.6	13.9	7.4
DO	94.5	99.3	98.4	26.8	24.8	21.5

Atendiendo a la composición y superficie BET del char de los tres materiales, mostrados en la Tabla 4, puede concluirse que su capacidad de desulfuración es independiente de la superficie específica de los mismos, y puede estar directamente relacionada con el contenido en cenizas y en especial de ciertos óxidos de metales, tales como Fe y Ca (este último muy abundante en el fango) y su capacidad para reaccionar directamente con el H_2S a altas temperaturas [5] según la Ecuación 3:

$$M_xO_y + y\ H_2S \rightarrow M_xS_y + y\ H_2O \qquad \text{Ec. 3}$$

En el caso de las cenizas, los resultados son notablemente diferentes. Para lignito y hulla (LA y BA), las eficiencias y capacidades de desulfuración son muy altas y equiparables al efecto producido por un lecho de dolomita (con la única excepción de BA a 700ºC). El gran aumento de eficiencia con respecto al char parece estar favorecido, por tanto, por la eliminación del contenido en carbono de los mismos durante la oxidación, quedando así expuestas mayores cantidades de compuestos metálicos activos en la superficie. En cambio, las cenizas de fango presentan resultados de orden similar a los obtenidos con char del mismo material, hecho que puede atribuirse a la similitud entre ambos materiales en cuanto al contenido en cenizas (el char de fango contenía mucho menos C que los producidos a partir de lignito y hulla). La evolución temporal de la eficiencia de desulfuración de las cenizas LA, BA y SSA, junto con la dolomita, se muestra en la Figura 12.

En dicha figura puede verse cómo las cenizas de lignito y hulla mantienen su actividad de desulfuración, eliminando la práctica totalidad de H_2S durante todo el tiempo de experimento (120 minutos), excepto en el caso de las cenizas de hulla a 700 ºC.

Por su parte, las superficies específicas de char y ceniza, tanto antes como después de los experimentos de desulfuración, se muestran en la Tabla 12.

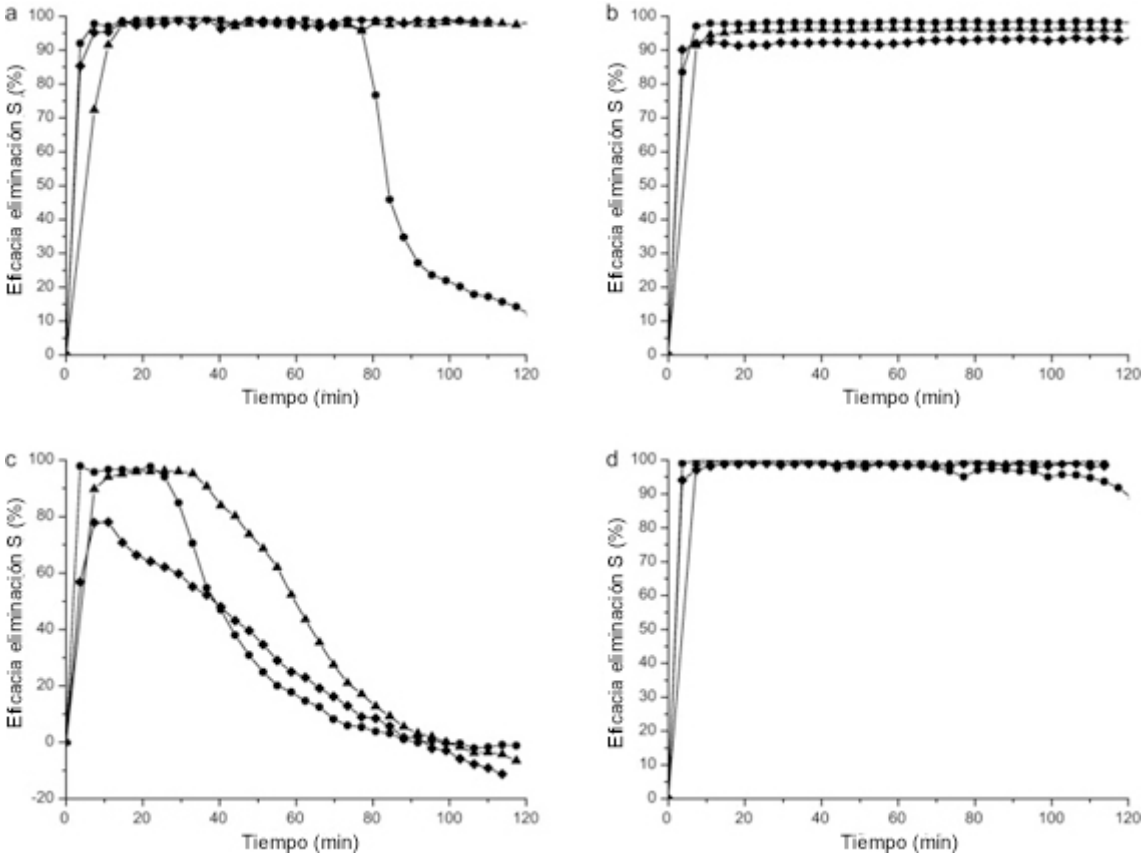

Figura 12. Eficiencia de desulfuración (% de S eliminado del gas) de las cenizas y de la dolomita. (a) BA; (b) LA; (c) SSA; (d) dolomita calcinada. ● 700 ºC; ▲ 800 ºC; ◆ 900 ºC.

Tabla 12. Superficies BET de los materiales empleados.

Superficie BET (m^2/g)					
		Hulla	**Lignito**	**Fango**	**Dolomita**
Char		244.7	173.8	59.1	-
Cenizas		5.0	13.0	5.8	18.8
Cenizas tras desulfuración	**700ºC**	4.9	18.5	-	2.3
	800ºC	5.0	10.6	-	8.0
	900ºC	3.4	4.5	-	8.3

Como puede observarse, una mayor superficie específica no produce un aumento de la eficiencia de desulfuración: las superficies específicas del char de cada material son entre 10 y 50 veces superiores a las de sus cenizas, pero las eficiencias de desulfuración son mucho mayores para estas últimas (excepto, como se ha comentado, en el caso del fango). Además, se determinó la variación de superficie específica de las cenizas de lignito y hulla tras la desulfuración, así como la de la dolomita. Estos datos también se muestran en la Tabla 12 y evidencian cambios poco significativos en cuanto a la estructura porosa de los materiales empleados. Por tanto, a alta temperatura, la superficie BET ejerce una influencia despreciable en la capacidad de desulfuración. Este resultado contrasta con los encontrados en bibliografía empleando materiales carbonosos para desulfuración a bajas temperaturas [42].

Con respecto a este Apartado de la presente Tesis Doctoral, puede concluirse que de los materiales empleados en el estudio de desulfuración, los chares presentan una modesta capacidad de desulfuración, siendo el char de fangos el único capaz de mantener cierta actividad de eliminación de H_2S a lo largo del tiempo. Al utilizar cenizas procedentes de lignito y hulla, la eliminación de H_2S se ve ampliamente mejorada (reducción de la concentración de sulfuro de hidrógeno de 0.50 a 0.05 % vol. para las cenizas de lignito en todo el rango de temperaturas investigado y para las cenizas de hulla a 800 y 900ºC), y es equiparable a la de la dolomita calcinada, el material de referencia de este estudio. Por su parte, las cenizas de fango sólo muestran una ligera mejora con respecto al char del mismo material.

2.4.3. Mejora catalítica del gas usando un catalizador comercial en lecho fijo

El objetivo de esta parte de la tesis consistió en el estudio de un sistema de limpieza catalítica del gas de co-gasificación mediante dos lechos fijos consecutivos; uno compuesto por dolomita, y otro por un catalizador comercial de Ni soportado sobre α-Al_2O_3. Como se ha comentado anteriormente, la inclusión de una etapa de desulfuración previa al lecho catalítico de Ni resulta imprescindible, puesto que la presencia de H_2S produce la rápida desactivación del mismo por envenenamiento. Es por ello que se optó por emplear dolomita como agente desulfurante de efectividad ampliamente conocida, si bien igualmente podría haberse utilizado alguno de los agentes desulfurantes empleados en la sección 2.4.2; en concreto, cenizas de hulla o lignito. La dolomita presenta además un efecto catalítico de craqueo de alquitranes, de acuerdo con la bibliografía existente [13,43].

Por otra parte, el uso de dos lechos diferenciados para ambos tratamientos permite el control independiente de temperaturas y velocidades espaciales (GHSV, gas hourly space velocity), pudiendo por tanto optimizar estos parámetros para ambos procesos de limpieza del gas. Adicionalmente, se realizaron una serie de experimentos previos incluyendo dolomita dentro del propio lecho fluidizado (sustitución del 25% del lecho de arena por dolomita); sin embargo, esta opción fue desechada debido a la presencia de cantidades muy elevadas de este material en los sistemas de colección de partículas y alquitranes [44]. En los experimentos llevados a cabo en esta etapa, se emplearon cantidades de catalizador suficientes para el estudio de la composición de gases una vez alcanzado el estado estacionario en el sistema, por lo que no se incluyó un análisis detallado de los procesos de desactivación y/o regeneración.

Los resultados referentes a la composición de los gases obtenidos se muestran en la Figura 13. Cada experimento se denota de la forma: X-T, siendo X el tipo de lecho

empleado (B: blanco, D: dolomita; D-Ni: dolomita + Ni), y T la temperatura de operación del mismo (800, 850 y900ºC).

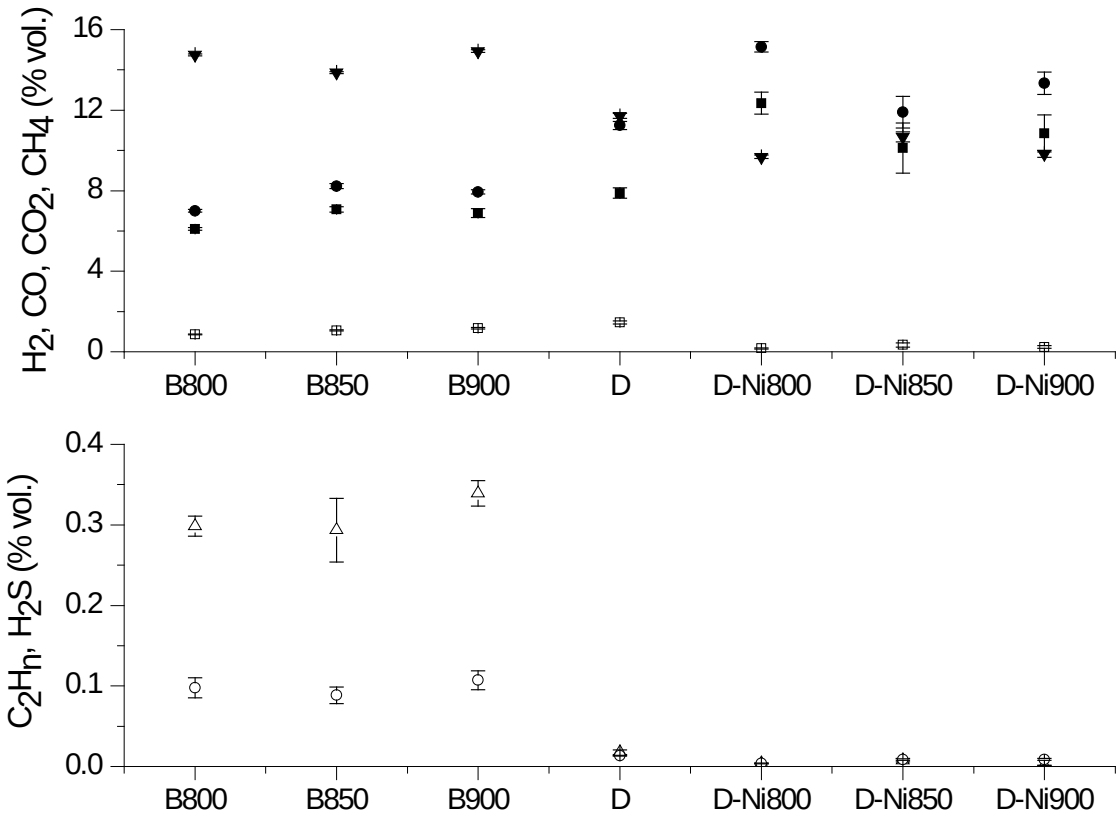

Figura 13. Composición media de los gases obtenidos tras cada lecho (■ H_2, ● CO, ▼ CO_2, □ CH_4, △ C_2H_n, ○ H_2S).

Con respecto a los experimentos de referencia, la presencia de un lecho de dolomita produce un descenso de la concentración de CO_2 y un ligero aumento de la de H_2, CO y CH_4. Por su parte, los hidrocarburos ligeros (C_2H_n) desaparecen casi por completo, lo que puede atribuirse a reacciones de craqueo o reformado promovidas por la dolomita sobre estos hidrocarburos y los alquitranes [45,46]. Por su parte el conocido efecto de desulfuración de la dolomita viene dado por su reacción con el H_2S para formar CaS:

$CaO + H_2S \rightarrow CaS + H_2O$ Ec. 4

Si a continuación se añade un lecho de catalizador de Ni, se observa un incremento en la concentración de H_2 y CO y un descenso en la de CO_2. Además, el contenido en metano del gas desciende abruptamente. Todas estas observaciones pueden atribuirse al efecto de las reacciones de reformado catalizadas por el níquel [47].

Además de los efectos positivos en cuanto a composición promedio del gas, conviene conocer la evolución temporal de esta composición a lo largo de cada experimento, puesto que sus variaciones pueden indicar posibles cambios de actividad catalítica de los materiales de ambos lechos. Esta evolución temporal se muestra (para el experimento D-Ni800) en la Figura 14.

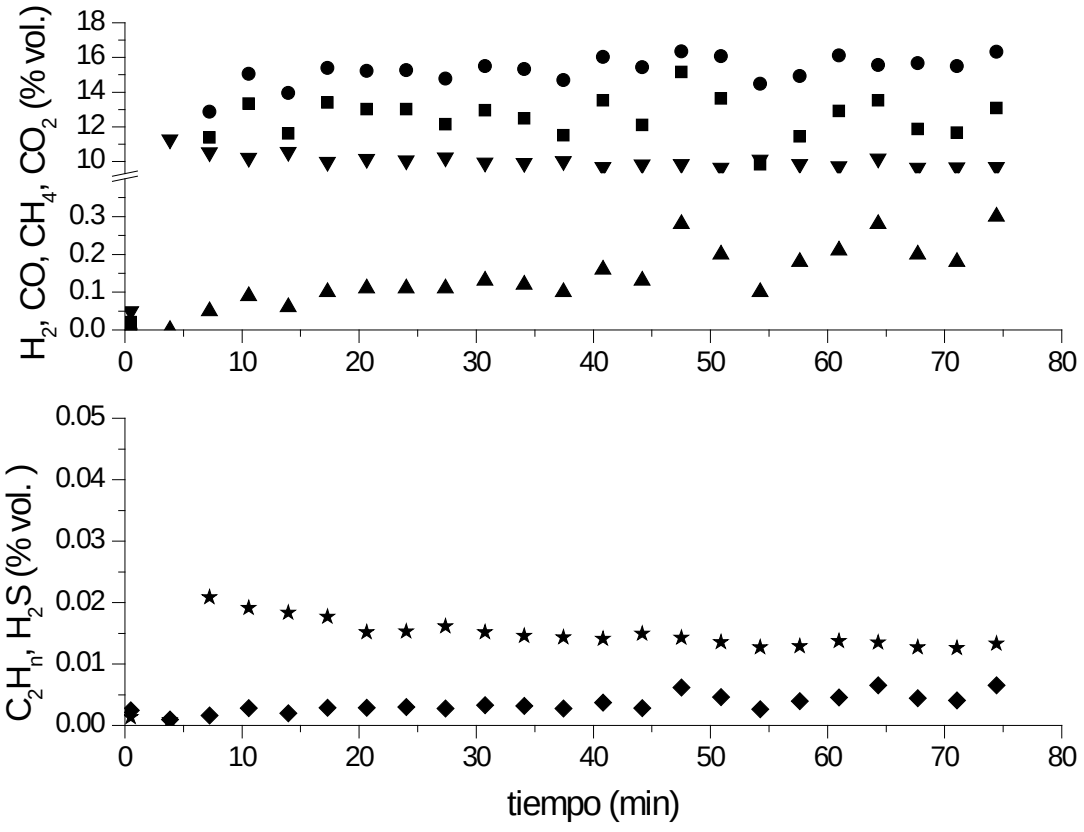

Figura 14. Evolución de la composición del gas en base seca (■ H_2, ●CO, ▲CH_4, ▼ CO_2, ◆ C_2H_n, ★ H_2S). Experimento D-Ni800.

Como puede apreciarse, la variación temporal de la composición de los principales gases producidos (CO, CO_2 y H_2) es poco significativa, pero el metano aumenta de forma constante a lo largo del experimento. Por su parte las concentraciones de H_2S y C_2H_n permanecen a valores muy bajos y sufren poca variación durante el experimento. La detección de H_2S puede indicar cierta desactivación adicional del catalizador de Ni por envenenamiento. La caracterización detallada del catalizador usado en el lecho proporciona resultados que respaldan estas suposiciones [48].

El mencionado aumento de CH_4 representa un indicio de posible desactivación del catalizador de Ni [49,50], por lo que la evolución de este gas se estudió en detalle. Así, la Figura 15 muestra la evolución temporal de CH_4 en todos los experimentos realizados. A 800ºC, la producción de metano en el experimento blanco y en el correspondiente al lecho único de dolomita son muy similares, lo que sugiere que a esta temperatura la actividad de la dolomita con respecto al craqueo de este gas es aún baja.

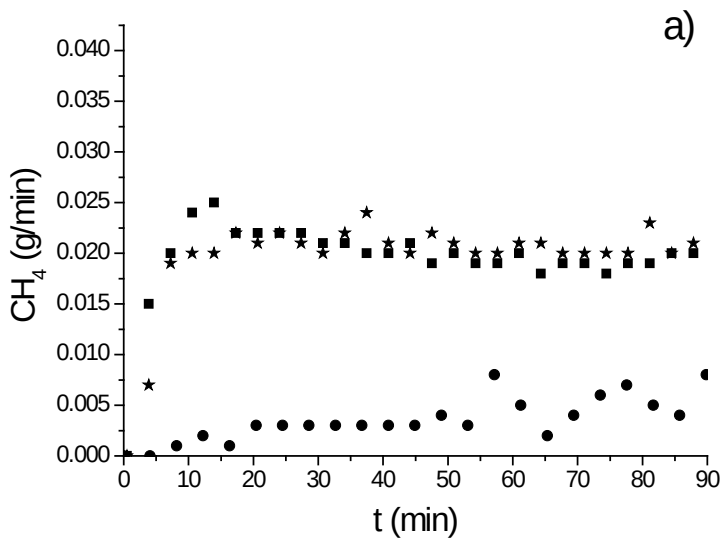

Figura 15. Evolución temporal del CH_4 (■ blanco, ● D-Ni, ★ D 800 ºC), a) 800ºC, b) 850ºC, c) 900ºC.

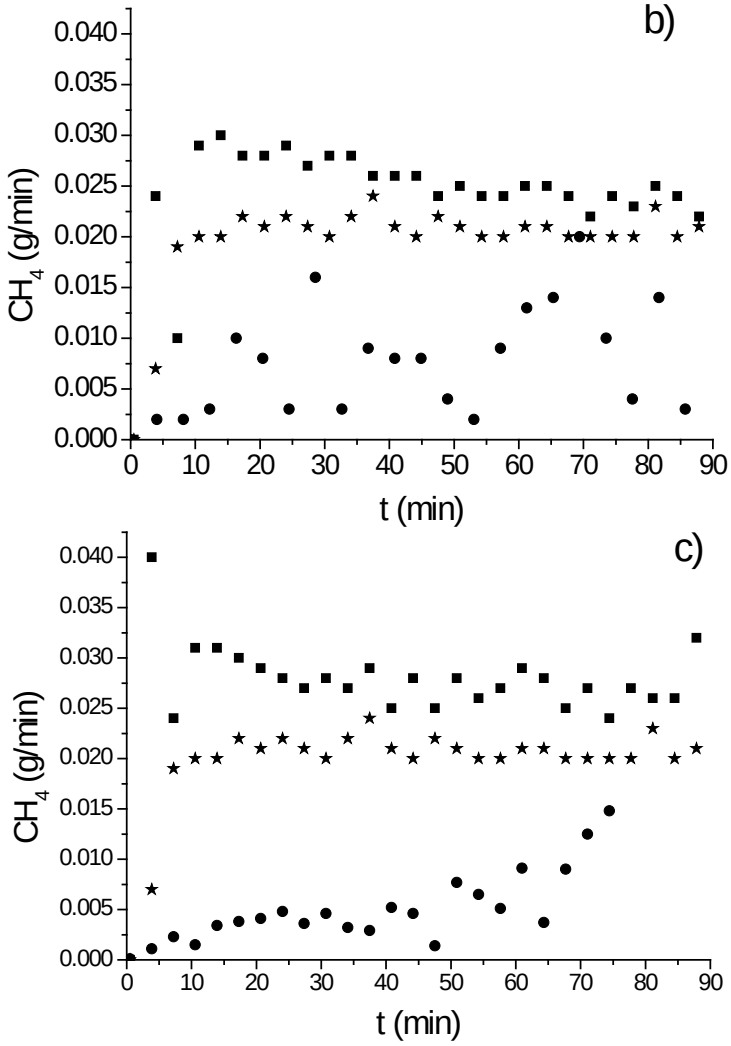

Figura 15 (Continuación). Evolución temporal del CH_4 (■ blanco, ● D-Ni, ★ D 800 ºC), a) 800ºC, b) 850ºC, c) 900ºC.

En cambio, tras el paso por el lecho de Ni se produce la práctica desaparición de todo el metano durante los primeros minutos de cada experimento, lo que indica la mayor actividad del catalizador hacia el craqueo de este gas. A temperaturas mayores (800 y 900ºC), este incremento de CH_4 se produce más rápidamente, lo que sugiere una mayor velocidad de desactivación.

Otro aspecto importante a investigar, relacionado con la composición del gas de gasificación, es el poder calorífico inferior (PCI). En la Figura 16 se representan los valores de PCI (kJ/m^3N) obtenidos a partir de la composición media de los gases en cada experimento. En los experimentos en blanco se obtienen valores aproximados de 2000 kJ/m^3N a 800ºC, y 2400 kJ/m^3N a 850 y 900ºC (diferencias que podrían atribuirse a cierto alcance de las reacciones de craqueo, formando gases combustibles, a las temperaturas más altas del intervalo estudiado). Tras el lecho de dolomita, el craqueo adicional de los productos de gasificación produce un incremento del poder calorífico hasta unos 2800 kJ/m^3N, mientras que el lecho de catalizador de níquel sólo produce un aumento significativo a 800ºC. Este hecho puede relacionarse con las mayores concentraciones de H_2 y CO encontradas a esta temperatura, como se mostraba en la Figura 13. Temperaturas más altas en el lecho de níquel no producen mejoras apreciables del poder calorífico, en comparación con el lecho de dolomita.

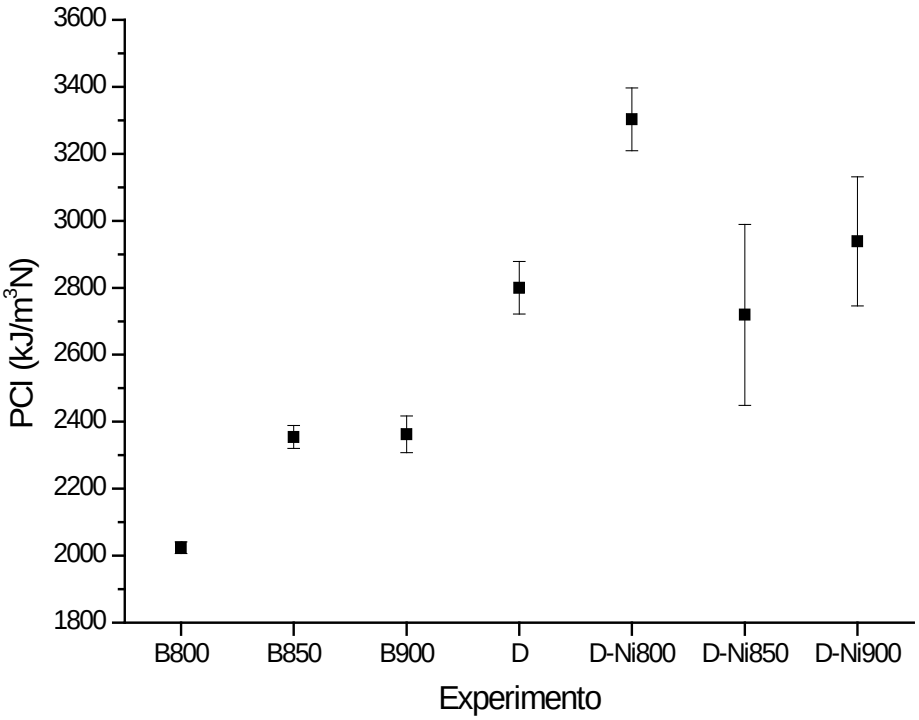

Figura 16. PCI del gas generado.

Algunos de los cambios previamente observados en la composición media de los gases pueden relacionarse con la producción específica de gas (Y_{gas}), mostrado en la Figura 17. El aumento en la producción de gas en los experimentos blancos a 850 y 900ºC puede explicarse por el mencionado craqueo de algunos componentes del alquitrán a esas temperaturas; mientras que el descenso adicional en la formación de gas después del lecho de dolomita puede atribuirse a la carbonatación parcial de la misma (observación consistente con el observado aumento de poder calorífico del gas resultante) y la eliminación del H_2S formado durante la gasificación. Por su parte, el lecho de catalizador de Ni sólo produce un aumento estadísticamente significativo de la producción específica de gas a la temperatura de 800ºC; a temperaturas superiores el gas producido es equivalente al obtenido sólo con dolomita. Este hecho puede indicar un cambio en la velocidad de desactivación del catalizador, que a su vez depende de la diferencia entre la velocidad de formación y de gasificación de depósitos carbonosos en la superficie del catalizador [50].

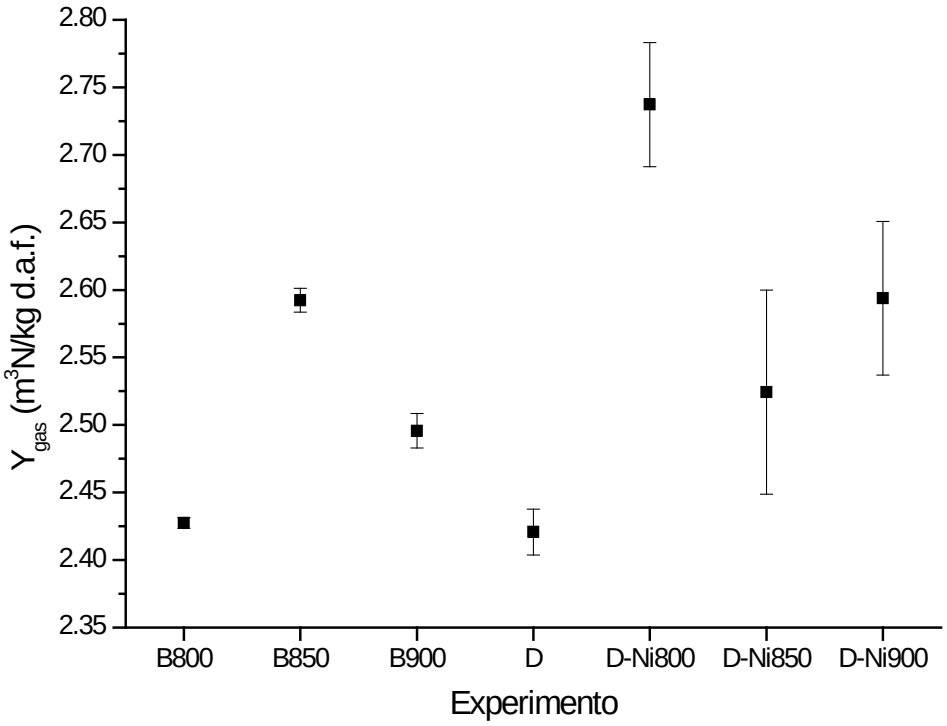

Figura 17. Producción específica de gas.

Con respecto a cada uno de los componentes principales del gas de gasificación, los rendimientos, expresados en gramos de gas por gramo de fango seco y en base libre de cenizas (d.a.f.) se han representado en la Figura 18.

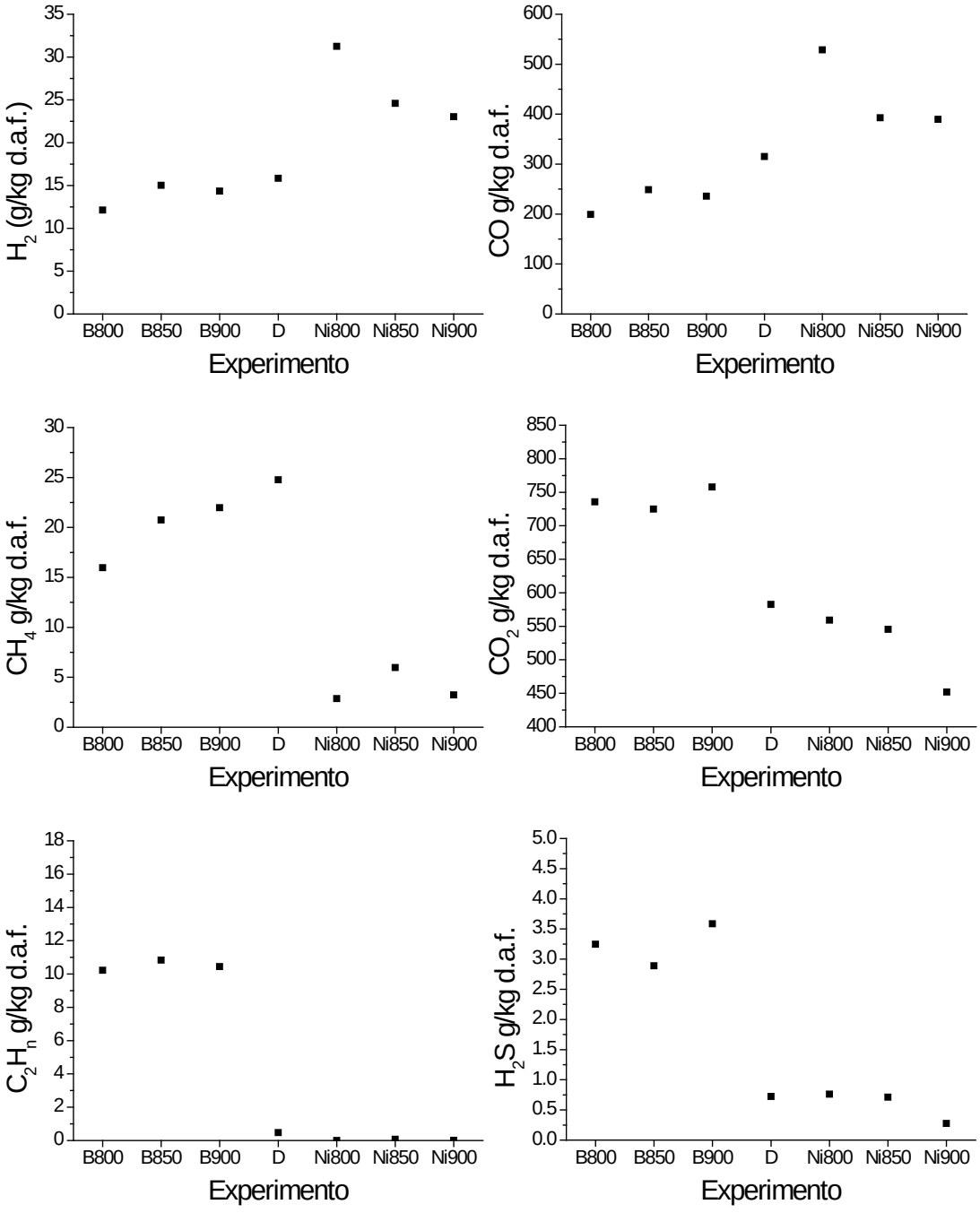

Figura 18. Producción específica (g/kg fango d.a.f.) de los componentes individuales del gas de gasificación.

Los cambios más importantes que provoca el lecho de dolomita son el acusado descenso en la formación de C_2H_n y H_2S. La dolomita produce también un descenso en la producción de CO_2, probablemente por la mencionada carbonatación parcial del material previamente calcinado. Por su parte, el lecho de Ni provoca considerables aumentos de H_2 y CO (especialmente a 800ºC) y un visible descenso en la producción de metano, que podría atribuirse a la reacción de reformado con vapor de este compuesto:

$$CH_4 + H_2O \leftrightarrow CO + 3H_2 \qquad \text{Ec. 5}$$

La eficiencia del proceso de gasificación se mide habitualmente mediante dos parámetros: por un lado, el rendimiento energético a gas, η_{gas}, indicador de la eficacia en la conversión del fango a gas combustible (calculado a partir del poder calorífico y la producción específica de gas según la Ecuación 1 del Apartado 2.4.1). Por otro lado, la eficiencia de conversión de carbono η_C se define de la forma siguiente:

$$\eta_C(\%) = \frac{g\ de\ C\ en\ el\ gas}{g\ de\ C\ alimentados} \cdot 100 \qquad \text{Ec. 6}$$

Ambas eficiencias se representan en la Figura 19 para cada tipo de experimento realizado. El rendimiento energético a gas se incrementa tanto tras el uso de dolomita como con el catalizador de Ni. En el caso del lecho de dolomita y como se ha comentado anteriormente, la carbonatación parcial del material conduce a la eliminación de parte del CO_2 y el consiguiente incremento en el PCI del gas, lo que contrarrestaría el descenso en la producción específica de gas observada en la Figura 17, produciendo un incremento neto en la eficiencia a gas frío. Para el lecho de catalizador de Ni, el incremento más acusado tiene lugar a 800ºC como resultado del incremento simultáneo del PCI de los gases y del rendimiento a gas.

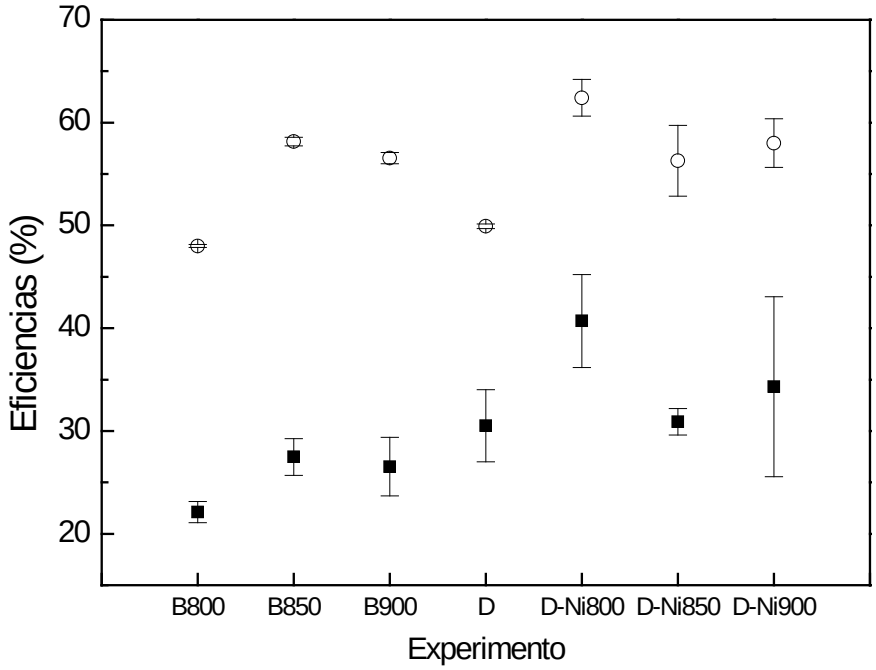

Figura 19. Rendimiento energético a gas (η_{gas}, ■) y eficiencia de conversión de C (η_C, ○).

Finalmente, la Figura 20 presenta el contenido en alquitranes del gas de gasificación. El efecto de un incremento de la temperatura de 800 a 900ºC produce un descenso en la cantidad de alquitranes generados debido al craqueo térmico de parte de los mismos (experimentos B800/B850/B900) [25], y una posible consecuencia de este hecho es el aumento de la cantidad de metano presente en el gas, como se refleja en la Figura 18.

Si bien el lecho de dolomita es capaz de reducir la concentración de alquitranes en más de un orden de magnitud, hasta 0.21 g/m^{3}N, esta cantidad todavía es apreciable; sin embargo, el lecho de catalizador de Ni, operando a cualquiera de las temperaturas probadas, es capaz de eliminar la práctica totalidad de los alquitranes presentes en el gas, tal y como observaron Pinto y cols. [33]. La eliminación total del alquitrán se constató realizando análisis de cromatografía de gases-espectrometría de masas

(GC/MS). A pesar de la progresiva desactivación del catalizador previamente mencionada, la eliminación de alquitranes se produce en todos los experimentos realizados, debido a la presencia de cantidades suficientemente grandes de catalizador.

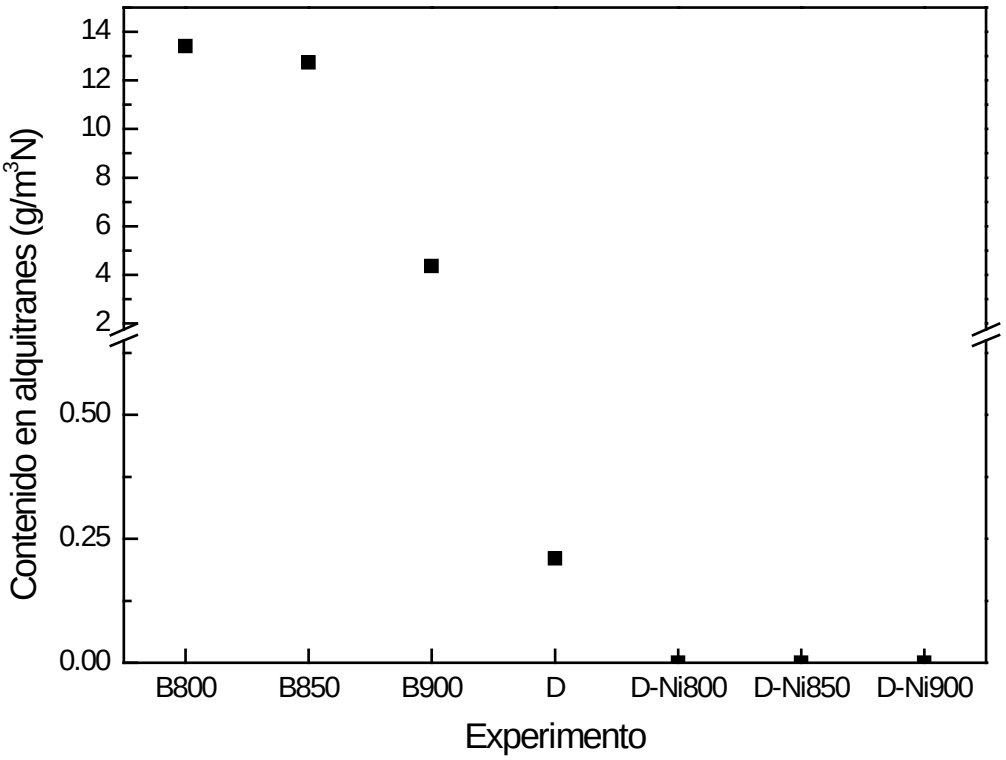

Figura 20. Contenido en alquitranes del gas.

Las conclusiones principales de este apartado de la presente tesis son las siguientes: El uso de un lecho de dolomita operando a 800ºC produce un descenso en el contenido en H_2S del gas de un 0.1 % vol. hasta 0.01 % vol., mientras que un lecho de catalizador comercial de níquel colocado a continuación es capaz de disminuir el contenido en alquitranes de gas hasta niveles indetectables con las técnicas empleadas en este trabajo. Todas las temperaturas probadas para el lecho de catalizador de Ni (800, 850 y 900ºC) provocan la completa eliminación de alquitranes.

En cuanto a las condiciones óptimas de funcionamiento, operando ambos lechos a 800ºC produce los mejores resultados en cuanto a poder calorífico inferior del gas final (produciéndose un incremento de 2000 a 2800 kJ/m^3N tras el lecho de dolomita y hasta 3300 kJ/m^3N tras el lecho de catalizador, respectivamente) y eficiencias del proceso (η_{gas}, η_C), rendimiento a gas (2.4 a 2.7 m^3N/kg d.a.f.). Sin embargo, se observó la desactivación parcial del lecho de catalizador de Ni, probablemente producido debido a la deposición de materia carbonosa procedente del craqueo de los alquitranes e hidrocarburos ligeros presetnes en el gas de gasificación, así como al envenenamiento por parte del H_2S no convertido en el lecho de dolomita.

2.4.4. Mejora catalítica del gas usando un reactor de lecho fluidizado de dos zonas

Este estudio se usó catalizador preparado en el laboratorio, y no catalizador comercial como en el estudio de limpieza de gas en lecho fijo. El catalizador se caracterizó mediante porosimetría, XRD, TPR y SEM. Se comprobó como el Ni se incorpora al catalizador en forma de espinela de níquel, siendo γ-alúmina la única fase cristalina atribuible al soporte. En la Figura 21 se muestra una microfotografía SEM-EDX que muestra que el níquel se encuentra disperso homogéneamente en la superficie, con una relación Ni/Al de 0.28 constante aproximadamente en toda la superficie escaneada.

En los ensayos de actividad del catalizador, realizados en lecho fijo, se comprobó como el soporte tiene cierta actividad en el reformado de hidrocarburos salvo para el metano, y que en presencia de H_2S, el catalizador se desactiva, dejando de producirse el reformado de metano.

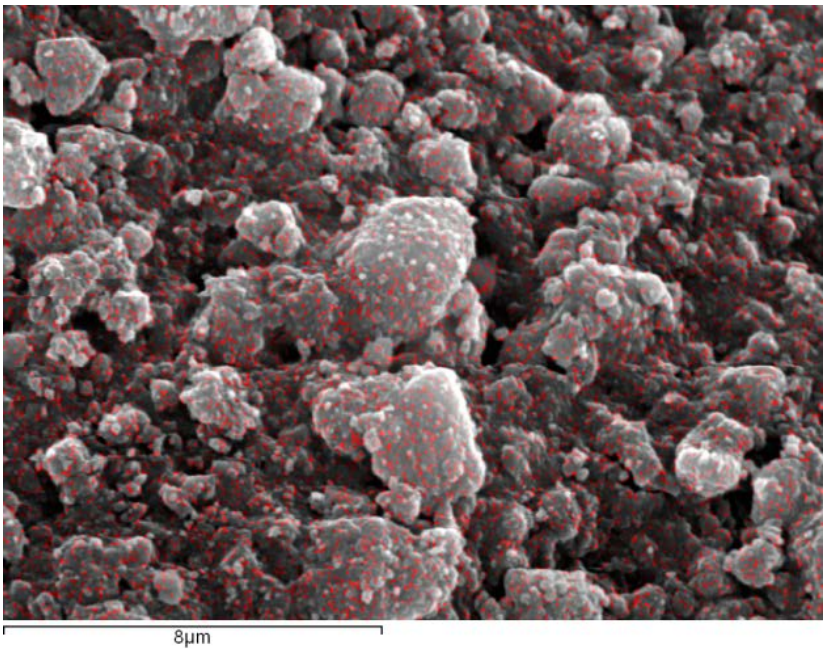

Figura 21. Fotografía SEM-EDX del catalizador preparado

Como se ha comentado en el Apartado 2.3.2, tras el gasificador, se situó el reactor de lecho fijo con dolomita para eliminar H_2S del gas. El uso del lecho de dolomita calcinada permite además, disminuir la cantidad de alquitrán, que disminuye de 15 g/m^3N a 0.21 g/m^3N. El reformado adicional que se consigue con el catalizador de Ni en el RLFDZ reduce el contenido en alquitrán del gas a límites no detectables. En el laboratorio, realizando análisis con un cromatógrafo de gases con espectrómetro de masas (GC/MS), se comprobó que este contenido es menor que 2 mg/m^3N de naftaleno, que es el compuesto mayoritario detectado en el alquitrán producido, por lo que se puede concluir que la limpieza del gas producido es total.

Por lo que respecta a la composición del gas, en las Figuras 22 y 23 se muestra la composición media del gas seco para los compuestos más representativos, obtenida en las distintas configuraciones usadas, tanto por el uso del RLFDZ como el efecto de alimentar, en la zona de regeneración distintos porcentajes de oxígeno para llevar a cabo la combustión selectiva del coque depositado en el catalizador.

Se puede observar como el uso de dolomita prácticamente no afecta al contenido en H_2 del gas, mientras que la concentración de CO y CH_4 aumentan ligeramente, mientras que CO_2 y C_2H_n (la suma de C_2H_2, C_2H_4 y C_2H_6) disminuyen significativamente. Las tendencias observadas pare el CO_2 y CO pueden ser debidas al desplazamiento de la reacción de intercambio inversa así como a las reacciones de reformado de alquitrán provocadas por el lecho de dolomita calcinada.

Aunque el uso de alúmina en el RLFDZ aumenta H_2 y CO, el efecto se ve incrementado por el catalizador de Ni/γ-alúmina. Con catalizador y sin alimentar oxígeno o con únicamente un 1 % de oxígeno en el gas de regeneración se obtiene un máximo en la concentración del gas para estos compuestos. Sin embargo hay que tener en cuenta en estas circunstancias, el sistema no opera de modo estable.

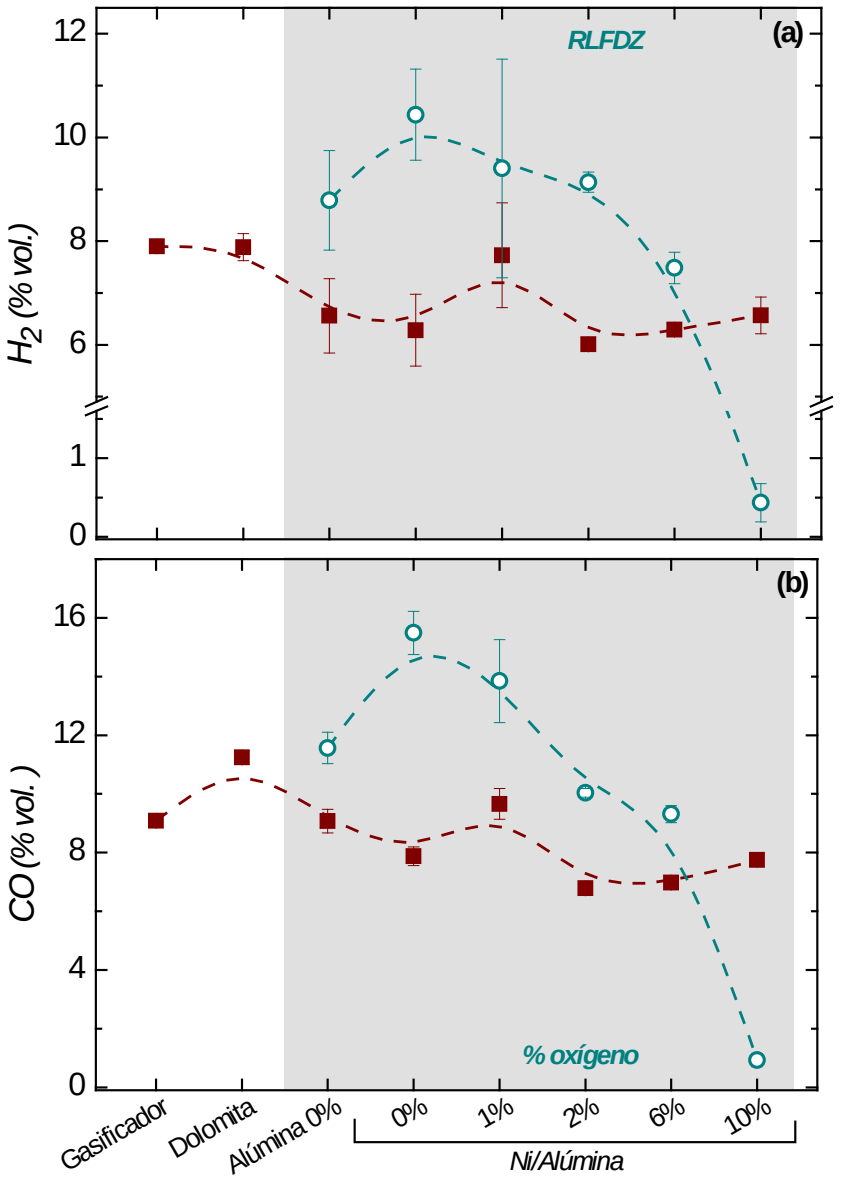

Figura 22. Contenido en hidrógeno (a) y monóxido de carbono (b) en el gas sin reformar (■) y reformado (○).

Al aumentar el porcentaje de oxígeno en el gas de regeneración, el sistema se comporta de modo más estable, aunque disminuye la concentración de H_2 y CO en el gas. Al usar un 10 % de O_2 en el gas de regeneración, la concentración de estos gases cae por debajo de la del gas sin reformar, lo que indica que hay un exceso de oxígeno

para la combustión del coque depositado en el catalizador, que llega a la zona de reformado y produce la oxidación del gas de gasificación.

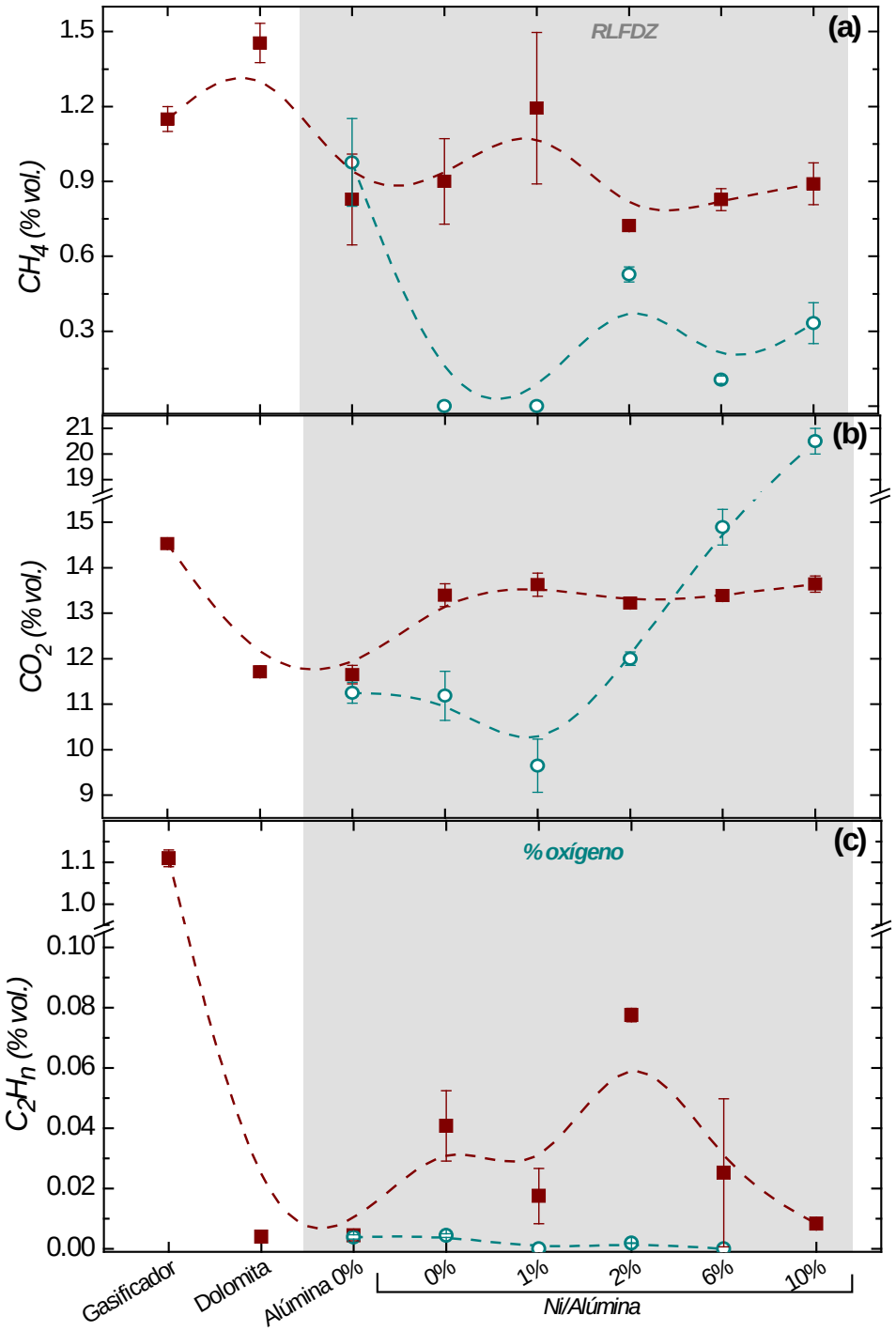

Figura 23. Contenido en metano (a), dióxido de carbono (b), y C_2H_n (c) en el gas sin reformar (■) y reformado (○).

De los porcentajes de oxígeno en el gas de regeneración utilizados, el 2 % es el que ofrece el mejor resultado en cuanto a aumento del PCI del gas, tal y como se aprecia en la Figura 24 (excluido el 0 % de oxígeno, que como se ha comentado no permite la regeneración del catalizador, dado que no se produce combustión del coque).

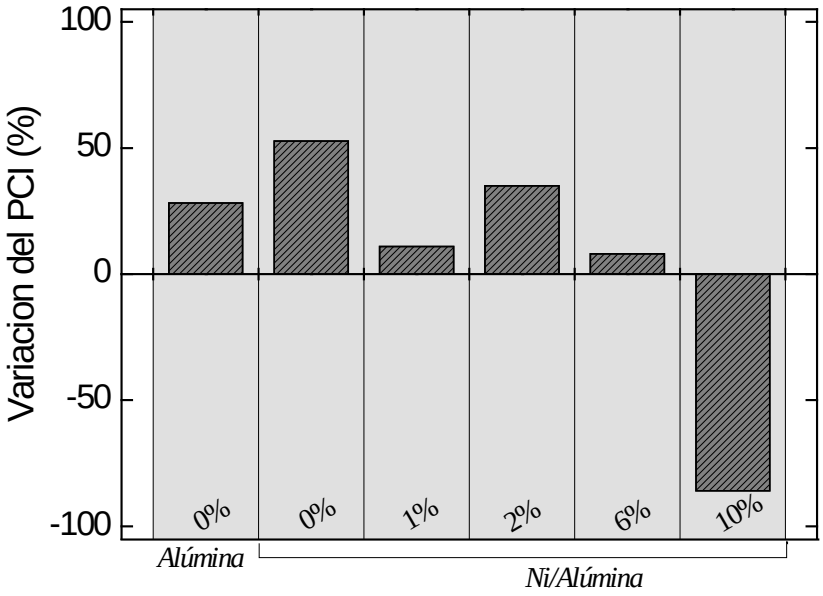

Figura 24. Variación del PCI del gas (%).

Como conclusiones más relevantes de este estudio se puede destacar que se ha conseguido una operación de modo estable del sistema experimental completo. En las mejores condiciones probadas, usando un 2 % en volumen de oxígeno en el gas de regeneración del reactor de dos zonas, se consigue un aumento del 37 % en el poder calorífico inferior y una eliminación completa del alquitrán en el gas, menor que el límite de detección mediante GCMS.

2.4.5. Trabajos futuros

Este trabajo se ha centrado en el estudio de la co-gasificación de fango de EDAR y carbón con aire en lecho fluidizado, dando especial importancia al tratamiento de limpieza de gases. Aunque se han implementado con éxito dos estrategias para la limpieza del gas, en lo que a la eliminación de alquitranes se refiere, y antes de pasar el estudio a otra escala, quedan todavía líneas de mejora para continuar la investigación.
Por lo que respecta a la limpieza de los gases, aunque el funcionamiento de los catalizadores ha sido satisfactorio, el trabajo debería completarse con:

- Un estudio en profundidad de la vida del catalizador, con tiempos de funcionamiento más largos.

- Un estudio de desulfuración con otros materiales, incluso en otras condiciones de operación que pudiesen llegar a simular las condiciones de procesos donde se elimina el azufre, como puede ser el proceso Claus.

- Ampliar el rango de contaminantes a otros compuestos, bien con azufre como COS que se conoce que se forman en la gasificación y que por falta de medios materiales no se ha abordado en este trabajo, bien de distinta naturaleza, como es el NH_3, que también se forma en la gasificación de compuestos con N en su composición elemental.

Por otra parte, este estudio se llevó a cabo en un reactor y en una condiciones que, si bien para la biomasa pueden ser adecuadas, cuando se usa carbón se ha obtenido una conversión del mismo baja, con eficacias energéticas y conversión del carbono a gas que se pueden mejorar, por lo que un estudio ampliando la temperatura de la gasificación y/o incluyendo vapor de agua y mezclas del mismo con oxígeno sería de gran interés, aunque para ello habría que diseñar y construir un sistema experimental distinto.

3. Bibliografía

[1] Manyà JJ, Sánchez JL, Ábrego J, Gonzalo A, Arauzo J. Influence of gas residence time and air ratio on the air gasification of dried sewage sludge in a bubbling fluidised bed. Fuel 2006;85(14-15):2027–2033.

[2] Manyà JJ, Sánchez JL, Gonzalo A, Arauzo J. Air gasification of dried sewage sludge in a fluidized bed: effect of the operating conditions and in-bed use of alumina. Energy and Fuels 2005;19(2):629–636.

[3] Fonts I, Juan A, Gea G, Murillo MB, Sánchez JL. Sewage sludge pyrolysis in fluidized bed, 1: influence of operational conditions on the product distribution. Industrial & Engineering Chemistry Research 2008;47(15):5376–5385.

[4] Fonts I, Juan A, Gea G, Murillo MB, Arauzo J. Sewage sludge pyrolysis in a fluidized bed, 2: influence of operating conditions on some physicochemical properties of the liquid product. Industrial & Engineering Chemistry Research 2009;48(4):2179–2187.

[5] Ábrego J, Arauzo J, Sánchez JL, Gonzalo A, Cordero T, Rodríguez-Mirasol J. Structural changes of sewage sludge char during fixed-bed pyrolysis. Industrial & Engineering Chemistry Research 2009;48(6):3211–3221.

[6] Casajus C, Ábrego J, Marias F, Vaxelaire J, Sánchez JL, Gonzalo A. Product distribution and kinetic scheme for the fixed bed thermal decomposition of sewage sludge. Chemical Engineering Journal 2009;145:412–419.

[7] Aznar M. Estudio de la gasificación con aire en lecho fluidizado de lodos procedentes de estaciones depuradoras de aguas residuales urbanas. Universidad de Zaragoza, 2009.

[8] Gonzalo A. Procesado termoquímico de fangos procedentes de estaciones depuradoras de aguas residuales. Universidad de Zaragoza, 2004.

[9] Ábrego J. Características y aplicación del sólido obtenido mediante pirólisis de fangos de EDAR. Universidad de Zaragoza, 2010.

[10] Fonts I. Estudio experimental de la pirólisis en lecho fluidizado de lodos de EDAR. Obtención y propiedades del producto líquido. Universidad de Zaragoza, 2010.

[11] Aznar M, Manyà JJ, García G, Sánchez JL, Murillo MB. Influence of freeboard temperature, fluidization velocity and particle size on tar production and

composition during the air gasification of sewage sludge. Energy and Fuels 2008;22(4):2840–2850.

[12] Fonts I, Cascarosa E, García G, Aznar M, Ábrego J, Arauzo J. Sewage sludge and meat bone meal valorisation by means of pyrolysis and gasification. In: San José MJ, editor. Advances in chemical engineering. Transworld Research Network, 2010. p. 15–32.

[13] Sutton D, Kelleher B, Ross JRH. Review of literature on catalysts for biomass gasification. Fuel Processing Technology 2001;73(3):155–173.

[14] Maniatis K. Progress in biomass gasification: an overview, vol. 1. Blackwell Science, 2002.

[15] Milne TA, Evans RJ, Abatzoglou N. Biomass gasifier "tars": their nature, formation, and conversion. report NREL/TP-570-25357. 1998.

[16] Abad A, Adánez J, García-Labiano F, De Diego LF, Gayán P. Hot coal-gas desulfurization with calcium-based sorbents in a pressurized moving-bed reactor. Energy and Fuels 2004;18(5):1543–1554.

[17] Hepola J, Simell P. Sulphur poisoning of nickel-based hot gas cleaning catalysts in synthetic gasification gas: I. effect of different process parameters. Applied Catalysis B: Environmental 1997;14(3-4):287–303.

[18] de Diego LF, Adánez J. Factors affecting the H2S reaction with noncalcined limestones and half-calcined dolomites. Energy and Fuels 1999;13(1):146–153.

[19] Corella J, Aznar MP, Gil J, Caballero MA. Biomass gasification in fluidized bed: where to locate the dolomite to improve gasification? Energy and Fuels 1999;13(6):1122–1127.

[20] Álvarez-Rodríguez R, Clemente-Jul C. Hot gas desulphurisation with dolomite sorbent in coal gasification. Fuel 2008;87(17-18):3513–3521.

[21] Pinto F, Lopes H, André RN, Gulyurtlu I, Cabrita I. Effect of catalysts in the quality of syngas and by-products obtained by co-gasification of coal and wastes. 2: heavy metals, sulphur and halogen compounds abatement. Fuel 2008;87(7):1050–1062.

[22] Gascón J. Nuevos reactores de lecho fluidizado de dos zonas para valorización de hidrocarburos. Universidad de Zaragoza, 2006.

[23] Unión Europea. Directiva 91/271/CEE sobre el tratamiento de las aguas residuales urbanas. 1991.

[24] Li C, Suzuki K. Tar property, analysis, reforming mechanism and model for biomass gasification—an overview. Renewable and Sustainable Energy Reviews 2009;13(3):594–604.

[25] Han J, Kim H. The reduction and control technology of tar during biomass gasification/pyrolysis: an overview. Renewable and Sustainable Energy Reviews 2008;12(2):397–416.

[26] Simell PA, Bredenberg JB. Catalytic purification of tarry fuel gas. Fuel 1990;69(10):1219–1225.

[27] Bangala DN, Abatzoglou N, Martin J-P, Chornet E. Catalytic gas conditioning: application to biomass and waste gasification. Industrial & Engineering Chemistry Research 1997;36(10):4184–4192.

[28] Zhang R, Brown RC, Suby A, Cummer K. Catalytic destruction of tar in biomass derived producer gas. Energy Conversion and Management 2004;45(7-8):995–1014.

[29] Meng X, De Jong W, Pal R, Verkooijen AHM. In bed and downstream hot gas desulphurization during solid fuel gasification: a review. Fuel Processing Technology 2010;91(8):964–981.

[30] Adánez J, Abad A, García-Labiano F, De Diego LF, Gayán P. H2s retention with ca-based sorbents in a pressurized fixed-bed reactor: application to moving-bed design. Fuel 2005;84(5):533–542.

[31] Cheah S, Carpenter DL, Magrini-Bair K a. Review of mid- to high-temperature sulfur sorbents for desulfurization of biomass- and coal-derived syngas. Energy and Fuels 2009;23(11):5291–5307.

[32] Elseviers WF, Verelst H. Transition metal oxides for hot gas desulphurisation. Fuel 1999;78(5):601–612.

[33] Pinto F, André RN, Franco C, Lopes H, Gulyurtlu I, Cabrita I. Co-gasification of coal and wastes in a pilot-scale installation 1: effect of catalysts in syngas treatment to achieve tar abatement. Fuel 2009;88(12):2392–2402.

[34] Caballero MA, Aznar MP, Gil J, Martín JA, Francés E, Corella J. Commercial steam reforming catalysts to improve biomass gasification with steam−oxygen

mixtures. 1. hot gas upgrading by the catalytic reactor. Industrial & Engineering Chemistry Research 1997;36(12):5227–5239.

[35] Hong S-P, Dong J-I, Yeo S-K, Park I-H, Chung M-S, Kim D-I, Park Y-K. Reduction of tar using cheap catalysts during sewage sludge gasification. Journal of Material Cycles and Waste Management 2011;13(3):186–189.

[36] Kuhn JN, Zhao Z, Felix LG, Slimane RB, Choi CW, Ozkan US. Olivine catalysts for methane- and tar-steam reforming. Applied Catalysis B: Environmental 2008;81(1-2):14–26.

[37] Rapagnà S, Gallucci K, Di Marcello M, Matt M, Foscolo PU. Improvement of gas yield from biomass gasification by using fe/olivine as gasifier bed inventory. Chemical Engineering Transactions 2010;21:415–420.

[38] Azhar Uddin M, Tsuda H, Wu S, Sasaoka E. Catalytic decomposition of biomass tars with iron oxide catalysts. Fuel 2008;87(4-5):451–459.

[39] Cheah S, Carpenter DL, Magrini-Bair K a. Review of mid- to high-temperature sulfur sorbents for desulfurization of biomass- and coal-derived syngas. Energy and Fuels 2009;23(11):5291–5307.

[40] Yuan W, Bandosz TJ. Removal of hydrogen sulfide from biogas on sludge-derived adsorbents. Fuel, 2007;86(17-18):2736–2746.

[41] Ansari A, Bagreev A, Bandosz TJ. Effect of adsorbent composition on h2s removal on sewage sludge-based materials enriched with carbonaceous phase. Carbon 2005;43(5):1039–1048.

[42] Bagreev A, Bandosz TJ. On the mechanism of hydrogen sulfide removal from moist air on catalytic carbonaceous adsorbents. Industrial & Engineering Chemistry Research 2005;44(3):530–538.

[43] Abu El-Rub Z, Bramer E a., Brem G. Review of catalysts for tar elimination in biomass gasification processes. Industrial & Engineering Chemistry Research 2004;43(22):6911–6919.

[44] Devi L. A review of the primary measures for tar elimination in biomass gasification processes. Biomass and Bioenergy 2003;24(2):125–140.

[45] Corella J, Toledo JM, Aznar MP. Improving the modeling of the kinetics of the catalytic tar elimination in biomass gasification. Industrial & Engineering Chemistry Research 2002;41(14):3351–3356.

[46] Pérez P, Aznar MP, Caballero MA, Gil J, Martí JA, Corella J. Hot gas cleaning and upgrading with a calcined dolomite located downstream a biomass fluidized bed gasifier operating with steam-oxygen mixtures. Energy and Fuels 1997;0624(97):1194–1203.

[47] Bimbela F, Chen D, Ruiz J, García L, Arauzo J. Ni/al coprecipitated catalysts modified with magnesium and copper for the catalytic steam reforming of model compounds from biomass pyrolysis liquids. Applied Catalysis B: Environmental 2012;119-120:1–12.

[48] García G, Monzón A, Bimbela F, Sánchez JL, Ábrego J. Desulfurization and catalytic gas cleaning in fluidized bed co-gasification of sewage sludge-coal blends. Energy and Fuels 2013: DOI: 10.1021/ef400259g.

[49] Czernik S, Evans R, French R. Hydrogen from biomass-production by steam reforming of biomass pyrolysis oil. Catalysis Today 2007;129(3-4):265–268.

[50] Bartholomew CH. Mechanisms of catalyst deactivation. Applied Catalysis A: General 2001;212(1-2):17–60.

Anexo I. Informe de contribución.

Mi contribución como autor en cada uno de los artículos de esta memoria ha sido:

Artículo I: Publicado en Chemical Engineering Journal, factor de impacto: 3.461 (2011).
Área temática: Chemical Engineering (11/133)

Responsable de la experimentación y análisis de datos, redacción de la parte de resultados.

Artículo II: Publicado en Chemical Engineering Journal, factor de impacto: 3.461 (2011).
Área temática: Chemical Engineering (11/133)

Responsable del trabajo experimental y del análisis de resultados y colaboración en la redacción.

Artículo III: Publicado en Energy & Fuels, Factor de impacto: 2.721 (2011).
Área temática: Chemical Engineering (18/133)

Responsable de la parte experimental y análisis de resultados. Redacción de la parte experimental y análisis de resultados.

Artículo IV: Publicado en Energy & Fuels, Factor de impacto: 2.721 (2011).
Área temática: Chemical Engineering (18/133)

Responsable de la parte experimental, análisis de resultados y redacción.

Estos artículos se pueden encontrar en el apartado final de esta memoria (Anexo III).

Además, fruto del trabajo realizado en esta Tesis Doctoral, se ha participado en los siguientes congresos:

c2yƎNŜă2 I:

Cascarosa, E; García, G; Monzón, A; Sánchez, JL; Arauzo, J (2011)

Gas cleaning from coal and sewage sludge co-gasification process with a Ni catalyst bed.

Fifth International Conference on Clean Coal Technologies (CCT2011).

Zaragoza (España). 8-12 Mayo 2011. Tipo de contribución: Póster.

ConƎ₪Ŝă2 II:

Cascarosa, E., Ábrego , J., G., Gonzalo, A., García, G., Sánchez, J.L.(2010)

Use of different residues for high temperature desulphuration of co-gasification syngas

ECSM 2010 – 2nd European Conference on Sludge Management

Budapest, Hungary, 9&10 Septiembre 2010

Tipo de contribución: Póster

ConƎ₪Ŝă2 III:

García, G., Cascarosa, E., Sánchez, J.L., Arauzo, J. (2009)

Analysis of catalytic co-gasification of two types of coal with sewage sludge and olive bagasse

17h European Biomass Conference

Hamburgo (Alemania) 29 Junio-3 Julio 2009

Tipo de contribución: Póster

ConƎ₪Ŝă2 IV:

García, G., Ábrego, J., Sánchez, J.L., Arauzo, J. (2009)

Influence of feed composition on the co-gasification of two types of coal with sewage sludge and olive bagasse

16th European Biomass Conference

Valencia, 2-6 Junio 2008

Tipo de contribución: Póster

Anexo II. Artículos publicados.

Reprinted from Chemical Engineering Journal, Vol 22 (2), G. García, J. Arauzo, A. Gonzalo, J.L. Sánchez, J. Ábrego, Influence of feedstock composition in fluidised bed co-gasification of mixtures of lignite, bituminous coal and sewage sludge, 345-352, Copyright (2013), with permission from Elsevier

Chemical Engineering Journal 222 (2013) 345–352

Contents lists available at SciVerse ScienceDirect

Chemical Engineering Journal

journal homepage: www.elsevier.com/locate/cej

Influence of feedstock composition in fluidised bed co-gasification of mixtures of lignite, bituminous coal and sewage sludge

G. García [a], J. Arauzo [b], A. Gonzalo [b], J.L. Sánchez [b], J. Ábrego [b,*]

[a] AEMA Servicios, Pol. Ind. El Pilar, C/Fitero 9, E-26540 Alfaro, Spain
[b] Thermo-Chemical Processes Group, Aragón Institute of Engineering Research (I3A), I+D Building, University of Zaragoza, c/Mariano Esquillor s/n, E-50018 Zaragoza, Spain

HIGHLIGHTS

- Design of experiments to study effect of sewage/coal blends on co-gasification.
- Co-gasification produces synergistic effects on product composition (tar).
- Improved LHV and gas yields (d.a.f. + air) with addition of sewage sludge.

ARTICLE INFO

Article history:
Received 1 October 2012
Received in revised form 8 February 2013
Accepted 18 February 2013
Available online 28 February 2013

Keywords:
Co-gasification
Sewage sludge
Coal
Experimental design

ABSTRACT

Energy recovery from sewage sludge can be achieved by several thermochemical processes, including its co-processing with other fuels. In this work, co-gasification of mixtures of sewage sludge with two types of coal (bituminous and lignite) was performed in a laboratory-scale fluidised bed reactor. The influence of the feedstock composition on key parameters of gasification—such as gas heating value and yield, cold gas efficiency and tar generation—was determined. Whereas some of these results can be explained as the sum of individual contributions of each feedstock component, some synergistic effects were also identified. Among these, the decrease of tar yield and the increase of H_2 and CO in the gas suggest that co-gasification of sewage sludge with certain types of coal may be energetically advantageous and improve the process performance.

© 2013 Elsevier B.V. All rights reserved.

1. Introduction

In the last decades, the increasing challenges on water management and pollution have led to the application of stricter wastewater treatment policies in most countries. As a result, the number of wastewater plants worldwide has increased dramatically, and so has done the amount of sewage sludge generated in these treatment plants [1].

Because of its origin, sewage sludge contains a significant organic fraction with good potential for energy recovery. Several technologies have been extensively investigated and reviewed in the recent literature, including combustion, co-combustion, gasification and pyrolysis [2–4]. While co-combustion of sewage sludge and coal has been subject of several works [5–13], co-gasification has been shortly reported yet. Research carried out at INETI, Portugal (now Laboratório Nacional de Energia e Geologia) is one of the most significant. Lopes and co-workers [14] and Pinto et al. [15] studied the effect of sewage sludge content (0–100% w/w, mixed with bituminous Puertollano coal), gasification temperature (750–900 °C) and equivalent ratio (0–0.3 at 850 °C) on the gas composition and HCl, NH_3 and H_2S contents from a fluidized bed gasifier. They also analysed the solid residue after gasification. In the second part of this work [16], the authors gasified sewage sludge–straw blends and compared the results with the ones from the previous article.

Wang and Xiao [17] simulated a sewage sludge/coal co-gasification power plant using Aspen Plus. Sewage sludge was fed at 80% moisture with the option of a previous step for drying. Results were compared to sludge gasification, coal gasification and co-incineration of both materials. It was found that a mixing weight ratio of 50–67% sludge (80% moisture) outperformed co-incineration, coal gasification or sludge gasification power plants.

Liu et al. [18] studied the transformation of phosphorus during gasification in a quartz tube reactor. Sewage sludge powder was mixed with a varying amount of coal powder to make the total phosphorus content in the mixture be 0.5, 1.0, 1.5, 2.0, 2.5, and 2.85 wt.%. The temperature range and the gasifying agent were 900–1300 °C and CO_2 respectively.

* Corresponding author. Tel.: +34 976762962; fax: +34 976761879.
E-mail address: javabr@unizar.es (J. Ábrego).

1385-8947/$ - see front matter © 2013 Elsevier B.V. All rights reserved.
http://dx.doi.org/10.1016/j.cej.2013.02.073

Reprinted from Chemical Engineering Journal, Vol 22 (2), G. García, J. Arauzo, A. Gonzalo, J.L. Sánchez, J. Ábrego, Influence of feedstock composition in fluidised bed co-gasification of mixtures of lignite, bituminous coal and sewage sludge, 345-352, Copyright (2013), with permission from Elsevier

At the Imperial College of London, Reed and co-workers [19] performed a 2 MWth pilot-plant study of air-blown, pressurised sewage sludge co-gasification with coal at 960 °C. The main objective was to study the distribution of trace elements to the output streams and the effect of temperature in the performance of a downstream hot gas filter. In other works by the same research group, sewage sludge gasification was compared to coal gasification, but these two materials were not co-gasified together. For instance, Paterson et al. [20] described the formation of HCN and NH_3 from gasification of sewage sludge and bituminous coal in a laboratory-scale spouted bed gasifier. Finally, Paterson and co-workers [21] also reviewed the design and development of the bench-scale pressurised fluidized bed reactor used in Ref. [20].

Some advantages over coal gasification have been pointed out in the mentioned works [15]. For instance, co-gasification of sewage sludge and coal mixtures was a better option than co-incineration [17], and caused an increase in fuel conversion and heating value [22].

The objective of this study was to investigate the co-gasification of blends of dry sewage sludge with two different types of coal: bituminous coal and lignite. More specifically, we focused on the influence of the blend composition on some key parameters of gasification, such as cold gas efficiency, gas heating value and composition, specific gas yield and tar generation. Experiments were made in a laboratory-scale fluidised bed reactor, according to a previously developed experimental design for mixtures. In this way, the statistical significance of the results could be adequately evaluated.

Although out of the scope of this work, the characteristics and behaviour of the solid products would require further research. For instance, the heavy metal content of the solid product (coming mainly from sewage sludge) should be considered. In this regard, Hernández and co-workers [23] performed leaching tests after gasification of similar sewage sludge, and concluded that thermal treatment significantly stabilized heavy metals in the solid product. Also, it should be noted that the mixture of chars produced as a result of co-gasification of sewage sludge and coals could be used as cheap desulfurization agent [24].

2. Experimental

2.1. Materials

Anaerobically digested and dried sewage sludge was received from a Spanish urban wastewater treatment plant. The bituminous coal and lignite were kindly supplied by the Spanish company Endesa. Hereinafter in this work, these materials will be referred to as BC (bituminous coal), LC (lignite coal) and SS (sewage sludge).

Table 1 shows the heating values, proximate and ultimate analyses of the raw materials. Table 2 shows the composition of their ashes. These analyses were performed by ICB-CSIC (Instituto de Carboquímica) in Zaragoza.

All the feedstock materials were crushed and sieved to particle sizes between 250 and 500 μm. Sand (SiO_2) with a mean particle size between 250 and 350 μm was used as bed material. 20 g of sand per 100 g of total solid feed were added to each blend to improve the feeding of the materials into the reactor. Prior to each experiment, each particular feedstock mixture was blended and dried for 24 h at 105 °C. Air was used as gasification agent.

In order to avoid fluidization problems, the possibility of ash melting must be assessed, especially considering the high ash content of some of the materials used in this work. The simplified correlation proposed by Seggiani [25] which was obtained for coal and biomass has been used to calculate the initial deformation temperature, obtaining 1340 °C for BC, 1130 for LC and 1000 for SS (with standard deviation of 80 °C from the correlation). At the gasification temperature of 850 °C, no fluidization problem or slag formation was observed.

Table 1
Heating values, ultimate and proximate analyses of the raw materials.

	Analysis method	BC	LC	SS
Proximate analysis				
Moisture (wt.%)	ISO-579-1981	6.9	19.2	6.5
Ash (wt.%)	ISO-1171-1976	14.3	26.3	41.3
Volatile (wt.%)	ISO-5623-1974	25.2	26.0	46.9
Fixed C (wt.%)		53.6	28.5	5.4
Ultimate analysis (dry basis)				
C (wt.%)	Carlo Erba 1108	65.3	37.6	27.8
H (wt.%)	Carlo Erba 1108	4.1	4.1	4.4
N (wt.%)	Carlo Erba 1108	1.8	0.5	4.0
S (wt.%)	Carlo Erba 1108	0.7	6.1	0.8
Heating value (dry basis)				
HHV[a] (MJ/kg)	ASTM-D-3286-96	25.4	14.6	12.0
LHV[a] (MJ/kg)	ASTM-D-3286-96	24.3	13.3	10.9

[a] HHV: higher heating value; LHV: lower heating value.

Table 2
Ash compositions of the feedstock materials.

(wt.% of ash)	BC	LC	SS
Al_2O_3	27.97	25.07	21.57
CaO	7.21	3.40	23.14
Fe_2O_3	2.71	28.04	8.56
K_2O	0.74	1.34	3.66
MgO	1.33	1.07	5.93
Na_2O	0.35	0.16	1.37
SiO_2	47.50	37.88	34.51
TiO_2	1.49	0.73	1.25

2.2. Experimental apparatus

The laboratory-scale fluidised bed experimental system has been described elsewhere [24,26]. For all the experiments, the bed temperature was 850 °C, the ratio between actual and minimum fluidization velocity in the bed was $V_f/V_{mf} = 5$, and the equivalence ratio was ER = 0.3 (defined as the ratio between actual oxygen used for gasification and stoichiometric oxygen for a complete combustion). Tar and water were trapped in a series of condensers refrigerated by ice, and in a cotton filter. Water content was determined by means of Karl-Fischer titration, and tar was quantified gravimetrically. Gas composition was measured with an Agilent 3000A MicroGC gas chromatograph. The total amount of gasification gas was quantified using a volumetric gas metre.

2.3. Experimental procedure

To establish the influence of the feedstock composition on the gasification outcomes, an experimental design based on a simplex lattice mixture was used. This design was augmented with ternary mixtures to determine the response within the experimental region [27]. A figure showing additional information about the experimental design points can be found in Supplementary Material.

Replicated experiments with pure raw materials, their binary mixtures and the centroid (1/3 of each raw material) were carried out in order to determine the experimental error as a basis for the analysis of variance (ANOVA) of the results. Design Expert 7.0.0 software has been used in this work for the statistical analysis and data representation. With the proposed experimental design, it is possible to distinguish whether there is any synergystic or

Reprinted from Chemical Engineering Journal, Vol 22 (2), G. García, J. Arauzo, A. Gonzalo, J.L. Sánchez, J. Ábrego, Influence of feedstock composition in fluidised bed co-gasification of mixtures of lignite, bituminous coal and sewage sludge, 345-352, Copyright (2013), with permission from Elsevier

antagonistic effect when the different raw materials are mixed. Thus, the effect of the feedstock composition can be empirically modelled with an equation:

$$RV = \beta_1 \cdot W_1 + \beta_2 \cdot W_2 + \beta_3 \cdot W_3 + \beta_{12} \cdot W_1 \cdot W_2 + \beta_{13} \cdot W_1 \cdot W_3 + \beta_{23} \cdot W_2 \cdot W_3 + \beta_{123} \cdot W_1 \cdot W_2 \cdot W_3 \quad (1)$$

In Eq. (1), RV is a response variable (any of the measured experimental results), and the equation represents a special cubic model [28], where the β_i coefficients represent the linear response of the pure components mass fraction (W_i), the β_{ij} coefficients the quadratic effect due to the synergetic effect of having two components in the mixture and β_{123} models the cubic effect due to the three components. Some of the coefficients may not appear in the model for a specific response, as some of them can be statistically not significant.

Thus, this work used this statistical methodology to examine the influence of gasifying different mixtures of the three raw materials on:

- Gas yield, measured as N m^3 of dry gas produced per kg of d.a.f. feedstock, Y_{gas}, and as the weight percentage of gas related to the feedstock, alone or with air, also in a d.a.f. basis, GY_{solid} (%) and $GY_{solid+air}$ (%).
- Tar generation (measured either as the tar content in the gas, in g/N m^3 (dry basis), or as the tar yield on a dry and ash free (d.a.f.) basis of the feedstock).
- Average dry gas composition (vol.% of H_2, CO, CH_4, C_2H_n and H_2S).
- Lower heating value (LHV) of the dry gas.
- Extent of gasification, expressed as carbon-to-gas efficiency, (η_C), which was calculated as the percentage of carbon in the feedstock converted into C-containing permanent gases (CO, CO_2, CH_4, C_2H_2, C_2H_4 and C_2H_6).
- The cold gas energy efficiency for gasification, η_{energ}, calculated as the ratio between the energy content of the product dry gas and the energy content of the feedstock, as shown in following equation:

$$\eta_{energ} = \frac{LHV_{gas} \cdot Y_{gas}}{LHV_{feed}} \times 100 \quad (2)$$

3. Results and discussion

Table 3 shows an overview of the experimental results obtained. At a first glance, it appears that variations of the feedstock composition produce a wide range of variation of all these parameters. For instance, and as can be observed in Table 3, tar content in the gas ranged between 5 and 65 g/N m^3, with the tar yield in a d.a.f. basis of the solid fed between 1.4% and 17.3% and gas yields between 2.4 and 3.1 N m^3/kg d.a.f. The lower heating value of the product gas ranged within 1700 and 4100 kJ/N m^3). A detailed assessment of the most relevant parameters for gasification will be presented in the following sections.

Table 4 shows the statistically significant coefficients, and their 95% confidence interval, as determined by the ANOVA analysis of the experimental results. R^2 is the multiple correlation coefficient also calculated from the ANOVA model, and R^2_{adj} is the correlation coefficient adjusted for the number of parameters in the model relative to the number of points in the experimental design. R^2 is an indicator of how well the model fits the experimental data. It can be seen that for some responses the regression coefficient is not close to 1, due to the experimental variability. Nevertheless, the statistically significant effect of mixing the three raw materials can be still observed and quantified, although a low regression coefficient means that the obtained model cannot be used for an accurate prediction of the response variables.

3.1. Gas yield

Results for the gas yield (Y_{gas}) are shown in Fig. 1. Firstly, the gas yield (measured as the volume of gas per kg of feedstock on d.a.f.) is shown in Fig. 1a. Y_{gas} is maximum for BC alone, and significantly lower for LC and SS. For bituminous coal–sewage sludge mixtures, Pinto and co-workers [15] observed a similar trend; i.e., a decrease in Y_{gas} at increasing amounts of sewage sludge. For this response variable, no interactions were observed between any of the feedstock components. Thus, Y_{gas} follows a linear relationship with each feedstock component fraction, and can be calculated directly from the feedstock composition using Eq. (1) with the corresponding β_i coefficients presented in Table 4. Nevertheless, in this case, low values of R^2 and R^2_{adj} were determined, as shown in Table 4. This poor fitting of the model limits its usefulness for prediction purposes, and is due to the influence of uncontrolled factors that also might mask some kind of interaction between the feedstock components.

The gas yield in a d.a.f. solid basis (GY_{solid}) is shown in Fig. 1b. The use of air as gasification agent causes these weight yields to be greater than 100%. Using this calculation basis, the highest gas yield is obtained from BC alone, due to the fact that higher air flows are needed with this material for a fixed stoichiometric ratio (mostly because of its higher C content). According to the obtained model, the nonlinear terms are not significant, which means that gas formation is not favoured by any feedstock mixture. Again, it should also be noticed that the experimental variability makes the R^2 value rather low.

Table 3
Experimental results (1). Tar, gas, energy and C-to-gas yields, gas LHV and average gas composition (vol.%).

Mass fraction BC/LC/SS	Tar (g/N m^3)	Tar (%)	η_C (%)	η_{energ} (%)	LHV (kJ/N m^3)	Y_{gas} (N m^3/kg)	GY_{solid} (%)	$GY_{solid+air}$ (%)	H_2	CO	CH_4	C_2H_n	H_2S
1/0/0	41.2/43.8	12.3/12.6	42.1/42.6	23.2/22.6	2293/2201	3.00/3.13	357/352	80.0/81.2	5.73/5.09	9.04/8.90	1.15/1.16	0.20/0.23	–0.01/0.04
0/1/0	58.4/64.5	15.6/15.6	47.2/46.6	20.2/22.4	1686/2070	2.67/2.42	337/298	83.6/82.8	5.44/7.50	6.01/7.84	0.80/0.60	0.09/0.10	1.00/0.82
0/0/1	38.4/64.2	10.2/17.3	79.7/79.5	47.3/51.7	4112/3949	2.65/2.69	322/328	86.8/86.6	8.24/7.56	8.52/8.14	3.13/3.14	1.75/1.67	0.10/0.11
0.5/0.5/0	41	11.7	52	22.7	2044	2.86	355	84.6	6.23	7.73	0.92	0.11	0.2
0.5/0/0.5	21.9/28.7	6.1/7.7	56.0/55.0	35.0/33.2	3191/3103	2.81/2.69	339/326	85.6/84.8	8.20/8.09	9.31/9.11	1.97/1.87	0.72/0.69	0.04/0.05
0/0.5/0.5	23.0/18.2	6.0/4.9	64.6/66.7	40.8/42.7	3293/3322	2.62/2.71	317/315	87.2/84.8	8.87/9.04	9.26/9.53	2.23/2.00	0.74/0.72	0.41/0.42
0.67/0.17/0.17	28.4	8.3	48.6	24.3	2302	2.9	359	84.7	6.41	8.25	1.13	0.29	0.07
0.17/0.67/0.17	5.2	1.4	52.7	25	2071	2.77	345	85.5	6.55	7.46	0.86	0.2	0.31
0.17/0.17/0.67	38.1	10.2	64.3	40.5	3477	2.69	325	86.5	8.81	9.32	2.15	0.99	0.14
0.41/0.41/0.18	12.5	3.1	43.3	20.5	2090	2.46	306	81.7	5.9	8.07	0.89	0.2	0.11
0.33/0.33/0.33	6.4/12.9	1.6/3.5	50.1/51.3	29.7/30.5	2882/2731	2.51/2.7	305/329	83.6/83.9	8.10/7.55	9.24/8.87	1.54/1.45	0.49/0.47	0.13/0.32
	20.5/20.7	5.4/5.5	46.9/46.4	28.4/27.9	2585/2510	2.62/2.66	319/323	81.0/80.6	6.86/6.65	9.77/9.69	1.10/1.01	0.37/0.35	0.14/0.12

Reprinted from Chemical Engineering Journal, Vol 22 (2), G. García, J. Arauzo, A. Gonzalo, J.L. Sánchez, J. Ábrego, Influence of feedstock composition in fluidised bed co-gasification of mixtures of lignite, bituminous coal and sewage sludge, 345-352, Copyright (2013), with permission from Elsevier

Table 4
ANOVA regression coefficients for the measured response variables.

Response variable	β_{BC}	β_{LC}	β_{SS}	β_{BC-LC}	β_{BC-SS}	β_{LC-SS}	$\beta_{BC-LC-SS}$	R^2/R^2_{adj}
Tar (g/N m^3)	43 ± 8	58 ± 7	54 ± 7	−80 ± 40	−90 ± 30	−150 ± 30	*	0.75/0.64
Tar yield (%)	11 ± 2	13 ± 2	15 ± 2	*	−30 ± 10	−40 ± 10	*	0.65/0.54
η_{energ} (%)	23 ± 1	21 ± 1	50 ± 1	−2 ± 7*	−7 ± 6	26 ± 6	−130 ± 40	0.98/0.97
η_C (%)	44 ± 1	47 ± 1	80 ± 1	26 ± 9	−23 ± 7	11 ± 7	−260 ± 50	0.98/0.97
LHV (kJ/N m^3)	2100 ± 90	1900 ± 100	4100 ± 100	*	*	*	*	0.94/0.93
Y_{gas} (N m^3/kg$_{daf}$)	2.96 ± 0.06	2.55 ± 0.07	2.63 ± 0.07	*	*	*	*	0.55/0.49
Gas yield (%)$_{daf\ solid}$	356 ± 7	317 ± 8	316 ± 8	*	*	*	*	0.49/0.43
Gas yield (%)$_{daf\ solid+air}$	82 ± 1	83 ± 1	87 ± 1	*	*	*	*	0.40/0.33
H_2 (%)	6.0 ± 0.4	6.2 ± 0.5	8.4 ± 0.5	*	*	5 ± 2	*	0.62/0.55
CO (%)	9.0 ± 0.3	6.7 ± 0.3	8.6 ± 0.4	*	*	7 ± 2	*	0.69/0.63
CH_4 (%)	1.1 ± 0.1	0.6 ± 0.1	3.2 ± 0.1	*	−1.6 ± 0.6	*	*	0.93/0.92
C_2H_n	0.17 ± 0.03	0.069 ± 0.04	1.73 ± 0.04		−1.1 ± 0.2	−0.8 ± 0.2	*	0.99/0.98
H_2S	0.05 ± 0.04	0.86 ± 0.05	0.06 ± 0.04	−1.3 ± 0.3				0.93/0.92

* Not significant.

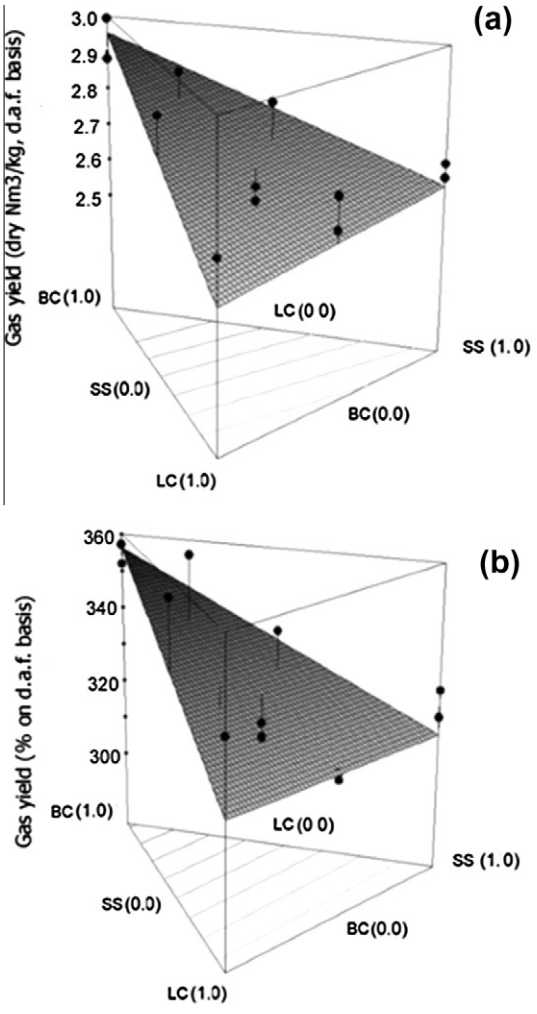

Fig. 1. Influence of feedstock composition on gas yield: (a) N m^3/kg on d.a.f. basis; (b) % on d.a.f. basis.

Calculating the gas yield on an air plus solid d.a.f. basis ($GY_{solid+air}$) can provide a more intuitive way of presenting these results. Values are smaller than 100%, and a change in the previously observed trend can be seen: as shown in Fig. 2, the highest yield corresponds to sewage sludge alone, owing to its higher volatile and ash content and lower fixed carbon content, shown in Table 1, especially if compared to bituminous coal.

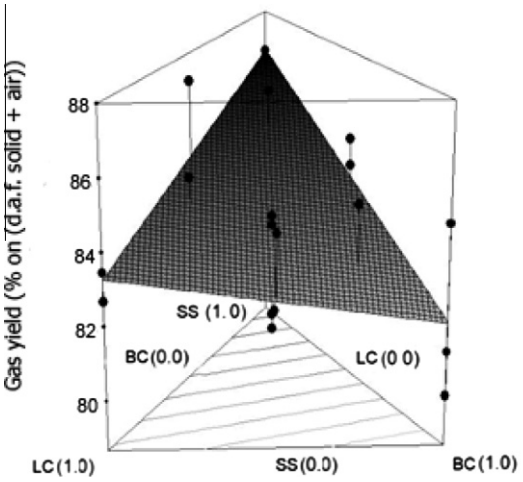

Fig. 2. Influence of feedstock composition on gas yield, % on (d.a.f. solid + air) basis.

3.2. Tar generation

Results for tar generation are shown in Fig. 3. Fig. 3a depicts the subsequent proposed model for tar content of the gas, according to the coefficients of the adjusted model shown in Table 4. Tar is the main undesirable product obtained from gasification; thus, it should be minimised. From the linear coefficients of the model, it can be seen that both lignite and sewage sludge produce more tar than bituminous coal when gasified alone.

It is interesting to notice that the three quadratic coefficients (β_{ij} at Table 3) are statistically significant and have negative sign, indicating that any binary or ternary mixture of the materials causes a decrease in tar yield, if compared to gasification of any of the raw materials alone. This antagonistic effect is presented in Fig. 3a and may be due to the different composition of the inorganics of the three feedstock materials (see Table 2). Al, Ca, Fe and Mg, among other metals, are present in different proportions in the ash of BC, LC and SS, and are widely known to have a catalytic effect towards tar abatement [29–37].

It is likely that a specific combination of these metal compounds within the fluidized bed might optimise tar cracking at these fluidization and temperature conditions. Moreover, differences in the nature of volatiles released and their subsequent gas phase reac-

Reprinted from Chemical Engineering Journal, Vol 22 (2), G. García, J. Arauzo, A. Gonzalo, J.L. Sánchez, J. Ábrego, Influence of feedstock composition in fluidised bed co-gasification of mixtures of lignite, bituminous coal and sewage sludge, 345-352, Copyright (2013), with permission from Elsevier

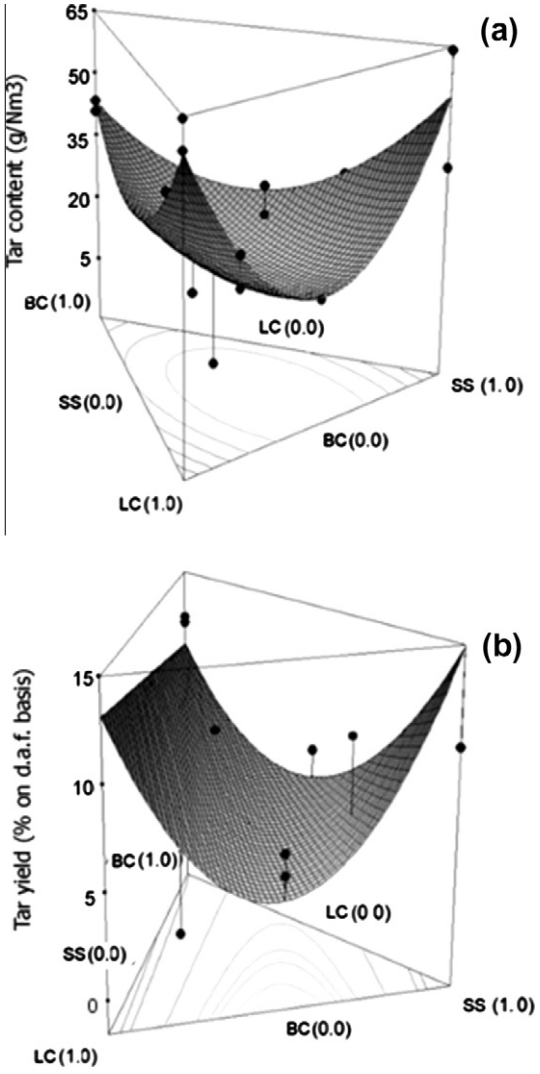

Fig. 3. Influence of feedstock composition on tar yield: (a) g/N m^3 of dry gas; (b) % on d.a.f. basis.

tions [38] may also cause different compositions of the formed tars, as pointed out by several authors for coal and wood co-gasification [39,40]. These compositional differences of tars might also enhance the catalytic action of some of the metals present in the ashes. Unfortunately, no further analyses of tar composition were done in this study.

Tar yield can also be measured as the weight percentage of feedstock that goes to tar on a dry and ash free basis, as shown in Fig. 3b. This measure seems more convenient for comparison, since it represents the fraction of organic matter converted into tar regardless of the amount of gas formed. As can be seen, there is a quadratic effect caused by the mixtures of SS–LC and SS–BC, whereas the LC–BC mixture is merely linear. The observed antagonistic response (excluding the LC–BC linear behaviour) is similar to that previously shown for tar content in the gas (g/N m^3), decreasing the tar concentration.

3.3. Average composition of the dry gas

The influence of the feedstock composition on the average content (% by volume) of the main combustible gas components (H_2, CO, CH_4, C_2H_n), as well as H_2S (an important gaseous pollutant), is presented in this section.

The volume percent (on a dry gas basis) of each one of the main combustible gases are shown in Fig. 4. For instance, the average volume% of H_2 in the dry gas is shown in Fig. 4a. In this work, H_2 changed within the range 5–9%. Paterson and co-workers [22] found somewhat higher concentrations of H_2 and CO, probably because or the use of air/steam mixtures, similarly to the results by Pinto et al. [15]. Wang and Xiao [17] also obtained higher concentrations of these two gases as a result of co-gasifying sewage sludge with high moisture content.

It can be seen that the mixtures of LC–BC and SS–BC can be described by a linear combination of the H_2 % produced in the gasification of those materials alone, whereas the SS–LC mixtures show a maximum evidencing a synergistic effect. Unlike our results, Pinto et al. [15] observed a decrease in H_2 concentration with a rise in the sludge content of the feedstock, which could be attributed to the addition of steam.

CO contents range between 6% and 10%, as shown in Fig. 4b. The same trend than for H_2 is found: a synergistic effect of feeding SS–LC mixtures and linear effects for the rest of binary mixtures.

However, methane shows a slightly different behaviour: for this gas there is an antagonistic (although quantitatively weak) effect between BC–SS, as shown in Fig. 4c.

Regarding C_2 hydrocarbons, there is also an antagonistic effect caused by the mixture of sewage sludge with any of the two coals, similarly to the previously shown results for tar generation. The antagonistic effects mentioned for CH_4 and C_2 hydrocarbons are statistically significant although not very important, as can be inferred from the slight curvature shown in Fig. 4d and from the low values of the quadratic terms calculated with the ANOVA analysis (Table 4).

Both CH_4 and C_2 hydrocarbons increase with increasing amounts of sewage sludge in the feedstock mixture, as previously noted by Pinto et al. [15], who attributed this fact to the rapid release of volatiles that do not crack substantially due to short residence times in the bed.

Finally, results for H_2S are presented in Fig. 5. The antagonistic effect is created by the combination of both coals, but not with sewage sludge. Additionally, and due to the very high sulphur content of lignite, the formation of this gas is maximum for this individual feedstock. In contrast, the H_2S contents are much lower for BS and SS as individual feedstock. Moreover, both materials produce very similar H_2S concentrations in the product gas, due to their almost identical S content, as shown in Table 1.

3.4. Lower heating value of the gas

As observed from Fig. 6 and from the significant coefficients in Table 4, the lower heating value (LHV, on a dry basis) of the produced gas can be simply calculated by averaging the LHV contribution of each one of the single components in the feedstock, being the quadratic and cubic effects from the composition not significant.

The gas produced by gasification of sewage sludge has a noticeably higher LHV than the produced in the gasification of any of the coals tested. This could be related to the increased release of methane and light hydrocarbons with higher sewage sludge contents, as previously mentioned.

3.5. Carbon-to-gas (η_C) and cold gas energy (η_{energ}) efficiencies

The carbon-to-gas efficiency, η_C, has been calculated from the gas composition and production, as a way to compute the gasification conversion. As shown in Fig. 7a and b, it is clear that the obtained models for carbon-to-gas conversion and cold gas efficiency are almost identical in shape, as could be expected since both parameters measure the conversion towards gas. In both

Reprinted from Chemical Engineering Journal, Vol 22 (2), G. García, J. Arauzo, A. Gonzalo, J.L. Sánchez, J. Ábrego, Influence of feedstock composition in fluidised bed co-gasification of mixtures of lignite, bituminous coal and sewage sludge, 345-352, Copyright (2013), with permission from Elsevier

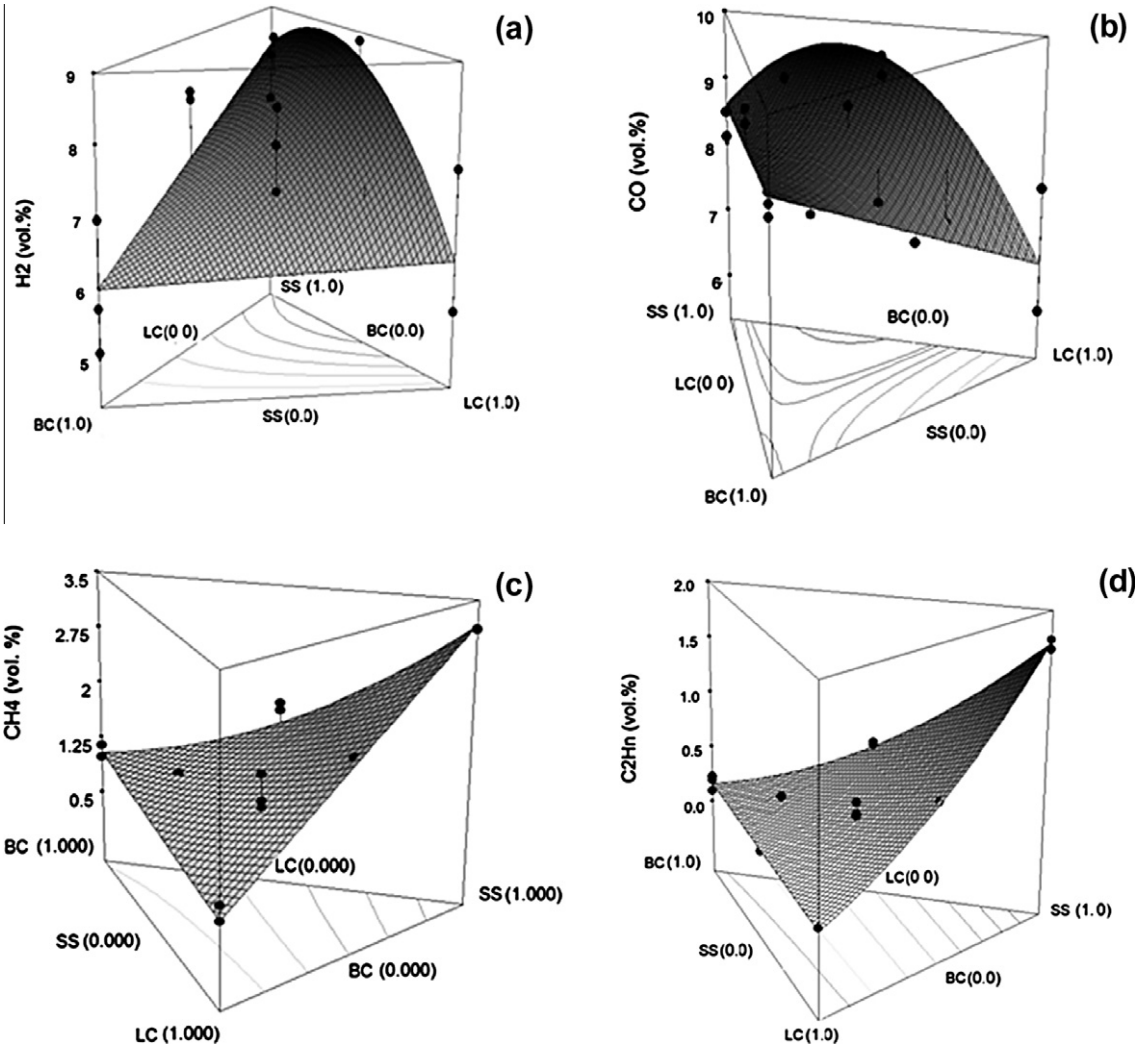

Fig. 4. Influence of feedstock composition on gas composition, vol.%: (a) H_2; (b) CO; (c) CH_4; (d) C_2H_n.

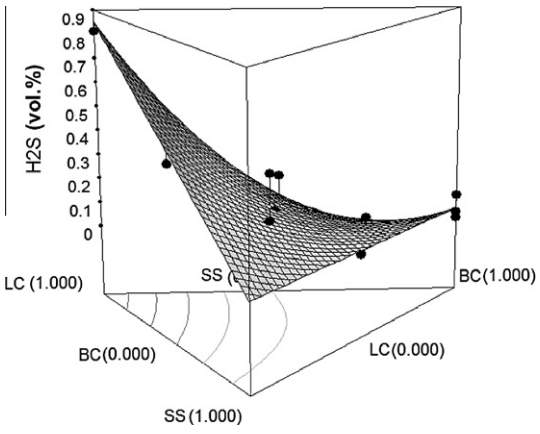

Fig. 5. Influence of feedstock composition on H_2S content (vol.%).

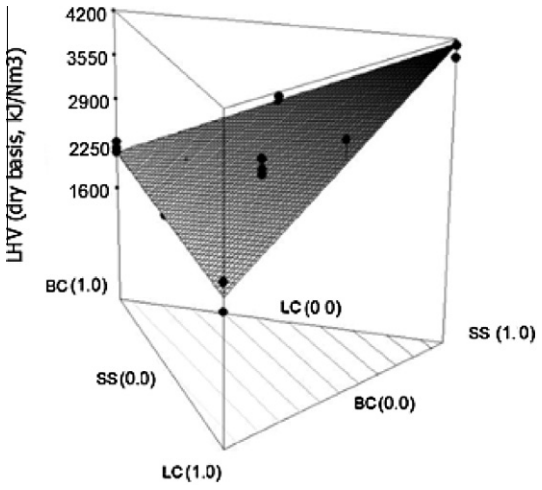

Fig. 6. Influence of feedstock composition on the lower heating value of gas (dry basis).

models, it is shown that sewage sludge exhibits the higher conversion towards gas, whereas the two coals have lower conversions. This fact agrees with the work of Pinto et al. [15] and Paterson et al. [22]. In the case of sludge alone, approximately 80% of the original C content can be converted into permanent gases [33] in the conditions used in this work. Comparing to values reported by Paterson et al. [22], carbon-to-gas and cold gas efficiencies are rather low, which can be explained by the use of an air/steam mixtures as gasifying agent in the mentioned work.

Reprinted from Chemical Engineering Journal, Vol 22 (2), G. García, J. Arauzo, A. Gonzalo, J.L. Sánchez, J. Ábrego, Influence of feedstock composition in fluidised bed co-gasification of mixtures of lignite, bituminous coal and sewage sludge, 345-352, Copyright (2013), with permission from Elsevier

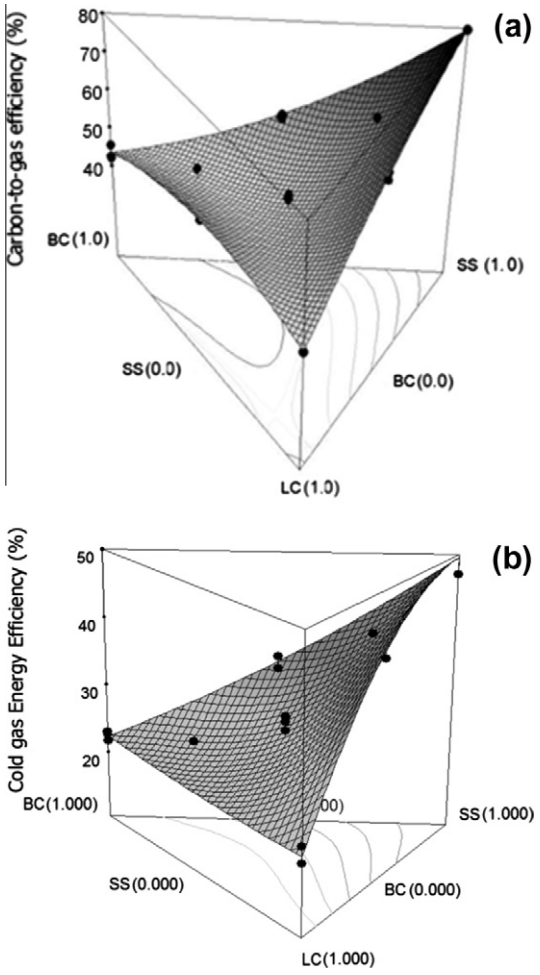

Fig. 7. Influence of feedstock composition on gasification efficiencies: (a) carbon-to-gas efficiency; (b) cold gas efficiency.

From the regression coefficients shown in Table 4, it can be observed that the highest gas energy efficiencies (up to 50%) are obtained when SS alone or sludge-enriched mixtures are used. This fact could be due to the higher volatile (and lower fixed carbon) content of sludge compared to the coals used. Accordingly, BC and LC show low cold gas efficiencies (and also tar production, as shown in Fig. 3). As a consequence, chars produced from BC and LC still have high organic (mainly carbon) contents. Results from a previous work [24] (carried out in the same experimental facility, with the same raw materials and at similar operating conditions) showed that the carbon content of chars from gasification were 47% for BC, 25% for LC and 14% for SS.

Fig. 7b showing the results of the ANOVA model for cold gas efficiency, depicts a rather flat surface. Thus, there are no relevant synergistic effects when using any mixture of the three raw materials, despite the statistical significance of the parameters shown in Table 4.

4. Conclusions

In this work, the influence on several gasification parameters of mixing two types of coal (bituminous and lignite) with sewage sludge was studied with the help of a mixture design. Many of the observed effects on the gasification performance can be simply described as a linear combination of the individual contributions by each feedstock component; however, some synergistic or antagonistic effects were also found. For instance, a noteworthy reduction on tar generation was found when mixtures of coal and sewage sludge were gasified. The type of coal had a minor influence on this reduction. This fact might be due to the combined catalytic effect of the inorganics coming from coals and sludge.

Regarding gas composition, the main combustible components of the gas (H_2 and CO, in vol.%) were increased with increasing contents of sewage sludge, with a synergistic effect from lignite-sewage sludge mixtures that caused maximum concentrations of both gaseous products. Methane and C_2 hydrocarbons also increased with increasing contents of sewage sludge.

The positive effect of adding sewage sludge was also evidenced on the gas lower heating value, carbon-to-gas conversion and gas energy efficiencies.

According to these results, co-gasification of coals and sewage sludge might improve the overall process performance at the operational conditions tested in this work.

Appendix A. Supplementary material

Supplementary data associated with this article can be found, in the online version, at http://dx.doi.org/10.1016/j.cej.2013.02.073.

References

[1] A. Kelessidis, A.S. Stasinakis, Comparative study of the methods used for treatment and final disposal of sewage sludge in European countries, Waste Manage. (Oxford) 32 (2012) 1186–1195.
[2] P. Manara, A. Zabaniotou, Towards sewage sludge based biofuels via thermochemical conversion – a review, Renew. Sust. Energy Rev. 16 (2012) 2566–2582.
[3] I. Fonts, G. Gea, M. Azuara, J. Ábrego, J. Arauzo, Sewage sludge pyrolysis for liquid production: a review, Renew. Sust. Energy Rev. 16 (2012) 2781–2805.
[4] J. Werther, T. Ogada, Sewage sludge combustion, Prog. Energy Combust. 25 (1999) 55–116.
[5] M.B. Folgueras, R.M. Díaz, J. Xiberta, I. Prieto, Thermogravimetric analysis of the co-combustion of coal and sewage sludge, Fuel 82 (2003) 2051–2055.
[6] M. Otero, X. Gómez, A.I. García, A. Morán, Effects of sewage sludge blending on the coal combustion: a thermogravimetric assessment, Chemosphere 69 (2007) 1740–1750.
[7] B. Wang, R. Yan, H. Zhao, Y. Zheng, Z. Liu, C. Zheng, Investigation of chemical looping combustion of coal with $CuFe_2O_4$ oxygen carrier, Energy Fuel. 25 (2011) 3344–3354.
[8] T. Kupka, M. Mancini, M. Irmer, R. Weber, Investigation of ash deposit formation during co-firing of coal with sewage sludge, saw-dust and refuse derived fuel, Fuel 87 (2008) 2824–2837.
[9] S. Stelmach, R. Wasielewski, Co-combustion of dried sewage sludge and coal in a pulverized coal boiler, J. Mater. Cycles Waste Manage. 10 (2008) 110–115.
[10] W.P. Barber, Potential for sewage sludge co-combustion in the UK based on German experience, Water Environ. J. 16 (2002) 270–276.
[11] A.-L. Elled, L.-E. Åmand, B. Leckner, B.-Å. Andersson, The fate of trace elements in fluidised bed combustion of sewage sludge and wood, Fuel 86 (2007) 843–852.
[12] M.B. Folgueras, R. María Díaz, J. Xiberta, Sulphur retention during co-combustion of coal and sewage sludge, Fuel 83 (2004) 1315–1322.
[13] M.B. Folgueras, R.M. Díaz, J. Xiberta, M. Alonso, Effect of inorganic matter on trace element behavior during combustion of coal–sewage sludge blends, Energy Fuel. 21 (2007) 744–755.
[14] H. Lopes, F. Pinto, A.T. Crujeira, R. André, M. Dias, I. Gulyurtlu, et al., Environmental impact of sewage sludge co-gasification with coal, in: Volume 2: Aircraft Engine; Ceramics; Coal, Biomass and Alternative Fuels; Controls, Diagnostics and Instrumentation; Environmental and Regulatory Affairs, ASME, 2006: pp. 401–408.
[15] F. Pinto, H. Lopes, R.N. André, M. Dias, I. Gulyurtlu, I. Cabrita, Effect of experimental conditions on gas quality and solids produced by sewage sludge cogasification. 1. Sewage sludge mixed with coal, Energy Fuel 21 (2007) 2737–2745.
[16] F. Pinto, R.N. André, H. Lopes, M. Dias, I. Gulyurtlu, I. Cabrita, Effect of Experimental conditions on gas quality and solids produced by sewage sludge cogasification. 2. Sewage sludge mixed with biomass, Energy Fuel 22 (2008) 2314–2325.
[17] X. Wang, Y. Xiao, Analysis of sludge and coal co-gasification power plant, in: ASME Turbo Expo 2004: Power for Land, Sea, and Air, Vienna (Austria), 2004, pp. 131–139.
[18] Q. Zhang, H. Liu, W. Li, J. Xu, Q. Liang, Behavior of phosphorus during co-gasification of sewage sludge and coal, Energy Fuel. (2012). 120412125009002..

Reprinted from Chemical Engineering Journal, Vol 22 (2), G. García, J. Arauzo, A. Gonzalo, J.L. Sánchez, J. Ábrego, Influence of feedstock composition in fluidised bed co-gasification of mixtures of lignite, bituminous coal and sewage sludge, 345-352, Copyright (2013), with permission from Elsevier

[19] G.P. Reed, D.R. Dugwell, R. Kandiyoti, Control of trace elements in gasification: distribution to the output streams of a pilot scale gasifier, Energy Fuel. 15 (2001) 794–800.
[20] N. Paterson, Y. Zhuo, D. Dugwell, R. Kandiyoti, Formation of hydrogen cyanide and ammonia during the gasification of sewage sludge and bituminous coal, Energy Fuel. 73 (2005) 1016–1022.
[21] A. Cousins, Y. Zhuo, A. George, N. Paterson, D.R. Dugwell, R. Kandiyoti, Development of a bench-scale high-pressure fluidized bed reactor and its sequential modification for studying diverse aspects of pyrolysis and gasification of coal and biomass, Energy Fuel. 22 (2008) 2491–2503.
[22] N. Paterson, G.P. Reed, D.R. Dugwell, R. Kandiyoti, Gasification tests with sewage sludge and coal/sewage sludge mixtures in a pilot scale, air blown, spouted bed gasifier, in: Volume 1: Turbo Expo 2002, ASME, 2002: pp. 197–202.
[23] A.B. Hernandez, J.H. Ferrasse, P. Chaurand, H. Saveyn, D. Borschneck, N. Roche, Mineralogy and leachability of gasified sewage sludge solid residues, J. Hazard M. 191 (2011) 219–227.
[24] G. García, E. Cascarosa, J. Ábrego, A. Gonzalo, J.L. Sánchez, Use of different residues for high temperature desulphurisation of gasification gas, Chem. Eng. J. 174 (2011) 644–651.
[25] M. Seggiani, Empirical correlations of the ash fusion temperatures and temperature of critical viscosity for coal and biomass ashes, Fuel 78 (1999) 1121–1125.
[26] G. García, E. Cascarosa, J.L. Sánchez, Analysis of catalytic co-gasification of two types of coal with sewage sludge and olive bagasse, in: Proceedings of the 17th European Biomass Conference and Exhibition, Hamburg, Germany, 2009, pp. 721–724.
[27] J.A. Cornell, Experiments with Mixtures: Designs, Models, and the Analysis of Mixture Data, 3rd ed., Wiley, New York, 2002.
[28] G.F. Piepel, J.A. Cornell, Mixture experiment approaches: examples, discussion, and recommendations, J. Qual. Technol. 26 (1994) 177–196.
[29] S.-P. Hong, J.-I. Dong, S.-K. Yeo, I.-H. Park, M.-S. Chung, D.-I. Kim, et al., Reduction of tar using cheap catalysts during sewage sludge gasification, J. Mater. Cycles Waste Manage. 13 (2011) 186–189.
[30] J.N. Kuhn, Z. Zhao, L.G. Felix, R.B. Slimane, C.W. Choi, U.S. Ozkan, Olivine catalysts for methane- and tar-steam reforming, Appl. Catal. B-Environ. 81 (2008) 14–26.
[31] S. Rapagnà, K. Gallucci, M. Di Marcello, M. Matt, P.U. Foscolo, Improvement of gas yield from biomass gasification by using Fe/olivine as gasifier bed inventory, Chem. Eng. Trans. 21 (2010) 415–420.
[32] M. Azhar Uddin, H. Tsuda, S. Wu, E. Sasaoka, Catalytic decomposition of biomass tars with iron oxide catalysts, Fuel 87 (2008) 451–459.
[33] M. Virginie, C. Courson, D. Niznansky, N. Chaoui, A. Kiennemann, Characterization and reactivity in toluene reforming of a Fe/olivine catalyst designed for gas cleanup in biomass gasification, Appl. Catal. B-Environ. 101 (2010) 90–100.
[34] L. Di Felice, C. Courson, D. Niznansky, P.U. Foscolo, A. Kiennemann, Biomass gasification with catalytic tar reforming: a model study into activity enhancement of calcium- and magnesium-oxide-based catalytic materials by incorporation of Iron, Energy Fuel 24 (2010) 4034–4045.
[35] J.M. de Andrés, A. Narros, M.E. Rodríguez, Behaviour of dolomite, olivine and alumina as primary catalysts in air–steam gasification of sewage sludge, Fuel 90 (2011) 521–527.
[36] Y. Sun, J. Jiang, E. Kantarelis, J. Xu, L. Li, S. Zhao, et al., Development of a bimetallic dolomite based tar cracking catalyst, Catal. Commun. 20 (2012) 36–40.
[37] J.J. Manyà, J.L. Sánchez, A. Gonzalo, J. Arauzo, Air gasification of dried sewage sludge in a fluidized bed: effect of the operating conditions and in-bed use of alumina, Energy Fuel. 19 (2005) 629–636.
[38] F. Pinto, C. Franco, H. Lopes, R.N. André, I. Gulyurtlu, I. Cabrita, et al., Effect of used edible oils in coal fluidised bed gasification, Fuel 84 (2005) 2236–2247.
[39] I. Aigner, C. Pfeifer, H. Hofbauer, Co-gasification of coal and wood in a dual fluidized bed gasifier, Fuel 90 (2011) 2404–2412.
[40] K. Kumabe, T. Hanaoka, S. Fujimoto, T. Minowa, K. Sakanishi, Co-gasification of woody biomass and coal with air and steam, Fuel 86 (2007) 684–689.

Reprinted from Chemical Engineering Journal, 174, G. García, E. Cascarosa, J. Ábrego, A. Gonzalo, J.L. Sánchez, Use of different residues for high temperature desulphurisation of gasification gas, 644– 651, Copyright (2011), with permission from Elsevier

Chemical Engineering Journal 174 (2011) 644–651

Contents lists available at SciVerse ScienceDirect

Chemical Engineering Journal

journal homepage: www.elsevier.com/locate/cej

Use of different residues for high temperature desulphurisation of gasification gas

G. García[a], E. Cascarosa[b], J. Ábrego[c], A. Gonzalo[b], J.L. Sánchez[b,*]

[a] Aema Servicios, Pol. Ind. El Pilar, C/Fitero 9, E-26540 Alfaro, Spain
[b] Thermo-chemical Processes Group, Aragón Institute of Engineering Research (I3A), I+D building, University of Zaragoza, c/Mariano Esquillor s/n, E-50018, Zaragoza, Spain
[c] Instituto de Carboquímica (CSIC), c/Miguel Luesma Castán, 4, E-50018, Zaragoza, Spain

ARTICLE INFO

Article history:
Received 11 May 2011
Received in revised form
15 September 2011
Accepted 17 September 2011

Keywords:
H_2S removal
Gasification
Sewage sludge
Coal
Hot gas cleaning

ABSTRACT

H_2S is an important constraint for the final use of gas from coal or biomass gasification. Its content varies depending on the sulphur present in the feedstock raw material. In parallel, char and ash from biomass and coal gasification or combustion usually have significant amounts of metals, some of which have shown activity towards H_2S abatement. Thus, these materials could be a feasible and cheap alternative for H_2S removal, as they are generated inside the gasification process. This work evaluates the feasibility of using ash and char from several materials (lignite, bituminous coal and sewage sludge) for H_2S removal. Experiments were carried out in a fixed bed reactor at 700–900 °C, using a synthetic gas with 0.5 vol.% of H_2S (similar to that obtained by air gasification of sewage sludge).

The highest H_2S removal was achieved using lignite ash (at all temperatures) and bituminous coal (at $T > 700$ °C), obtaining, in these conditions, an outlet gas with less than 0.05 vol.% H_2S after 2 h of experiment.

© 2011 Elsevier B.V. All rights reserved.

1. Introduction

Gasification is a thermochemical process that can transform a carbonaceous feedstock – such as biomass or coal – into a fuel gas containing mainly hydrogen, carbon monoxide and methane. However, this gas mixture may also contain several impurities that can significantly restrict the final use of the produced gas, and thus additional steps of gas cleaning may be required. Hydrogen sulphide is one of these contaminants. It is produced after gasification of sulphur-containing raw materials; for instance, several types of coal and biomass [1]. The amount of H_2S emissions depends both on the S content in the solid feedstock and on several experimental conditions [2]. A typical fuel gas obtained from coal gasification may contain 0.1–1.5 vol.% H_2S, whereas the values produced in wood gasification may be as low as 0.01 vol.% H_2S [2,3].

H_2S removal is critical for the success of gasification technologies. It is needed to avoid environmental problems such as global warming or acid rain [4], but also because of operational problems like corrosion in pipes, turbines or other equipment. Additionally, if H_2S is present in the gasification gas, the use of a Ni-based catalyst for tar cracking and gas reforming is not advisable because this gas deactivates the Ni catalyst [5,6] by NiS formation.

H_2S removal may be achieved by low temperature processes, such as wet scrubbing with selected solvents, or by high temperature processes, which are advantageous in terms of energy recovery (they do not require gas cooling) and may be applied *in situ* (inside the fluidised bed) or after the bed as a downstream operation. High temperature processes have been recently reviewed by Meng et al. [3]. Although several metallic compounds have been tested (Zn, Mn, Cu and Fe), calcium compounds are still the most widely used sorbents for hot gas desulphurisation in gasification and co-gasification processes [7–9]. Among calcium containing compounds, the most effective seems to be dolomite, which can reach desulphurisation efficiencies of up to 90% [2,10].

Some authors have used a bed of dolomite to avoid Ni catalyst deactivation prior to cracking and reforming stages, with promising results [1,4,11].

Carbonaceous by-products from pyrolysis and gasification processes (namely chars) have also been used as desulphurisation agents in lab-scale tests. Their desulphurisation capacity is due to their specific surface and their catalytic metallic content [12–14]. Ash is also a solid by-product of combustion; albeit its low carbon content and surface area, it usually contains iron and calcium compounds that may be able to interact with H_2S at high operational temperatures [2].

The application of both materials – chars and ashes – for H_2S removal in gasification processes may be very attractive due to its low cost. Manyà et al. [15] described the catalytic effect of sewage sludge ash in the air gasification process of sewage sludge; however, it is difficult to find research works that deal specifically with the use of char or ashes in high-temperature desulphurisation processes. Thus, the main objective of this preliminary work was to study the high-temperature desulphurisation ability of several solid materials (chars and ashes) coming from gasification or

* Corresponding author. Tel.: +34 976762962; fax: +34 976761879.
E-mail address: jlsance@unizar.es (J.L. Sánchez).

1385-8947/$ – see front matter © 2011 Elsevier B.V. All rights reserved.
doi:10.1016/j.cej.2011.09.085

Reprinted from Chemical Engineering Journal, Vol 22 (2), G. García, J. Arauzo, A. Gonzalo, J.L. Sánchez, J. Ábrego, Influence of feedstock composition in fluidised bed co-gasification of mixtures of lignite, bituminous coal and sewage sludge, 345-352, Copyright (2013), with permission from Elsevier

Table 1
Synthetic gas composition.

Component	vol.%
H_2	10.0
N_2	58.6
CH_4	4.0
CO	10.0
CO_2	15.0
C_2H_4	1.5
C_2H_6	0.2
C_2H_2	0.2
H_2S	0.5

combustion of three raw materials: sewage sludge, bituminous coal and lignite. Their H_2S removal efficiencies were evaluated and compared to a commercial grade calcined dolomite, used as reference material. Desulphurisation tests were carried out in a lab-scale fixed bed reactor, using a dry synthetic gas with a similar composition to the one obtained in sewage sludge gasification, with a H_2S content of 0.5% by volume.

2. Material and methods

Table 1 shows the composition of the synthetic gas used in this study. As said before, is similar to the dry gas obtained from air gasification of sewage sludge [15]. No water was added in this preliminary study, although it is also a very significant product of gasification. Thus, it must be noticed that additional interactions (which are beyond the scope of this work) may exist if water is present in the product gas. These interactions were pointed out by Seredych and Bandosz, who studied H_2S removal from digester gas or air [16] at low temperatures. According to the mentioned work, the presence of water has opposite effects: it improves the desulphurisation efficiency when it is adsorbed on the material surface, while can negatively affect desulphurisation due to the deactivation of basic sites on the surface. At high temperatures, the effect of steam is strongly dependent on the active metal, but desulphurisation capacity is generally reduced when water is present, as reported by Meng et al. in their review [3].

The raw materials used to obtain char and ash were bituminous coal, a Spanish lignite and sewage sludge from an urban wastewater treatment plant in Spain. Proximate and ultimate analyses of raw materials are shown in Table 2. As said before, calcined dolomite at 800 °C was also selected as a reference material, due to its well-known performance for this application [17].

Chars from lignite (LC), bituminous coal (CC) and sewage sludge (SSC) were obtained in the fluidized bed reactor depicted in Fig. 1, after gasification [18]. The bed temperature for the gasification experiments was 850 °C, with $V_f/V_{mf} = 5$ (ratio between actual and minimum fluidization velocity), and an equivalence ratio ER = 0.3 (ratio between actual oxygen used for gasification and stoichiometric oxygen for a complete combustion). Ultimate analysis, ash content and BET surface of the chars are shown in Table 3.

Table 2
Ultimate and proximate analyses of raw materials.

	Analysis method	Bituminous coal	Lignite coal	Sewage sludge
Proximate analysis				
Moisture (wt.%)	ISO-579-1981	3.7	12.1	7.1
Ash (wt.%)	ISO-1171-1976	14.8	28.6	41.0
Volatile (wt.%)	ISO-5623-1974	26.1	28.3	46.6
Fixed carbon (wt.%)		55.4	31.0	5.3
Ultimate analysis				
C (wt.%)	Carlo Erba 1108	67.6	40.9	27.7
H (wt.%)	Carlo Erba 1108	3.8	3.4	4.4
N (wt.%)	Carlo Erba 1108	1.9	0.5	3.9
S (wt.%)	Carlo Erba 1108	0.7	6.6	0.8

Table 3
Ultimate analyses, ash content and BET surface of the used chars.

	CC	LC	SSC
C (wt.%)	46.8	25.2	13.8
H (wt.%)	0.5	0.6	0.2
N (wt.%)	1.4	0.2	0.7
S (wt.%)	0.5	5.7	0.7
Ash (wt.%)	43.6	67.3	83.0
BET (m^2/g)	244.7	173.8	59.1

Ash was obtained from the raw materials according to standard method UNE 32-004-84. Ash composition was analysed by Inductively Coupled Plasma-Optical Emission Spectroscopy (ICP-OES). Table 4 shows the composition and BET surface of coal (CA), lignite (LA) and sewage sludge (SSA) ash as well as of the dolomite used.

A schematic diagram of the installation that was used for the desulphurisation study is shown in Fig. 2. Experiments were performed in a tubular fixed bed reactor made of quartz, of 0.012 m i.d. and 0.40 m in length that enabled a continuous flow of the gas through a batch of solid material.

The solids (1 g for each experiment) were placed inside the reactor on a fiberglass bed located 0.185 m from the top. The system was electrically heated to the final temperature (700, 800 or 900 °C) while nitrogen was flushed through the system to ensure inert atmosphere and thus to avoid char oxidation. Once the desired temperature was reached, the H_2S-containing gas was introduced, with a flowrate of 0.05 l_{SPT}/min (where SPT means standard temperature and pressure at 0 °C and 1 atm) regulated by a previously calibrated mass flow controller. The weight hourly space velocity (WHSV) during the experiments was set at 3.6 h^{-1}. After the reactor, gas composition was determined semi-continuously by means of an Agilent Micro-GC 3000.

Only single desulphurisation tests were done; thus, the recovery of these waste materials has not been considered in this study, although it might be possible to re-utilize them in multiple cycles.

Blank runs (without any bed material) were carried out at each temperature in order to avoid any side effect of the experimental system in the desulphurisation process. Although partial gasification of organic carbon in the used chars might take place at such high temperatures, its effect has not been analysed in this paper.

3. Results and discussion

Fig. 3 shows the calculated flow rates of sulphur (mg/min) at the outlet of the reactor, for all the temperatures and materials tested. The use of chars for desulphurisation did not render good results: only LC at 700 °C (Fig. 3a) produces a gas essentially free of H_2S for

Table 4
Ash and dolomite composition and BET surface.

Component	CA (wt.%)	LA (wt.%)	SSA (wt.%)	Dolomite (wt.%)
Al_2O_3	27.97	25.07	21.57	0.09
CaO	7.21	3.40	23.14	30.34
Fe_2O_3	2.71	28.04	8.56	0.01
K_2O	0.74	1.34	3.66	N.A.
MgO	1.33	1.07	5.93	20.63
Na_2O	0.35	0.16	1.37	N.A.
SiO_2	47.50	37.88	34.51	N.A.
TiO_2	1.49	0.73	1.25	N.A.
CO_2	N.A.	N.A.	N.A.	48.93
BET (m^2/g)	5.0	13.0	5.8	18.8

N.A.: not analysed.

Reprinted from Chemical Engineering Journal, Vol 22 (2), G. García, J. Arauzo, A. Gonzalo, J.L. Sánchez, J. Ábrego, Influence of feedstock composition in fluidised bed co-gasification of mixtures of lignite, bituminous coal and sewage sludge, 345-352, Copyright (2013), with permission from Elsevier

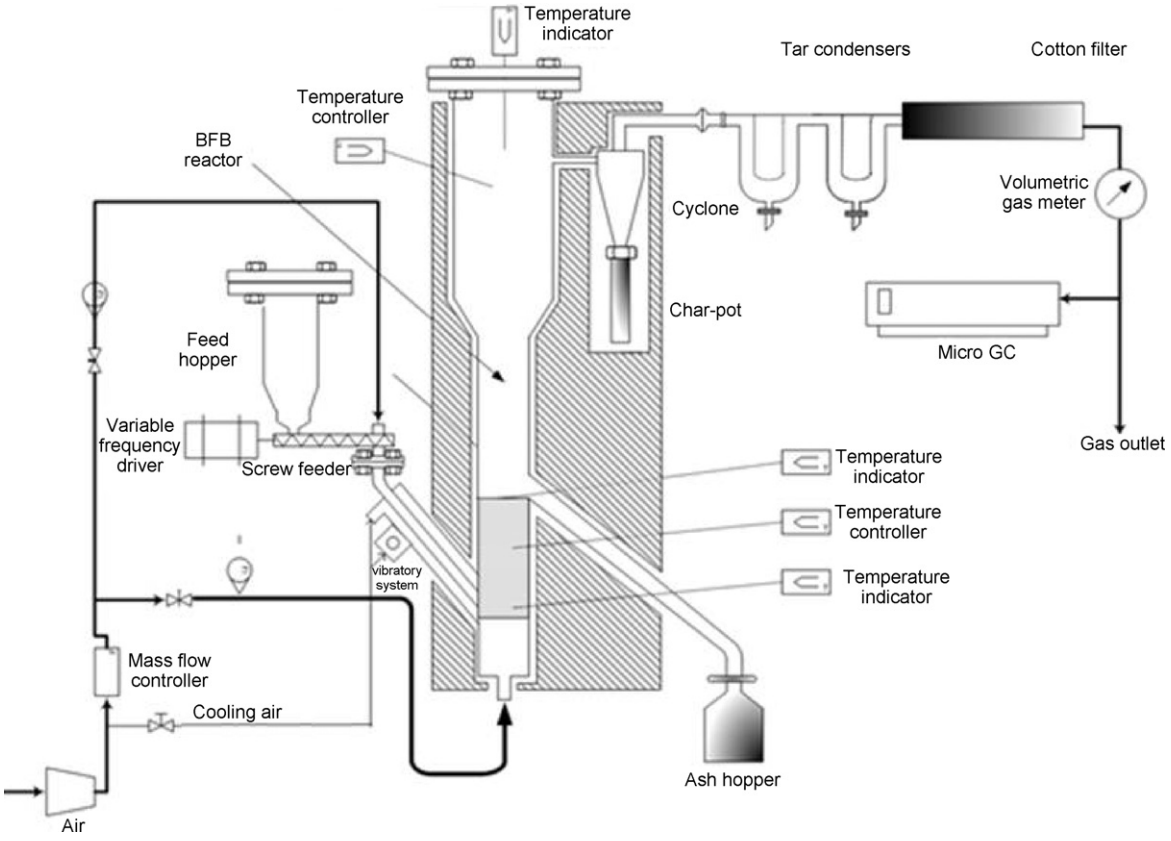

Fig. 1. Fluidised bed reactor used for char production.

less than 20 min, whereas at higher temperatures (Fig. 3c and e), H_2S is released from the beginning of the experiment. The use of ash from bituminous coal or lignite at 700 °C (Fig. 3b), 800 °C (Fig. 3d) and 900 °C (Fig. 3f), improves H_2S retention at all temperatures, compared with chars. In contrast, SSA presents the worst results for sulphur removal: after a few minutes of experiment (or right from the beginning in the case of 900 °C), the outlet gas contains a very noticeable amount of S. As can be observed in Fig. 3b, CA at 700 °C is only is able to retain H_2S for about 80 min in the conditions tested. Using CA over 700 °C, or LA at any temperature, yields higher H_2S retentions with outlet H_2S concentrations of less than 0.05 vol.%. Additionally from Fig. 3, and regarding the blank runs, it can be seen that the higher the temperature, the lower the sulphur flow rate at the outlet.

3.1. Desulphurisation with char

The extent of H_2S removal (expressed as percentage of H_2S removed from the gas) is shown in Fig. 4 for CC (Fig. 4a), LC (Fig. 4b) and SSC (Fig. 4c) at the three temperatures tested. These values have been calculated using data from the blank experiments at the same temperature as a reference, see Eq. (1):

$$\text{S removal efficiency} = \frac{D_b - D_e}{D_b} \times 100 \quad (1)$$

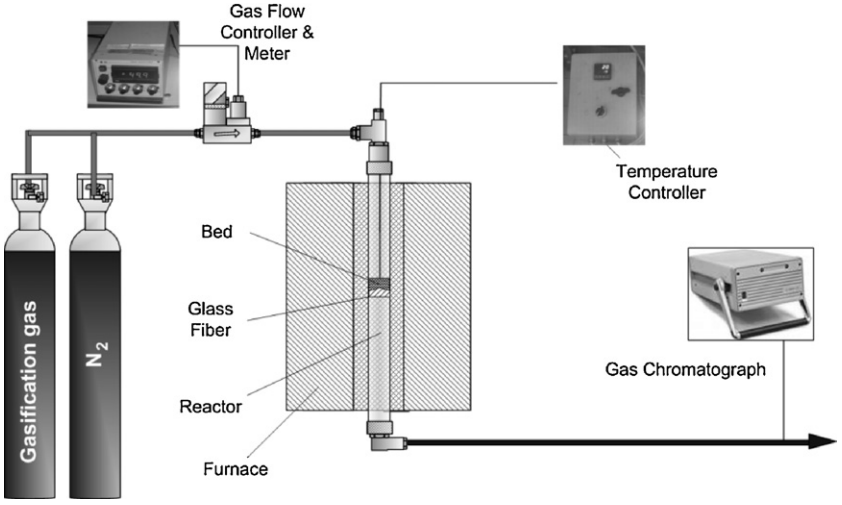

Fig. 2. Fixed bed reactor used in the desulphurisation experiments.

Reprinted from Chemical Engineering Journal, Vol 22 (2), G. García, J. Arauzo, A. Gonzalo, J.L. Sánchez, J. Ábrego, Influence of feedstock composition in fluidised bed co-gasification of mixtures of lignite, bituminous coal and sewage sludge, 345-352, Copyright (2013), with permission from Elsevier

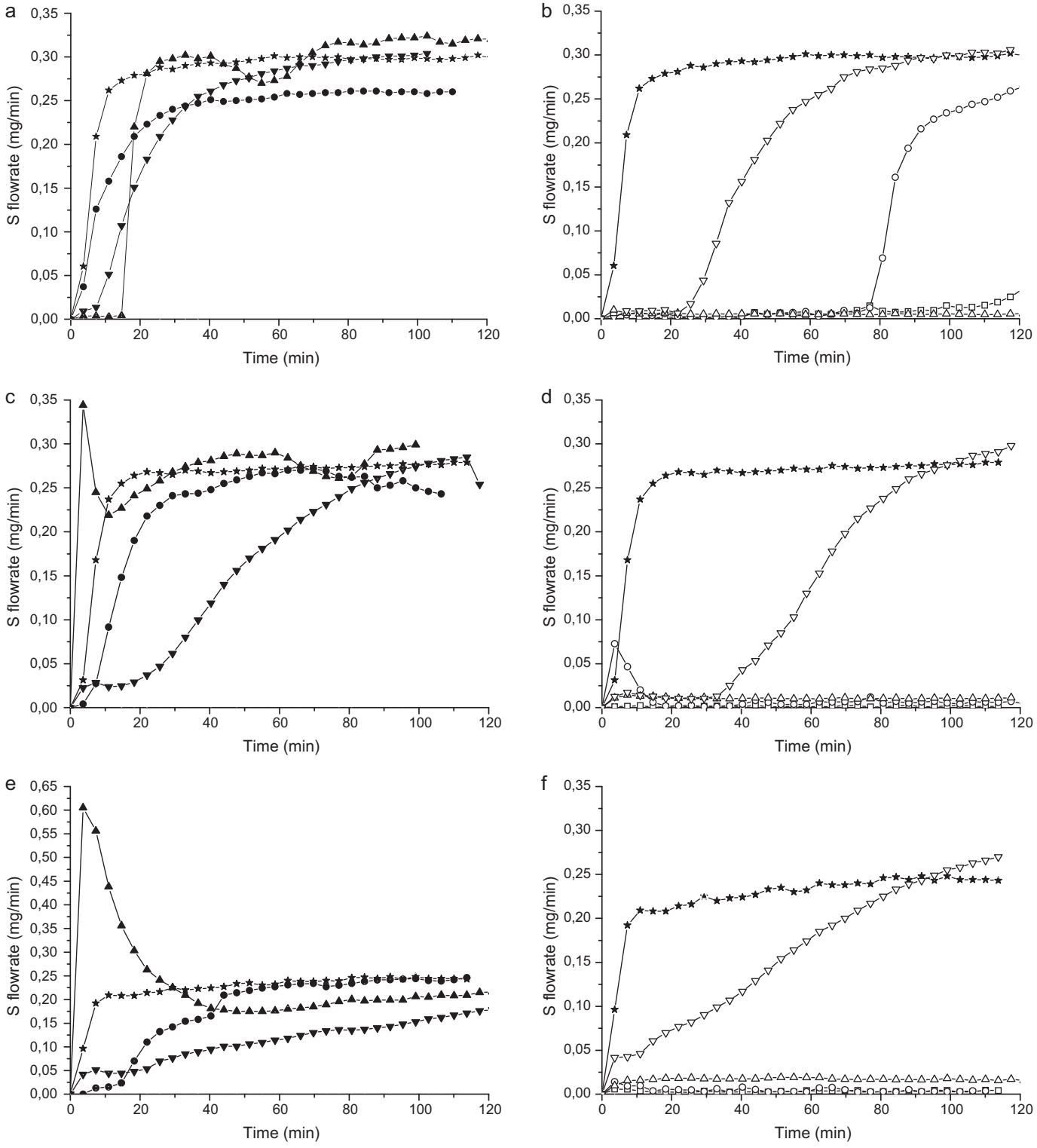

Fig. 3. S flowrate at 700 °C (a and b), 800 °C (c and d), and 900 °C (e and f). ⋆ Blank run, ● CC, ○ CA, ▲ LC, △LA, ▼ SSC, ▽ SSA, □ calcined dolomite.

being D_b the H_2S values from the blank experiments and D_e the H_2S values from the corresponding experiment.

As can be seen in Fig. 4a, when using bituminous coal char (CC) the H_2S removal percentage drops abruptly in the first 20–40 min of each experiment. An increase of temperature seems to slightly delay this descent. This fact is especially noticeable at 900 °C. In the last minutes of the experiments, H_2S removal is almost non-existent for the highest temperatures (800 and 900 °C), whereas there is still some activity at 700 °C.

For lignite chars (LC, Fig. 4b), the descent in H_2S removal efficiency takes place at even earlier stages of the experiment carried out at 700 °C (before 20 min). After that period, some activity is observed for chars at 900 °C. Due to the high sulphur content of lignite char, some H_2S formation (by means of reaction with

Reprinted from Chemical Engineering Journal, 174, G. García, E. Cascarosa, J. Ábrego, A. Gonzalo, J.L. Sánchez, Use of different residues for high temperature desulphurisation of gasification gas, 644– 651, Copyright (2011), with permission from Elsevier

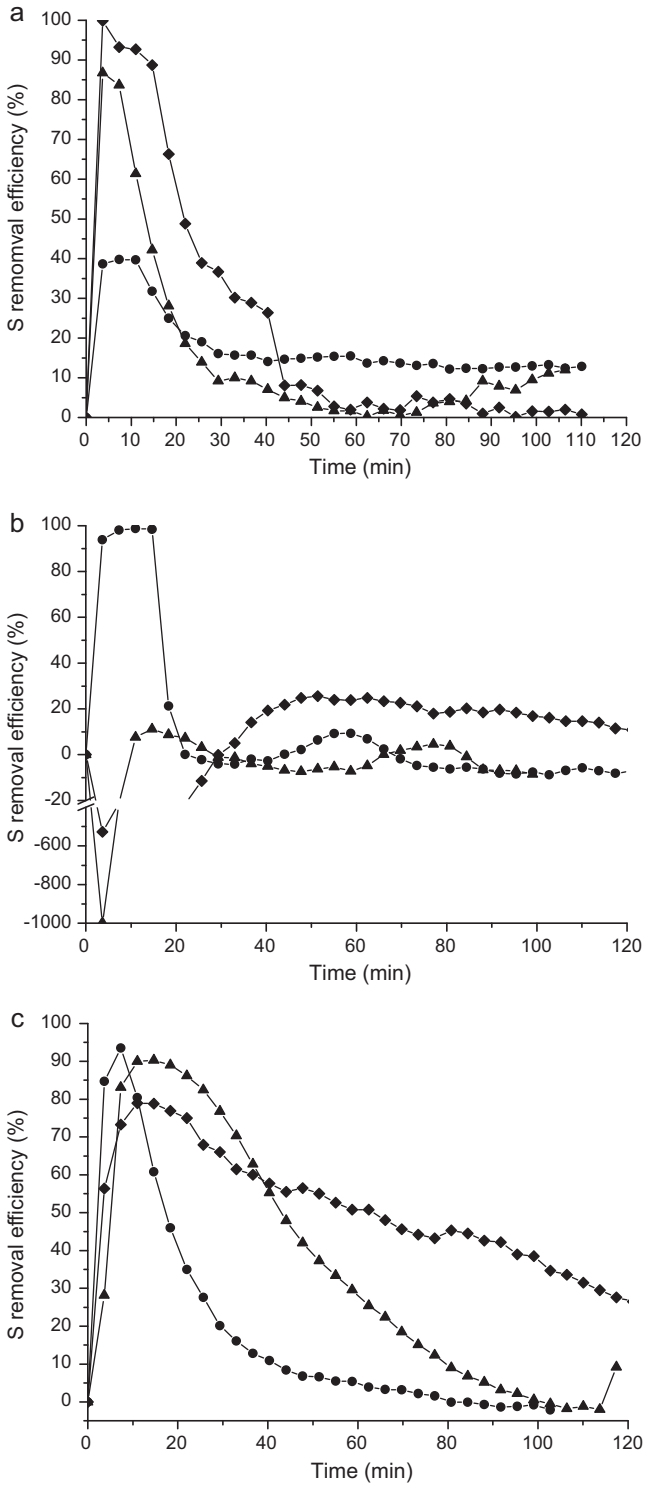

Fig. 4. S removal efficiency using chars: (a) CC, (b) LC; (c) SSC, at different temperatures: ● 700 °C, ▲ 800 °C, ♦ 900 °C.

H_2-containing gas) may occur at high temperatures. As a result of this fact, the H_2S concentration in the outlet flow at 800 and 900 °C is higher than in the blank experiment. This may cause the observed negative values for H_2S removal, as seen in Fig. 4b.

In contrast, sewage sludge char (SSC) shows a different behaviour, as depicted in Fig. 4c. A gradual descent in H_2S removal capacity is observed, instead of a dramatic decrease. Additionally, the higher the experiment temperature, the slower is this descent.

Table 5
Removal efficiencies and capacities of the materials tested.

	Average removal efficiency (% of S removed)			Removal capacity (after 100 min) (mg of S per gram of solid)		
	700 °C	800 °C	900 °C	700 °C	800 °C	900 °C
CC	17.8	15.8	23.0	4.7	3.1	5.1
LC	10.1	−39.7	−15.6	2.8	−1.7	−2.0
SSC	18.9	35.3	50.5	4.5	10.4	12.1
CA	72.2	97.2	97.6	23.2	24.0	21.3
LA	97.7	94.9	92.5	26.7	23.9	20.1
SSA	34.8	46.4	29.7	10.6	13.9	7.4
DO	94.5	99.3	98.4	26.8	24.8	21.5

At 900 °C, this char removes 30% of the incoming H_2S after 120 min. Overall, it is able to retain a significant amount of the total H_2S in the gas. More specifically, at 900 °C, a simple integration of the curve from Fig. 4c through the entire experiment length yields an overall H_2S removal of 50.5% of the amount obtained in the blank run at the same temperature. Expressed in terms of capacity, sewage sludge can remove up to 12.1 mg S/g char in the specified time interval, similarly to reported values in previous works [19,20].

As a general conclusion, chars from these materials seem to have fair H_2S removal capacities. Among the three materials tested, sewage sludge char is more effective than bituminous coal and lignite chars for H_2S removal. This can be observed by a simple comparison of the graphs in Fig. 4, as well as by the average removal efficiency and the calculated removal capacity in mg of S per mg of material, shown in Table 5.

In light of these results, it seems that BET surface area does not play a significant role in H_2S removal at the temperature range of this work. Bituminous coal and lignite chars have higher BET surfaces than sewage sludge char, as shown in Table 3; nevertheless, sewage sludge char show the best H_2S capacity among the three chars. SSC is the char with the lowest carbon content (and therefore with the lowest carbonaceous porous structure), thus indicating than the organic content of the coal chars might difficult the access of H_2S to the metallic centres.

Therefore, the higher performance of SSC may be due to its higher ash content, which might provide active centres for H_2S removal at high temperatures (from the metallic oxides present in ash [21]). Several metallic oxides present in sewage sludge chars, such as iron and calcium oxides, are known to carry out direct sulphidation reactions (Eq. (2)) [2]:

$$M_xO_y + yH_2S \rightarrow M_xS_y + yH_2O \quad (2)$$

3.2. Desulphurisation with ash and dolomite

Results obtained using ash from the different raw materials and commercial dolomite are shown in Fig. 5a (ash from bituminous coal), Fig. 5b (ash from lignite), Fig. 5c (ash from sewage sludge) and Fig. 5d (dolomite).

A simple comparison of Fig. 4 and Fig. 5 evidences great differences between the H_2S removal capacity of chars and ashes from lignite and bituminous coal. Unlike the analogue chars, ash produced from both materials can remove nearly 100% of the incoming H_2S from the gaseous stream.

For bituminous coal ash (CA, Fig. 5a), a very different behaviour is found depending on temperature. At 700 °C, a dramatic decrease in H_2S removal is seen after approximately 80 min, but this is not the case at 800 and 900 °C. Despite this observed decrease, the amount of S retained in the bed is similar to those retained at higher temperatures, as seen in Table 5. Therefore, there seems to be a temperature threshold, between 700 and 800 °C, above which desulphurisation is complete or almost complete in the experimental conditions of this study. CA has a H_2S removal capacity of at least

Reprinted from Chemical Engineering Journal, 174, G. García, E. Cascarosa, J. Ábrego, A. Gonzalo, J.L. Sánchez, Use of different residues for high temperature desulphurisation of gasification gas, 644– 651, Copyright (2011), with permission from Elsevier

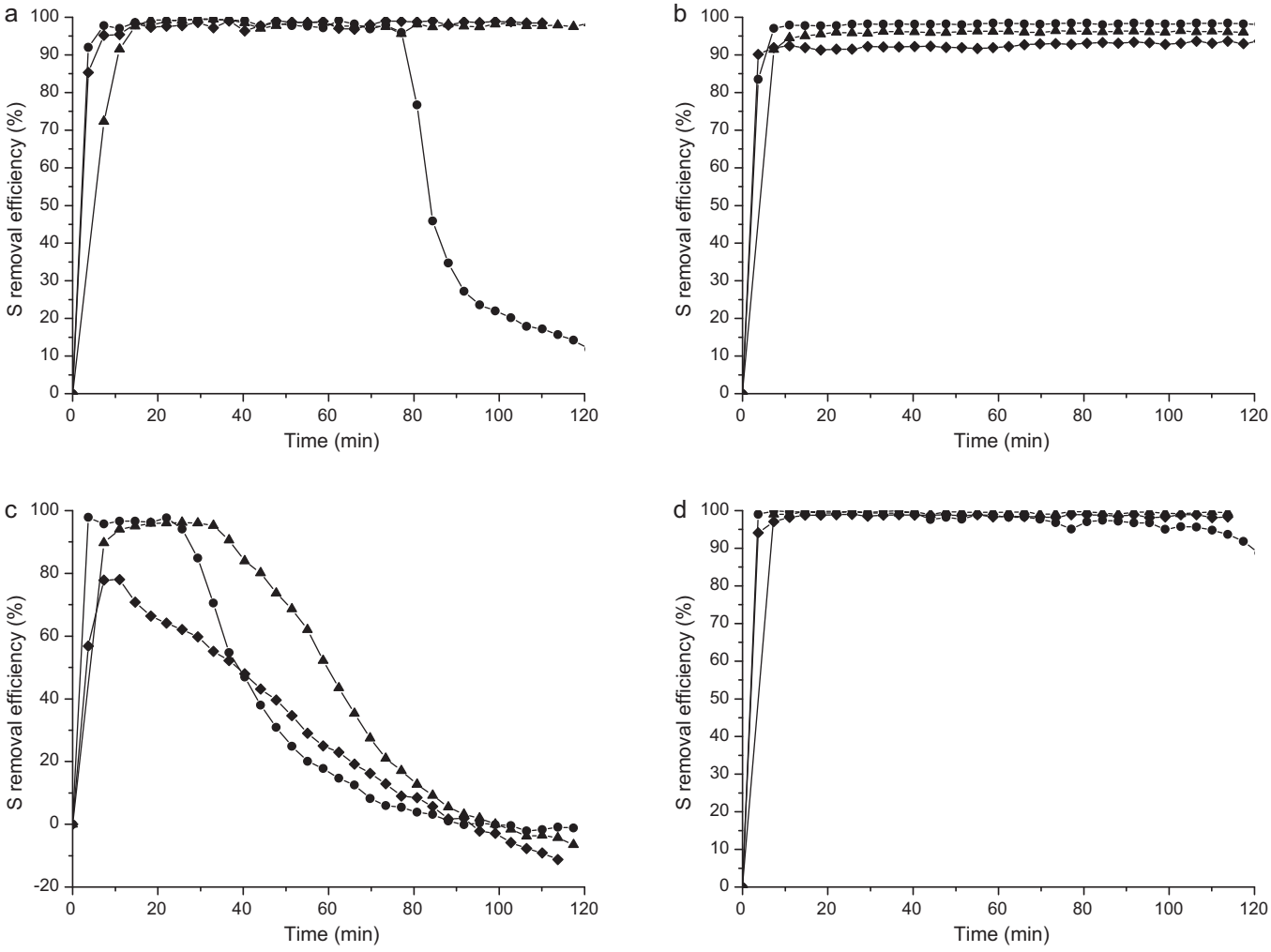

Fig. 5. S removal efficiency using ash: (a) CA, (b) LA; (c) SSA; and (d) commercial dolomite, at different temperatures: ● 700 °C, ▲ 800 °C, ♦ 900 °C.

21.3 mg S/g of ash above the mentioned temperature threshold (see Table 5).

For lignite ash (LA, Fig. 5b), a different trend is found. Almost 100% desulphurisation efficiency is achieved through all the experiment duration at 700 and 800 °C, but lower removal efficiency is detected at the higher temperature of 900 °C. No decay was observed in 120 min.

Efficiency curves for sewage sludge ash (SSA, Fig. 5c) are similar to that observed for char from the same raw material (Fig. 4c). At 700 °C, it can be seen a rapid decrease of the H_2S removal efficiency after a few minutes. This decrease is smoother at higher temperatures; indeed, at 900 °C the decrease rate of H_2S removal capacity is nearly constant. In contrast to SSC, sewage sludge ash loses all their H_2S removal capacity before the end of the experiment is reached (120 min).

As seen in Fig. 5d, and as previously observed by other authors [8], the desulphurisation efficiency of dolomite is very high through all the experiment duration. Thus, it can be considered the best of all the tested materials at any temperature, despite its low specific surface, 18.8 m^2/g. At all temperatures tested, H_2S concentration in the out flow gas was very low. At the highest temperatures tested (800 and 900 °C), coal ash is almost as efficient as dolomite, whereas lignite ash is more efficient at 700 and 800 °C, with a removal capacity similar to dolomite.

For the sake of comparison, the calculated removal efficiencies (% of incoming H_2S removed from the gas), as well as the removal capacities (mg of S per gram of solid) of the tested materials are shown in Table 5. It can be observed that, for the best performing materials (calcined dolomite and LA), the higher the temperature, the lower the capacity. Regarding this, it must be taken into account that in the blank runs, the H_2S concentration in the exiting gas diminished when temperature was increased, so less H_2S can be removed by the ash or char as temperature increases. Thus, no conclusion on the operating temperature can be drawn.

As can be seen, sewage sludge ash works better than char for H_2S removal at 700 and 800 °C, but not at 900 °C, where char shows the best performance of sewage sludge-based materials with 52.3% of H_2S removal.

As a conclusion, ashes from bituminous coal and lignite show a very high H_2S removal performance, much higher than those exhibited by char from the same materials, and similar, at the higher temperatures tested, to calcined dolomite. The main reason for this finding might be in the different carbon content of these materials. If (as stated previously) the inorganic content of these solids is responsible for its desulphurisation ability, converting char into ash is beneficial as it eliminates carbon from them almost completely. In the case of sewage sludge char, it already contained a low amount of carbon; thus, char and ash should not show such great differences in its desulphurisation ability, as seen before.

As observed in Fig. 5, ash from bituminous coal at 800 °C and 900 °C, and ash from lignite are able to retain H_2S during 120 min (excluding coal ash at 700 °C). Despite of the fact that the amount

Reprinted from Chemical Engineering Journal, 174, G. García, E. Cascarosa, J. Ábrego, A. Gonzalo, J.L. Sánchez, Use of different residues for high temperature desulphurisation of gasification gas, 644– 651, Copyright (2011), with permission from Elsevier

Table 6
BET surface of dolomite, CA and LA after the desulphurisation tests.

	BET (m^2/g)		
	700 °C	800 °C	900 °C
CA	4.93	5.01	3.43
LA	18.53	10.59	4.46
DO	2.29	8.00	8.31

of Ca, Na, K and Mg in the ash from sewage sludge is higher than in the ash from both types of coal (Table 4), the H_2S removal capacity of sewage sludge ash is the lowest of the three materials. These results indicate that the metallic oxides present in the material are not the unique variable that has influence on the capacity of H_2S removal.

The H_2S removal capacities of ashes from bituminous coal and lignite (CA and LA) are higher than those using char from the same materials (CC and LC), which can be related to the fact that ashes do not contain fixed carbon.

Regarding the specific surface of the tested materials, shown in Tables 3 and 4, it seems that this parameter does not play a significant role on the desulphurisation runs at this temperature range. The measured specific surface of CA is 5.0 m^2/g, about 50 times smaller than that of CC (244.7 m^2/g). For lignite, the specific surface of its ash and char is 173.8 m^2/g and 13 m^2/g, respectively. The specific surface of char from sewage sludge (59.1 m^2/g) is ten times higher than the specific surface of ash from sewage sludge (5.8 m^2/g).

The BET surface area of the best performing materials (dolomite, bituminous coal ash and lignite ash) was also determined after the desulphurisation experiments, as shown in Table 6. Additionally, the XRD diffraction patterns of these materials are shown in Figs. 6–8.

Fig. 6. XRD diffraction pattern of calcined dolomite (a), and after desulphurisation test at 700 (b), 800 (c) and 900 °C (d).

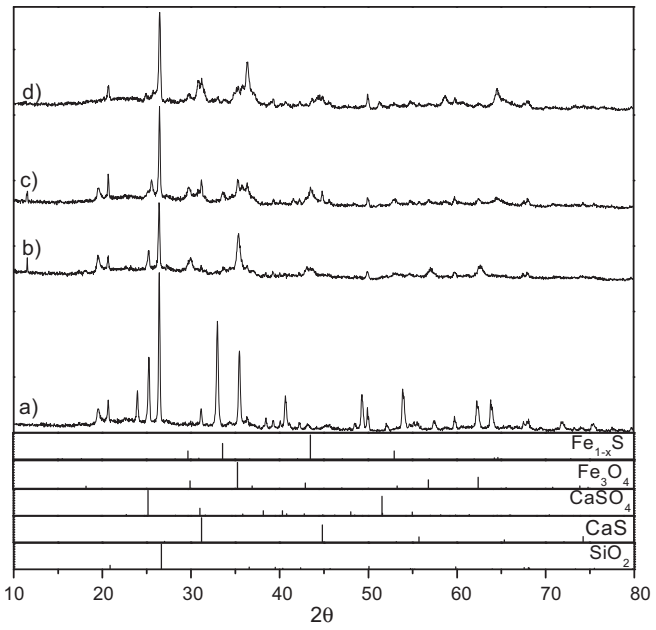

Fig. 7. XRD diffraction pattern of lignite ash (a), and after desulphurisation test at 700 (b), 800 (c) and 900 °C (d).

According to Table 6, surface area of CA does not show a significant change after desulphurisation, only at 900 °C it falls from 5 to about 3 m^2/g. The initial surface area of LA (13 m^2/g) increases slightly up to 18 m^2/g at 700 °C, and decreases again when the desulphurisation temperature increases (4 m^2/g at 900 °C), a similar value to that of CA at that temperature. Dolomite, which initially had the highest surface area (18 m^2/g), has a surface area of only 2 m^2/g after the 700 °C desulphurisation test. This can be related to the fact that partial re-carbonation occurs at this temperature, as observed in the XRD diffraction pattern shown in Fig. 6. After the desulphurisation tests at 800 and 900 °C, the surface area of used dolomite is 8 m^2/g.

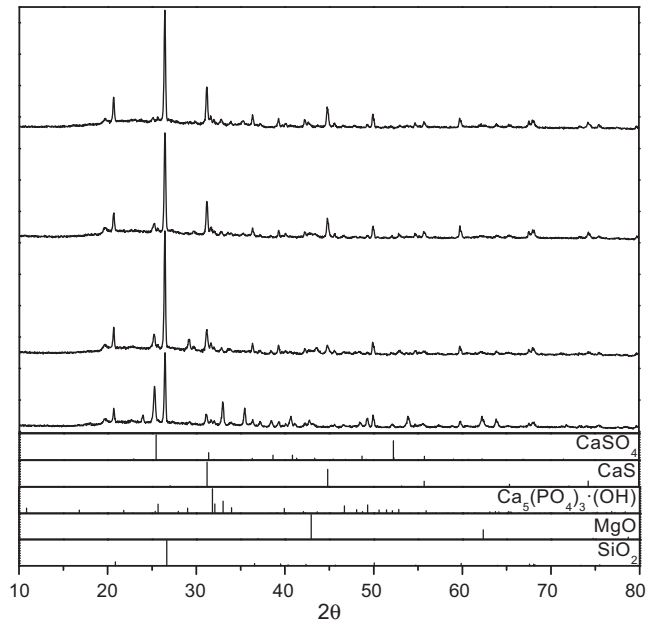

Fig. 8. XRD diffraction pattern of bituminous coal ash (a), and after desulphurisation test at 700 (b), 800 (c) and 900 °C (d).

Reprinted from Chemical Engineering Journal, 174, G. García, E. Cascarosa, J. Ábrego, A. Gonzalo, J.L. Sánchez, Use of different residues for high temperature desulphurisation of gasification gas, 644– 651, Copyright (2011), with permission from Elsevier

In another work [22] using catalytic carbonaceous materials, also at low temperature, it was found that surface area is also important, but, at high temperature this does not seem so be so important, as the best performing materials (LA, CA and calcined dolomite) have lower specific surfaces than the materials used in the cited paper, as shown in Table 4.

As could be expected, the XRD diffraction pattern of calcined dolomite sample (Fig. 6) reveals CaO y MgO as the predominant phases, with only small peaks adscribed to $Ca(OH)_2$. At 700 °C, the re-carbonation of CaO to $CaCO_3$ might be the cause for the low BET surface measured. At 800 and 900 °C, $CaCO_3$ is not observed, but a phase of $Ca(OH)_2$ can be clearly distinguished in the pattern. Small CaS peaks can be observed at 700 and 900 °C, but not at 800 °C. On the other hand, Mg only appears as MgO in the diffraction patterns, and no other crystalline Mg compounds were detected.

The diffraction patterns of lignite ash, shown in Fig. 7, evidence the more complex nature of this material. Previous to the desulphurisation experiments, the main crystalline phases observed in lignite ash are SiO_2, Fe_2O_3 (as hematite, pattern not shown in Fig. 7), and $CaSO_4$ (as anhydrite). At 700 °C, besides SiO_2 (which is the only compound appearing in the four lignite ash diffractograms), Fe_3O_4 and $CaSO_4$ (anhydrite) are present. No evidence of other S containing compounds is found at this temperature. At 800 °C, the diffraction pattern show iron and calcium sulphides, whereas at 900 °C only CaS can be observed.

The diffraction patterns of CA are shown in Fig. 8. As observed for lignite ash, the only compound present in all these samples is SiO_2. In CA before desulphurisation, CaO (pattern not shown in Fig. 8), $CaSO_4$, Fe_2O_3 (pattern not shown in Fig. 8) and MgO are also present as crystalline phases. After desulphurisation, CaS and hydroxylapatite ($Ca_5(PO_4)_3(OH)$) can be found in the patterns of the used CA at 700, 800 and 900 °C. It must be noticed that no crystalline compounds which can indicate that Mg is active for S retention have been observed in any of the samples of dolomite or ashes.

As observed by Seredych et al. [23] for desulphurisation at low temperatures, the presence of Fe and Ca compounds in these kinds of materials improves the desulphurisation capacity. As explained in the previous paragraphs, Ca and Fe sulphides have been detected in the XRD patterns of the used samples.

4. Conclusions

The desulphurisation of a synthetic gasification gas with a high H_2S content was studied with char from bituminous coal (CC), lignite (LA) and sewage sludge (SSC) in the 700–900 °C temperature range. From these materials, the sewage sludge char was the one able to keep its removal efficiency longer, although a significant H_2S percentage remained in the gas.

When ash from the same material was tested at the same temperatures, H_2S removal was dramatically improved in the cases of bituminous coal (CA) and lignite (LA), whereas only a slight improvement was found for sewage sludge (SSA).

The H_2S removal capacity of ash from the two coals tested is almost as high as the showed by calcined dolomite, the commercial material tested as reference. These materials have a low BET surface area and the XRD patterns once used revealed the presence of CaS and FeS. Using CA over 700 °C and LA at any of the temperatures tested, allows reducing the inlet H_2S concentration of 0.50 vol.% to less than 0.05 vol.%.

References

[1] F. Pinto, R.N. André, C. Franco, H. Lopes, I. Gulyurtlu, I. Cabrita, Co-gasification of coal and wastes in a pilot-scale installation. 1: effect of catalysts in syngas treatment to achieve tar abatement, Fuel 88 (2009) 2392–2402.
[2] S. Cheah, D.L. Carpenter, K.A. Magrini-Bair, Review of mid- to high temperature sulphur sorbents for desulphuration of biomass- and coal-derived syngas, Energy Fuels 23 (2009) 5291–5307.
[3] X. Meng, W. Jong, R. Pal, A.H.M. Verkooijen, In bed and downstream hot gas desulphurization during solid fuel gasification: a review, Fuel Process. Technol. 91 (2010) 964–981.
[4] R. Zhang, R.C. Brown, A. Suby, K. Cummer, Catalytic destruction of tar in biomass derived producer gas, Energy Convers. Manage. 45 (2004) 995–1014.
[5] J. Hepola, P. Simell, Sulphur poisoning of nickel-based hot gas cleaning catalysts in synthetic gasification gas. II. Chemisorption of hydrogen sulphide, Appl. Catal. B: Environ. 14 (1997) 305–321.
[6] Z. Abu El-Rub, E.A. Bramer, G. Brem, Review of catalysts for tar elimination in biomass gasification processes, Ind. Eng. Chem. Res. 43 (2004) 6911–6919.
[7] A. Abad, J. Adánez, F. García-Labiano, P. Gayan, Hot coal-gas desulphurization with calcium based sorbents in a pressurized moving-bed reactor, Energy Fuels 18 (2004) 1543–1554.
[8] R. Álvarez-Rodríguez, C. Clemente-Jul, Hot gas desulphurisation with dolomite sorbent in coal gasification, Fuel 87 (2008) 3513–3521.
[9] F. Pinto, H. Lopes, R.N. André, I. Gulyurtlu, I. Cabrita, Effect of catalysts in the quality of syngas and by-products obtained by co-gasification of coal and wastes. 2: heavy metals, sulphur and halogen compounds abatement, Fuel 87 (2008) 1050–1062.
[10] W.F. Elseviers, H. Verelst, Transition metal oxides for hot gas desulphurisation, Fuel 78 (1999) 601–612.
[11] M.A. Caballero, M.P. Aznar, J. Gil, J.A. Martín, E. Francés, J. Corella, Commercial steam reforming catalysts to improve biomass gasification with steam-oxygen mixtures. 1. Hot gas upgrading by the catalytic reactor, Ind. Eng. Chem. Res. 36 (1997) 5227–5239.
[12] T.J. Bandosz, Desulphurisation on activated carbons, in: T.J. Bandosz (Ed.), Activated Carbon Surfaces in Environmental Remediation, Elsevier Ltd., Oxford, 2006, pp. 231–291.
[13] W. Yuan, T.J. Bandosz, Removal of hydrogen sulphide from biogas on sludge-derived adsorbents, Fuel 86 (2007) 2736–2746.
[14] M. Seredych, T.J. Bandosz, Sewage sludge as a single precursor for development of composite adsorbents/catalysts, Chem. Eng. J. 128 (2007) 59–67.
[15] J.J. Manyà, M. Aznar, J.L. Sánchez, J. Arauzo, M.B. Murillo, Further experiments on sewage sludge air gasification: influence of the non-stationary period on the overall results, Ind. Eng. Chem. Res. 45 (2006) 7313–7320.
[16] M. Seredych, T.J. Bandosz, Desulphurisation of digester gas on catalytic carbonaceous adsorbents: complexity of interactions between the surface and components of the gaseous mixture, Ind. Eng. Chem. Res. 45 (2006) 3658–3665.
[17] M. He, B. Xiao, S. Liu, Z. Hu, X. Guo, S. Luo, F. Yang, Syngas production from pyrolysis of municipal solid waste (MSW) with dolomite as downstream catalysts, J. Anal. Appl. Pyrolysis 87 (2010) 181–187.
[18] G. García, E. Cascarosa, J.L. Sánchez, Analysis of catalytic co-gasification of two types of coal with sewage sludge and olive bagasse, in: Proceedings of the 17th European Biomass Conference and Exhibition, Hamburg, 29 June–3 July, 2009, pp. 721–724, ISBN 978-88-89407-57-3.
[19] W. Yuan, T.J. Bandosz, Removal of hydrogen sulfide from biogas on sludge-derived adsorbents, Fuel 86 (2007) 2736–2746.
[20] A. Ansari, A. Bagreev, T.J. Bandosz, Effect of adsorbent composition on H_2S removal on sewage sludge based materials enriched with carbonaceous phase, Carbon 43 (2005) 1039–1048.
[21] J. Aïbrego, J. Arauzo, J.L. Sánchez, A. Gonzalo, T. Cordero, J. Rodríguez-Mirasol, Structural changes of sewage sludge char during fixed-bed pyrolysis, Ind. Eng. Chem. Res. 48 (2009) 3211–3221.
[22] A. Bagreev, T.J. Bandosz, On the mechanism of hydrogen sulfide removal from moist air on catalytic carbonaceous adsorbents, Ind. Eng. Chem. Res. 44 (2005) 530–538.
[23] M. Seredych, C. Strydrom, T.J. Bandosz, Effect of fly ash addition on the removal of hydrogen sulphide from biogas and air on sewage sludge-based composite adsorbents, Waste Manage. 28 (1998) 1983–1992.

Reprinted with permission from Desulfurization and catalytic gas cleaning in fluidized bed co-gasification of sewage sludge-coal blends, G.García, A. Monzon, F. Bimbela, J. L. Sanchez, and J. Abrego, Energy Fuels, DOI: 10.1021/ef400259g , Publication Date (Web): 18 Apr 2013). Copyright (2013) American Chemical Society

energy&fuels

Article

pubs.acs.org/EF

Desulfurization and Catalytic Gas Cleaning in Fluidized-Bed Co-gasification of Sewage Sludge−Coal Blends

G. García,[†] A. Monzón,[‡] F. Bimbela,[§] J. L. Sánchez,[§] and J. Ábrego*[,§]

[†]Agua, Energia y Medio Ambiente, Servicios Integrales, S.L. (AEMA), Polígono Industrial El Pilar, C/Fitero 9, E-26540 Alfaro, Spain

[‡]Catalysis, Molecular Separations and Reactor Engineering Group, Department of Chemical and Environmental Engineering, and [§]Thermochemical Processes Group, Aragón Institute of Engineering Research (I3A), University of Zaragoza, I+D Building, C/Mariano Esquillor s/n, E-50018 Zaragoza, Spain

ABSTRACT: Energy recovery from digested sewage sludge can be achieved by means of co-gasification with coal in a fluidized-bed system. In this regard, one of the main hurdles in developing a feasible process is the need for gas cleaning, with special emphasis on desulfurization and minimization of the tar content of the product gas. In this work, high-temperature catalytic gas cleaning was investigated by means of two fixed beds placed in series downstream of the gasification system: the first containing dolomite for desulfurization and primary tar cracking and the second containing a nickel-based catalyst for additional gas reforming. The effect of the temperature on the performance of the Ni catalyst bed (800−900 °C) was assessed. The use of dolomite in a secondary bed at 800 °C allowed for a significant reduction in both tar [15−0.21 g/m^3 standard temperature and pressure (STP)] and H_2S (to less than 0.01%) and an increase in the heating value of the gas [lower heating value (LHV) from 2000 to 2800 kJ/m^3 STP]. The use of the Ni catalyst decreased the tar content of the gas to undetectable levels. The best results were obtained with the Ni-based catalyst at 800 °C, in terms of enhanced LHV (increasing from 2000 to 3300 kJ/m^3 STP), gas production, which increased from around 2.40 to 2.75 m^3 STP/kg on a dry and ash-free basis (daf), and energy requirements for the process. However, some evidence of Ni catalyst deactivation was found when operating under these conditions.

1. INTRODUCTION

Because of the constant increase in sewage sludge generation, it is widely accepted that alternative pathways for its valorization need to be investigated.[1] Among the alternatives, co-gasification with coal could be a feasible and environmentally sound option for energy recovery.[2,3]

One of the crucial steps to implement gasification at an industrial scale is gas cleaning and conditioning, particularly the removal of particulate matter, sulfur compounds, and tars.

The problem of tar elimination has traditionally been tackled by selecting appropriate process conditions and gasifier designs, by means of gas filtering and/or scrubbing or via thermal or catalytic tar cracking. Within the latter, the use of inexpensive catalytic bed materials, such as dolomite,[4−6] limestone,[7] and olivine,[8] has been explored, and also various metal-based catalysts have been tested.[9−12] However, one of the main operational problems in catalytic tar cracking is catalyst poisoning by sulfur.[13]

Besides their negative effect on catalysts, sulfur compounds are always undesirable in the product gas, regardless of its final use. Because of the high sulfur content of sewage sludge and some coals, significant amounts of sulfur compounds are expected to be present in the product gas after gasification, with H_2S being the most abundant.[14]

Among the different approaches that can be taken for sulfur abatement[15] is the use of dolomite, a well-known desulfurization agent[16−19] especially suitable for application in fixed-bed reactors. Furthermore, it also shows significant tar cracking activity.[6,20] Finally, nickel-containing catalysts have been widely studied for tar reforming of the product gas from coal or biomass gasification.[10,21,22] In this work, the effectiveness of these two materials for hot gas conditioning has been tested for the specific case of co-gasification of sewage sludge and coal blends.

The use of a secondary fixed bed for gas treatment allows for independent control of the operational conditions to be maintained. These conditions do not necessarily have to coincide with the fluidized-bed conditions, in terms of either temperature or gas hourly space velocity (GHSV). Additionally, the excessive carryover of particles can be avoided.

In a recent work, the influence of feedstock composition on air gasification was investigated for blends of bituminous coal, lignite, and sewage sludge.[23] It was found that tar generation was minimized when the three materials were mixed and compared to the gasification yield of each one of the materials used individually. Now that the effect of the feedstock composition has been determined, in this work, attention is mainly focused on the quality of the product gas. Thus, the objective of this work is to assess the performance of a sequential fixed-bed system (dolomite and Ni catalyst) for hot gas conditioning of a producer gas from co-gasification of coal and sewage sludge blends. In the experiments, large enough amounts of catalysts were used to determine the product gas composition that can be obtained after reaching steady-state conditions. To attain a complete development of this process, systematic studies of catalyst deactivation and the potential regeneration procedures will be carried out in further research.

Received: February 13, 2013
Revised: April 15, 2013

 © XXXX American Chemical Society dx.doi.org/10.1021/ef400259g | *Energy Fuels* XXXX, XXX, XXX−XXX

Reprinted with permission from Desulfurization and catalytic gas cleaning in fluidized bed co-gasification of sewage sludge-coal blends, G.García, A. Monzon, F. Bimbela, J. L. Sanchez, and J. Abrego, Energy Fuels, DOI: 10.1021/ef400259g , Publication Date (Web): 18 Apr 2013). Copyright (2013) American Chemical Society

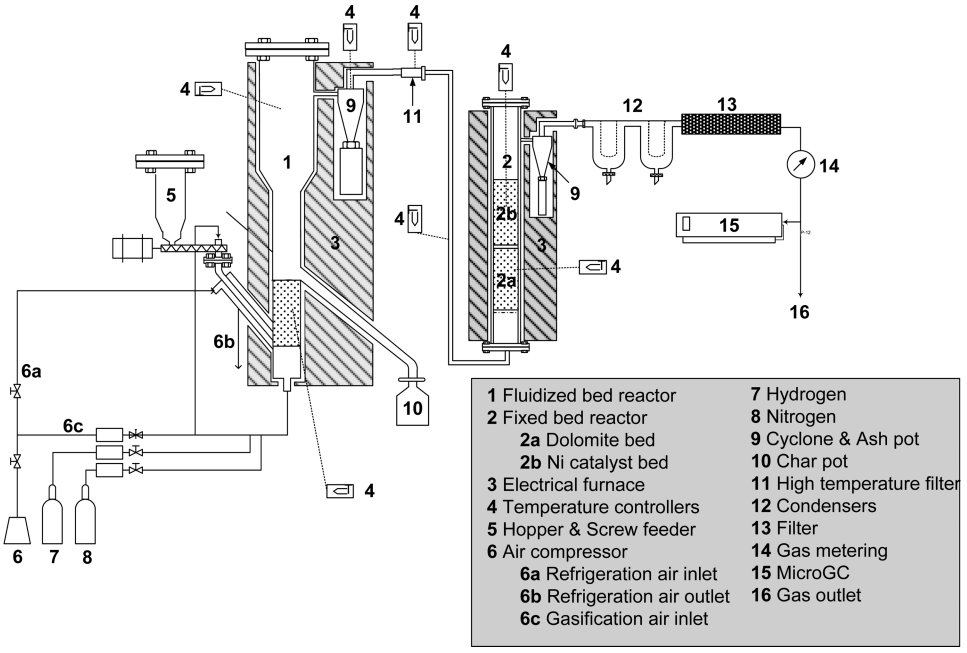

Figure 1. Scheme of the experimental laboratory-scale system.

2. EXPERIMENTAL SECTION

2.1. Experimental Setup. Figure 1 shows a schematic diagram of the experimental setup. The fluidized-bed gasification system has been described elsewhere.[19] An electrically heated pipe connects the fluidized-bed system to the fixed-bed catalytic reactor. This is maintained at 450 °C to prevent condensation of tar products on its inner wall. The fixed-bed reactor is 990 mm long and has a diameter of 35.5 mm. The gas enters the fixed-bed reactor from the bottom and passes through a distributor plate to the dolomite bed (250 g of fresh dolomite, with around 133 g after calcination). The Ni catalyst bed (135 g) is placed above the dolomite bed by means of a metal basket with a diameter almost identical to that of the inner reactor wall. Quartz wool is tightly placed above the dolomite bed to prevent fluidization and/or solid elutriation. The two independent heating zones in the electrical furnace mean that different operating temperatures can be set for each bed.

After exiting the fixed-bed system, the treated gas passes through a condensation system and a filter for tar and water collection. The water content of the collected liquid product is measured by Karl Fischer titration. The weight of the produced tar is calculated by difference with the water. The composition of the permanent gases is determined by an Agilent 3000 series MicroGC system [model G2801A, equipped with two analysis modules, Plot U with a Plot Q pre-column and MolSieve 5A, and thermal conductivity detectors (TCDs)], and the total gas flow rate is measured by a gas meter.

Prior to each experiment involving the reforming Ni catalyst, the catalyst was reduced by introducing a flow of 15% H_2 and 85% N_2 through the reactor system [800 °C, 2 h, 2.82 L standard temperature and pressure (STP)/min], with STP at 0 °C and 1 atm, similar to the reduction conditions proposed by Zhang et al.[22]

All of the experiments were carried out during a total time of 90 min, a fixed gasification temperature of 850 °C, and a stoichiometric ratio of 0.3 (air and solid flow rates of 2.8 L STP/min and 1.9 g/min, respectively). The temperature for the dolomite fixed bed was fixed at 800 °C with a GHSV of 2.18 h^{-1}, whereas the Ni catalyst operated between 800 and 900 °C with a weight hourly space velocity (WHSV) of 2.14 h^{-1}. Before starting to feed the coal−sewage sludge mixtures to the fluidized-bed reactor, the dolomite was calcined with air for 2 h and 800 °C in the same reactor system. After calcination, the system was purged with nitrogen and the previously mentioned H_2−N_2 mixture was introduced for catalyst reduction.

To discard possible additional thermal effects from the fixed-bed system on the results, blank experiments were performed by passing the gasification products through the secondary reactor without containing any bed material. These experiments were performed at 800, 850, and 900 °C.

The experiments will hereafter be referred to as B800/B850/B900, the so-called "blank experiments"; D, the experiment only involving a fixed bed of dolomite working at 800 °C; or D−Ni800/D−Ni850/D−Ni900, the experiments including the fixed bed of dolomite at 800 °C plus the fixed bed of the Ni catalyst working at a temperature of 800, 850, or 900 °C.

2.2. Materials. *2.2.1. Feedstock.* A mixture of sewage sludge (which was supplied thermally dried and anaerobically digested by the wastewater treatment plant "Madrid Sur", from Madrid, Spain), lignite coal (produced in Teruel, Spain), and bituminous coal (imported from South Africa, with both coals supplied by a power plant) was prepared by mixing identical weights of each component. Previously, the three materials were ground and sieved separately to obtain a uniform particle size of 250−500 μm. The composition and lower heating value (LHV) of the feedstock materials are shown in Table 1.

Table 1. Analysis of the Feedstock Materials

	bituminous coal (BC)	lignite coal (LC)	dried sewage sludge (SS)
	Ultimate Analysis		
C (%)	65.29	37.55	27.84
H (%)[a]	4.09	4.07	4.39
N (%)	1.84	0.46	3.95
S (%)	0.68	6.07	0.75
	Proximate Analysis		
moisture[b]	6.93	19.23	6.46
ash[c]	14.33	26.31	41.29
volatile matter[d]	25.19	26.01	46.89
fixed carbon	53.55	28.45	5.36
LHV (kJ/kg)[e]	24.32	13.25	10.87

[a]Includes hydrogen from water. [b]ISO 579-1981. [c]ISO 1171-1976. [d]ISO 5623-1974. [e]ASTM D3286-96.

dx.doi.org/10.1021/ef400259g | Energy Fuels XXXX, XXX, XXX−XXX

Reprinted with permission from Desulfurization and catalytic gas cleaning in fluidized bed co-gasification of sewage sludge-coal blends, G.García, A. Monzon, F. Bimbela, J. L. Sanchez, and J. Abrego, Energy Fuels, DOI: 10.1021/ef400259g , Publication Date (Web): 18 Apr 2013). Copyright (2013) American Chemical Society

Sand with a mean particle size of 273 μm was used as fluidization material.

2.2.2. Catalysts. Two catalytic materials have been used: dolomite for desulfurization and primary tar cracking and a nickel-based catalyst for gas reforming. Carbonated dolomite was supplied by the Spanish company Calcinor, whereas cylindrical monoliths (17 mm outer diameter, 9.5 mm long with six cylindrical holes, with 3 mm inner diameter each) of a commercial Ni-based catalyst supported on calcium aluminate and La-promoted (BASF SG9301) were used for the catalytic reforming.

These materials have been characterized by several analytical techniques. Dolomite was characterized by means of optical emission spectrometry with inductively coupled plasma (ICP−OES) and N_2 adsorption. With regard to the Ni-based catalyst, previous to the activation step, the Ni catalyst monoliths were characterized by N_2 adsorption, X-ray diffraction (XRD), temperature-programmed reduction (TPR), and X-ray photoelectron spectroscopy (XPS). After reaction, some spent catalyst samples were also characterized by XRD and XPS. The catalyst composition was supplied by the manufacturer.

The XRD analyses were made in a Bruker D8 Advance Series 2 diffractometer using a copper anode and a wavelength corresponding to that of copper (λ = 1.5418 Å). The measurements were completed in the 2θ range from 3° to 80°, using a scanning rate of 0.017°/s. Temperature-programmed reduction (TPR) analyses were carried out with a Micromeritics PulseChemisorb 2700 analyzer using a TCD. The samples were previously degasified at 110 °C in an Ar atmosphere. The samples were reduced using a gas mixture of 10% H_2 in Ar (50.14 cm^3 STP/min), starting at room temperature and setting a temperature ramp of 10 °C/min until a final temperature of 1050 °C was attained. Lastly, the XPS analyses of both fresh and spent catalyst samples were performed using a Kratos Axis Ultra DLD spectrometer, with monochromatic Al Kα ($h\upsilon$ = 1486.71 eV) as the X-ray source.

3. RESULTS AND DISCUSSION

3.1. Catalyst Characterization. *3.1.1. Dolomite.* Table 2 shows dolomite composition, determined by ICP−OES analysis and carried out at the Instituto de Carboquímica (ICB−CSIC), Zaragoza, Spain. Table 2 also includes data of the porous structure of the dolomite after calcination, as determined by N_2 adsorption at 77 K using a Micromeritics TriStar II 3000 V6.08A analyzer, taking a value of 0.162 nm^2 for the cross-sectional area of the N_2 molecule adsorbed.

Table 2. Composition of Carbonated Dolomite and Porous Structure of Calcined Dolomite

composition (carbonated dolomite)	
compound	wt %
Al_2O_3	0.09
CaO	30.34
Fe_2O_3	0.01
MgO	20.63
CO_2	48.93
porous structure (calcined dolomite)	
BET surface (m^2/g)	18.8
micropore area (m^2/g)	1.6
micropore volume (cm^3/g)	6×10^{-4}
mean pore diameter (nm)	20.0

3.1.2. Ni-Based Catalyst. Table 3 shows the catalyst composition (as determined by the manufacturer) as well as its porous structure data (determined by N_2 adsorption, using the same analyzer and in the same conditions as those used for the dolomite measurements). This catalyst has previously been reported for natural gas reforming.[24]

Table 3. Composition and Porous Structure of the Ni Catalyst

composition	
compound	wt %
α-Al_2O_3	70−75
CaO	5−10
La_2O_3	1.5
NiO	10−15
porous structure	
BET surface (m^2/g)	16.8
micropore area (m^2/g)	1.3
micropore volume (cm^3/g)	4.6×10^{-4}
average pore diameter (nm)	15.3

The porous structure of the as-received fresh catalyst (before activation) was determined by N_2 adsorption. The adsorption isotherm (not shown) can be ascribed to the type IV isotherm of the International Union of Pure and Applied Chemistry (IUPAC) classification, showing the usual hysteresis loop between the adsorption and desorption curves typical of mesoporous materials. The surface area determined by the Brunauer−Emmett−Teller (BET) method is relatively low, although in the range of other Ca-containing Ni/α-Al_2O_3 catalysts found in the literature, both commercial[25] and prepared in-house.[26] Most of the surface area (ca. 92%) is external, according to the *t* plot obtained using the Harkins and Jura thickness equation. This is logical given the low porosity of the material, as revealed by the BET value obtained. The fraction of micropores is small, and the average pore diameter is around 15 nm, determined from the pore size distribution obtained using the Barrett−Joiner−Halenda (BJH) technique, hence signaling the mesoporous nature of the catalyst.

Figure 2 shows the XRD pattern of the unreduced catalyst sample. The material possesses a high degree of crystallinity, showing very high and narrow peaks. The crystalline phases detected correspond to α-Al_2O_3, NiO (bunsenite), and a mixed calcium and aluminum oxide, $CaAl_4O_7$. Some secondary peaks could also be attributed to another mixed calcium and aluminum oxide, hibonite [$CaO(Al_2O_3)_6$]. These have not

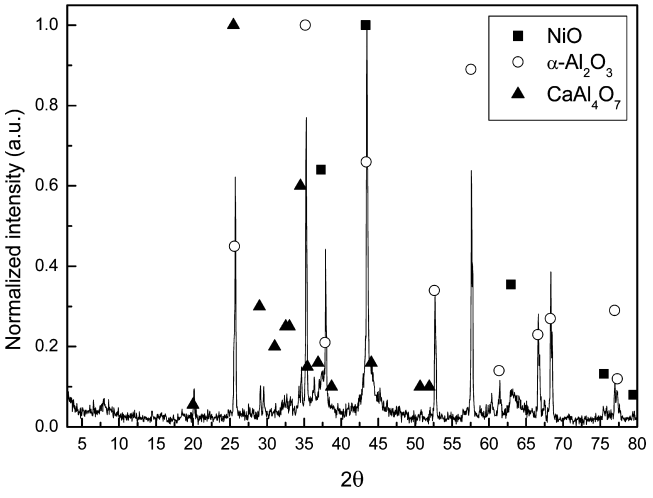

Figure 2. XRD pattern of the fresh Ni catalyst.

dx.doi.org/10.1021/ef400259g | Energy Fuels XXXX, XXX, XXX−XXX

Reprinted with permission from Desulfurization and catalytic gas cleaning in fluidized bed co-gasification of sewage sludge-coal blends, G.García, A. Monzon, F. Bimbela, J. L. Sanchez, and J. Abrego, Energy Fuels, DOI: 10.1021/ef400259g , Publication Date (Web): 18 Apr 2013). Copyright (2013) American Chemical Society

been included in Figure 2 for the sake of clarity. Standard diffraction patterns of lanthanum crystalline phases [La_2O_3, pattern ref 05-0602, and La_2NiO_4, pattern ref 70-0509, from the Joint Committee on Powder Diffraction Standards (JCPDS) database of the International Centre for Diffraction Data] were compared to the sample diffraction pattern. It could be concluded that no La crystalline phases were present, probably because of the low content of La in the catalyst.

Figure 3 shows the TPR profile of the as-received commercial Ni-based catalyst sample.

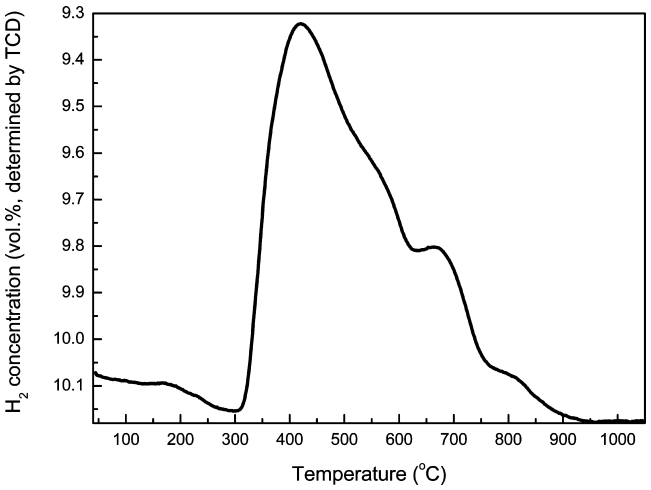

Figure 3. TPR profile of the commercial Ni-based catalyst.

The TPR profile shows a major reduction peak at 420 °C with a shoulder at around 540 °C. This major peak can be ascribed to the reduction of the Ni species that interact with the La-promoted calcium aluminate support. Requies et al.[27] correlated the presence of a peak at a reduction temperature of 532 °C with the reduction of "fixed NiO" species. Furthermore, similar TPR profiles of Ni/Al_2O_3 catalysts prepared by impregnation can be found in the literature.[26,28,29] A secondary peak appears at a temperature around 680 °C, and an additional small shoulder can be observed at ca. 820 °C. The peak at 680 °C could correspond to the reduction of NiO in intimate contact with the support.[26] A small shoulder at ca. 820 °C was also observed by Medrano et al.[29] in a Ni/Al_2O_3 catalyst modified with Ca with a high Ca/Al molar ratio (0.5). Hou et al.[26] attributed the presence of a peak at around 830 °C to the reduction of a $NiAl_2O_4$ phase. However, in the present work, the XRD pattern of the catalyst sample (Figure 2) did not reveal any crystalline phase corresponding to $NiAl_2O_4$, and the small shoulder observed in Figure 3 at 820 °C indicates a low H_2 consumption. Therefore, it could be concluded that such a shoulder could correspond to the reduction of highly dispersed non-stoichiometric amorphous nickel aluminate spinels. The formation of highly dispersed Ni spinels is favored by the addition of lanthanum as a modifier of the catalyst support in Ni/Al_2O_3 catalysts.[30]

Because the XPS analyses were conducted both to fresh and spent catalyst samples, the results of the XPS analyses are presented in section 3.3.1.2 (Table 4). According to the spectrum of the fresh catalyst sample, when analyzing the energy levels corresponding to Ni $2p_{3/2}$, a major peak at a binding energy (BE) equal to 855.4 eV is found, with a secondary peak at 862 eV. This has been attributed to the presence of superficial NiO having a certain degree of interaction with the support, concordant with the XRD and TPR analyses previously presented and the literature.[31,32]

3.2. Preliminary Experiments: In-Bed Use of Dolomite.

Before carrying out the experiments using the secondary fixed-bed reactor, it was considered of interest to check the possibility of using dolomite directly in the fluidized bed. Thus, preliminary experiments were performed with fixed amounts of dolomite, substituting 25% of the initial weight of the bed material (sand). The use of this material within the fluidized bed dramatically decreased the H_2S content of the product gas (from 0.13 to 0.01 vol %). Nevertheless, a large amount of dolomite fines were found in the condensable collection system, and changes in the tar production could not be quantified. This problem has been reported elsewhere in

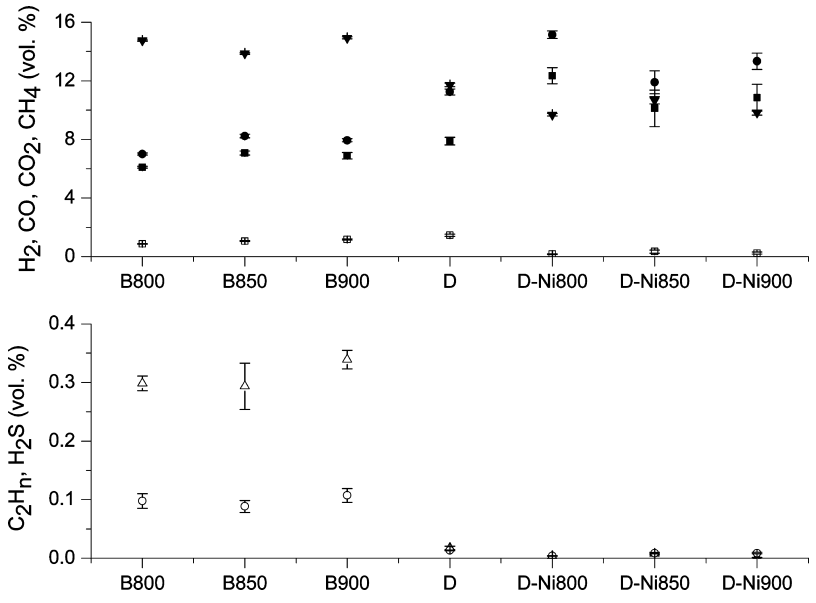

Figure 4. Average gas composition (■, H_2; ●, CO; ▼, CO_2; □, CH_4; △, C_2H_n; and ○, H_2S).

Reprinted with permission from Desulfurization and catalytic gas cleaning in fluidized bed co-gasification of sewage sludge-coal blends, G.García, A. Monzon, F. Bimbela, J. L. Sanchez, and J. Abrego, Energy Fuels, DOI: 10.1021/ef400259g , Publication Date (Web): 18 Apr 2013). Copyright (2013) American Chemical Society

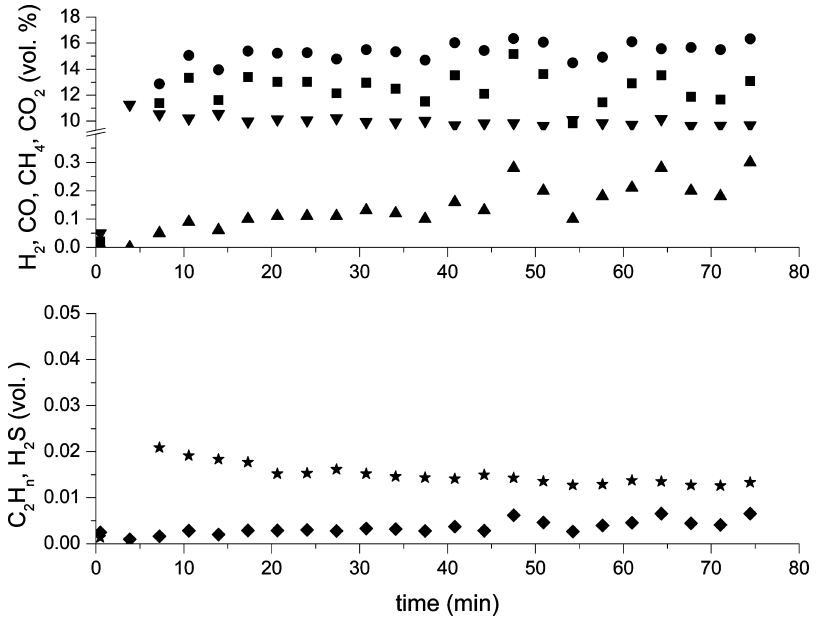

Figure 5. Evolution of dry gas composition (■, H_2; ●, CO; ▼, CH_4; ▼, CO_2; ♦, C_2H_n; and ★, H_2S). Experiment D−Ni800.

similar systems.[33] As a consequence of this excessive carryover, the use of in-bed dolomite was definitively discarded.

3.3. Use of a Secondary Fixed Bed with Dolomite and Ni Catalyst. *3.3.1. Gas Composition. 3.3.1.1. Average Gas Composition.* The average gas composition of the experiments is shown in Figure 4. The observed trends are consistent with previously published results for sewage sludge gasification.[34]

The dolomite bed produces a decrease in CO_2 and a slight increase in H_2.

Both CO and CH_4 contents increase after the dolomite bed, whereas C_2H_n hydrocarbons almost disappear. This might be related to steam reforming and/or cracking reactions for C_2H_n hydrocarbons and some tar compounds. Dolomite is known to have a certain catalytic activity for tar cracking.[35,36]

The low values that can be observed in Figure 4 for the H_2S concentration can be attributed to the sulfidation reaction with dolomite[37] according to the following reaction:

$$CaO + H_2S \rightarrow CaS + H_2O \quad (1)$$

Using the Ni catalyst bed, an increase in the H_2 and CO contents of the product gas and a slight decrease in the CO_2 concentration is observed at all of the temperatures tested and the CH_4 content falls dramatically. All of these observations are a consequence of the reforming reactions catalyzed by Ni.[32]

3.3.1.2. Evolution of Gas Composition. Data from Figure 4 show an overall positive effect of both fixed beds on the average gas composition and cleaning. Nevertheless, it would be interesting to detect any possible temporal change in the gas composition during the experiments, because this would provide evidence for changes in the catalytic activity of the fixed beds. Figure 5 depicts the evolution of the gas composition for the experiment carried out with a Ni catalyst bed temperature of 900 °C. The experiments carried out at 800 and 850 °C showed a similar gas evolution.

It is worth mentioning that the Ni catalytic beds after reaction showed two differentiated zones with different colors. The first two-thirds of the catalytic bed (situated at the reactor entrance) contained pellets with a much darker color than that of the initial calcined precursors, probably because of deposited coke. These pellets will be referred to as the black catalyst samples. However, the other third (closer to the reactor outlet) had a whitish look. These will be referred to as the white catalyst samples.

As seen in Figure 5, the main product gases from co-gasification (H_2, CO, and CO_2) show little variation during the total experiment time. On the other hand, CH_4 increases monotonically. The concentrations of C_2 hydrocarbons and H_2S remain almost constant and at very low values. The increase in CH_4, although still below the concentration observed in the absence of the Ni catalyst, may be an indication of catalyst deactivation, as described in other works.[38,39] Figure 6 shows the evolution of the CH_4 production rate (g/min) during each experiment. It can be observed that, at 800 °C, the CH_4 production rate in the blank experiment and after passing through the dolomite bed is roughly the same in both cases, suggesting that, at this temperature, the activity of dolomite toward methane cracking is low. As expected, the Ni catalyst is more active for methane cracking, and as commented before, the CH_4 increases over time at the three temperatures. It can also be observed, more clearly at 800 and 950 °C, that the higher the temperature, the quicker the increase in CH_4. This could be related to a faster deactivation of the catalyst occurring at higher temperatures. This is correlated with the gas production and heating value observed, which is discussed subsequently.

With regard to the evolution of H_2S with time, negligible amounts of H_2S were detected in the gas composition throughout. This might indicate additional deactivation of the Ni catalyst by sulfur poisoning.

To explain the tendencies observed, some characterization of the spent black and white Ni catalyst samples was carried out. Both fractions were characterized separately by means of XRD and XPS analyses. Figure 7 shows the XRD pattern of both samples (a) black and (b) white. The differences found in the crystalline phases corresponding to both samples are evident, even though both present high and narrow peaks, indicating a high degree of crystallinity. The crystalline phase corresponding to α-Al_2O_3 (corundum) could be identified in both cases.

Reprinted with permission from Desulfurization and catalytic gas cleaning in fluidized bed co-gasification of sewage sludge-coal blends, G.García, A. Monzon, F. Bimbela, J. L. Sanchez, and J. Abrego, Energy Fuels, DOI: 10.1021/ef400259g , Publication Date (Web): 18 Apr 2013). Copyright (2013) American Chemical Society

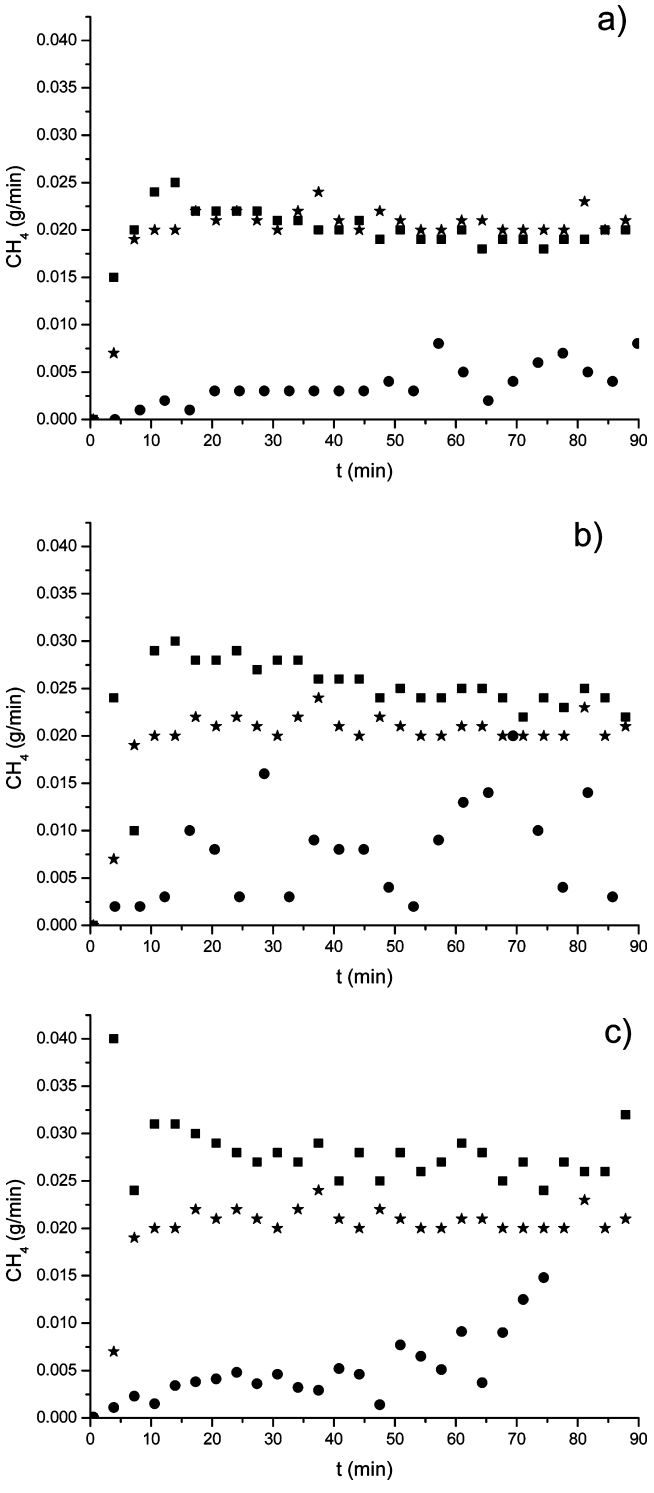

Figure 6. CH_4 evolution (■, blank experiment; ●, D−Ni; and ★, D 800 °C) at (a) 800 °C, (b) 850 °C, and (c) 950 °C.

However, the rest of the crystalline phases do not coincide. The most significant difference is found for metallic Ni (Ni^0), which is present in the black sample but not in the white. In addition, an additional crystalline phase of a mixed calcium aluminum oxide ($CaAl_4O_7$) was only identified in the black sample, whereas such a phase could not be detected in the white sample. Some secondary diffraction peaks corresponding to bunsenite (NiO) and hibonite [$CaO(Al_2O_3)_6$] could explain some of the small diffraction peaks detected in the white sample, at $2\theta = 62.9°$ and 79.5° (NiO) and at $2\theta = 20.1°$, 32.7°, 40.7°, 40.9°, 45.1°, 58.9°, and 60.0° [$CaO(Al_2O_3)_6$], respectively. However, the low intensities of the peaks corresponding to NiO and [$CaO(Al_2O_3)_6$] indicate a low degree of crystallinity for these phases in the sample.

Table 4 and Figure 8 show the results of the XPS analyses carried out on the black sample (Figure 8a) and the white sample (Figure 8b). For the sake of comparison, the XPS analysis of the fresh catalyst (already discussed in section 2) is also presented in Table 4 and Figure 8c. The region of interest for BE between 850 and 885 eV was analyzed, which can help in determining differences in the electronic state of surface Ni by analyzing the Ni $2p_{3/2}$ and $2p_{1/2}$ levels and also the characteristic satellite peaks. Deconvolution curves (not shown) of the overall experimental peaks were generated by applying a Gaussian/Laurentian mixed model of variable proportion. This procedure can help identify hidden secondary peaks that might explain some shoulders and non-Gaussian peak shapes observed in the curves. These curves have been fitted and compared to the overall experimental curves.

Again, the differences between the black and white samples are evident. The major peak observed for the black sample at a BE around 855 eV presents a shoulder. Hence, the observed peak can actually be considered as the sum of two peaks (see Figure 8a): one peak with its maximum at 855.7 eV and a second peak with its maximum at 853.1 eV. The latter can be attributed to reduced nickel, in agreement with the XRD analysis (Figure 6), whereas the peak at 855.7 eV, along with the satellite peak found at 862.1 eV, could correspond to stoichiometric NiO having a certain interaction with the support, consistent with the TPR analyses previously presented for the fresh catalyst sample. This is also consistent with the observations made by Salagre et al.,[31] who proposed that the shift from the BE corresponding to pure NiO (855.0 eV) toward 855.5 eV indicated a weak interaction with the support.

In contrast, the white sample presents a major peak with a maximum at 855.3 eV and a very small peak with a maximum at 851.7 eV. The latter was not detected in the XPS analysis of the black sample. The major peak at 855.3 eV, along with the satellite peak found at 861.9 eV, could again correspond to the presence of a surface NiO phase, concordant with the crystalline NiO phase revealed by the XRD analysis (Figure 6b), even though the slight decrease in the BE values found in the white sample indicate a weaker interaction with the support. On the other hand, the small peak at 851.7 eV could correspond to segregated surface Ni.[40] The peak size might indicate that only a small amount of surface Ni is present, in agreement with the literature,[31] which could explain the lack of detection of a crystalline Ni phase in the XRD analysis. It is also worth noting that the presence of surface S (BE between 160 and 175 eV, not shown) was only evidenced in the white sample. The preferential adsorption of sulfur in ceramic supports has also been previously reported in the literature.[41]

The crystalline phase corresponding to NiO was not detected in the XRD analysis of the black sample, meaning that the stoichiometric NiO may be affected by some "decorating" effect caused by dispersed species from the support, mainly Al^{3+} and La^{3+} ions.[30] Other authors have reported the existence of difficult to reduce NiO, especially if the particles are small and well-dispersed.[28] The intimate contact of a stoichiometric NiO phase "decorated" with the alumina surface could lead to a moderate interaction that might distort the crystalline structure of the stoichiometric NiO, also resulting in varying degrees of

Reprinted with permission from Desulfurization and catalytic gas cleaning in fluidized bed co-gasification of sewage sludge-coal blends, G.García, A. Monzon, F. Bimbela, J. L. Sanchez, and J. Abrego, Energy Fuels, DOI: 10.1021/ef400259g , Publication Date (Web): 18 Apr 2013). Copyright (2013) American Chemical Society

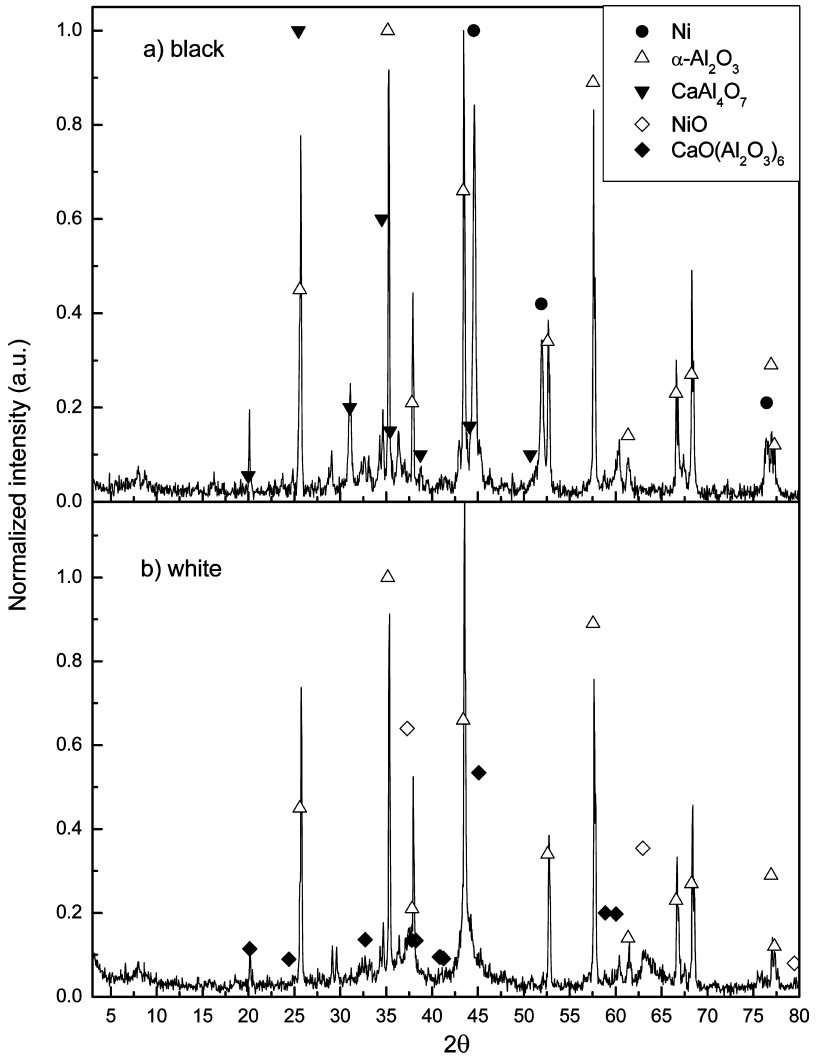

Figure 7. XRD analyses of the spent catalyst samples: (a) black and (b) white.

Table 4. XPS Analyses of the Ni Catalyst Samples

sample	primary peaks BE values (eV)	secondary peaks BE values (eV)	identified phase	Ni/Al atomic ratio
black	853.1		Ni^0	0.09
	855.7	862.1	NiO	
white	851.7		Ni^0	0.10
	855.3	861.9	NiO	
fresh	855.4	862.0	NiO	0.14

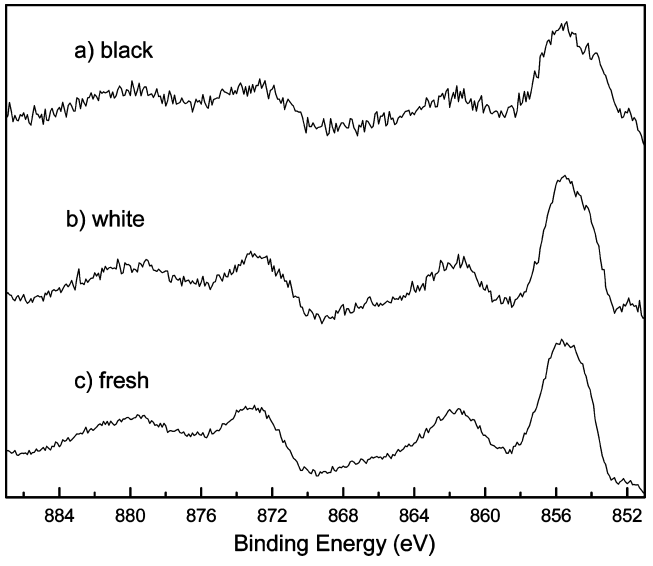

Figure 8. XPS analyses of (a) black, (b) white spent Ni catalyst, and (c) fresh Ni catalyst samples.

reducibility of the NiO phase as observed in the TPR. It might also hinder the reducibility of part of the NiO present in the fresh sample.

3.3.2. Gas LHV. The LHVs of the gases are shown in Figure 9. With regard to the blank experiments, values of around 2400 kJ/m^3 STP were found for B850 and B900, whereas run B800 produced a gas with a LHV of around 2000 kJ/m^3 STP. This difference can be attributed to some extent to tar cracking at the highest temperatures of the interval and the subsequent formation of gaseous products. In fact, H_2, CO, and CH_4 concentrations were found to be slightly higher at B850 and B900, as seen in Figure 4.

The additional catalytic cracking in the dolomite bed produces an increase in the LHV of the gas to 2800 kJ/m^3 STP. Afterward, the Ni catalyst bed produces a remarkable LHV increase at 800 °C (3300 kJ/m^3 STP), but higher

dx.doi.org/10.1021/ef400259g | *Energy Fuels* XXXX, XXX, XXX−XXX

Reprinted with permission from Desulfurization and catalytic gas cleaning in fluidized bed co-gasification of sewage sludge-coal blends, G.García, A. Monzon, F. Bimbela, J. L. Sanchez, and J. Abrego, Energy Fuels, DOI: 10.1021/ef400259g , Publication Date (Web): 18 Apr 2013). Copyright (2013) American Chemical Society

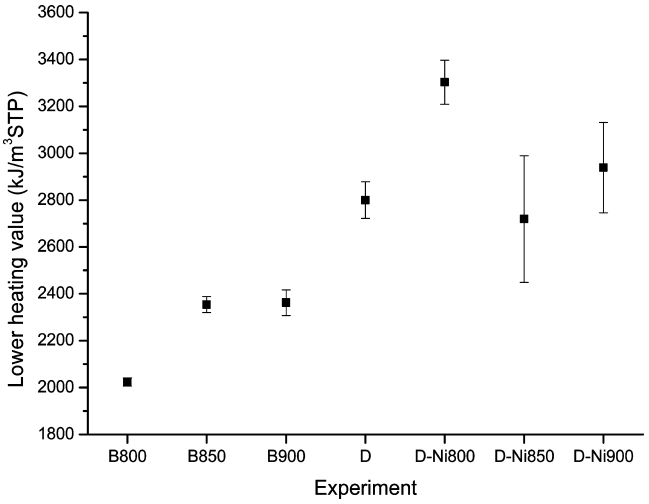

Figure 9. LHV of the product gas.

temperatures do not cause significant improvements compared to the gas exiting the dolomite bed. This can be related to the higher H_2 and CO concentrations found at 800 °C, as seen in Figure 4.

3.3.3. Gas Yield. Some of the previously observed changes in the gas composition can also be correlated to the gas yield, shown in Figure 10. The gas yield increase in the blank

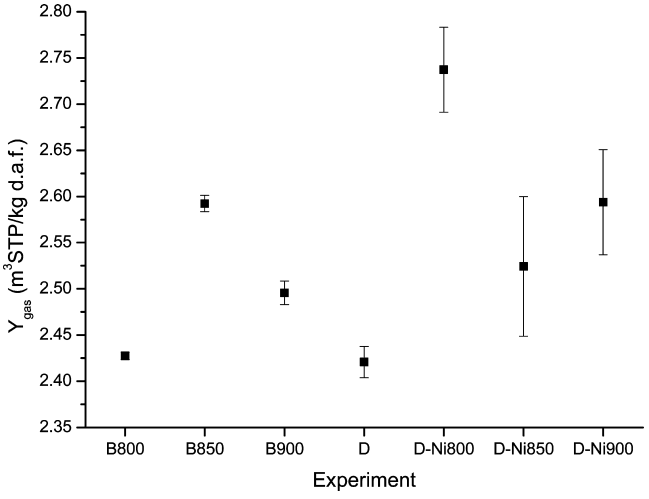

Figure 10. Gas yield.

experiments at higher temperatures can be explained as being a consequence of the cracking of some tar compounds. The dolomite bed produced a descent in the gas yield that might be caused by partial carbonation of the dolomite (consistent with the observed increase in the LHV) and the removal of H_2S.

With regard to the catalytic runs, the greatest gas yield was obtained at the lowest reaction temperature studied (800 °C), whereas between 850 and 900 °C, no statistically significant differences were found. The higher gas yield obtained at 800 °C compared to those obtained at higher temperatures might indicate a change in the deactivation rate, which is dependent upon the difference in the formation and gasification rates of carbon/coke precursors.[39]

Figure 11 shows the changes in individual gas yields expressed in grams of gas per kilograms of feedstock mixture [dry and ash-free basis (daf)]. Because air is used as a gasifying agent, the weight of gas produced is higher than the weight of organic solid fed. The most relevant changes induced by dolomite on the gas yield include a sharp descent in C_2H_n and H_2S. Also, lower amounts of CO_2 are found, probably as a result of the previously mentioned partial carbonation of dolomite. Afterward, the Ni catalyst bed produces high amounts of H_2 and CO (especially at 800 °C) and a substantial drop in CH_4. This could be attributed to the catalyzed steam reforming reaction of CH_4, according to eq 2.

$$CH_4 + H_2O \leftrightarrow CO + 3H_2 \quad (2)$$

On the other hand, the differences found in the individual gas yields in the catalytic runs with different reaction temperatures may be explained by the change in the total gas yield, which has previously been discussed.

3.3.4. Gasification Efficiencies and Energy Balance. Two important parameters for gasification systems have been calculated, namely, cold gas efficiency and carbon−gas efficiency. Their values are shown in Figure 12.

Cold gas efficiency (η_{gas}) serves as a measurement of the effectiveness of the gasification process for chemical energy conversion, according to eq 3

$$\eta_{gas}\ (\%) = \frac{LHV_{gas} Y_{gas}}{LHV_{gas}} \times 100 \quad (3)$$

where LHV_{gas} and LHV_{ss} are the lower heating values of the product gases and sewage sludge, respectively, and Y_{gas} is the previously calculated gas yield. The carbon−gas efficiency measures the effectiveness of C conversion within the gasification process and can be calculated by eq 4.

$$\eta_C\ (\%) = \frac{\text{grams of carbon in gas}}{\text{grams of carbon fed to the gasifier}} \times 100 \quad (4)$$

Cold gas efficiencies increase with the use of dolomite and Ni catalyst beds. In the case of the dolomite bed, partial carbonation would lead to removal of CO_2 and an increase in the LHV of the gases, as previously observed. This would counteract the previously observed decrease in Y_{gas} and produce a net increase in the cold gas efficiency. With regard to the Ni catalyst bed, the most significant increase takes place at 800 °C, as a result of increases in both the LHV of the gases and Y_{gas}.

The cold gas efficiency provides an estimate of energy in the feed stream, which is converted into fuel gas, but does not take into account the energy needed for the hot gas conditioning process. Air gasification can be carried out autothermally, because oxidation reactions supply the energy needed for the different steps (drying, thermal decomposition, dry and steam reforming, etc.). Nevertheless, energy requirements for the dolomite and nickel beds should be clarified. To do this, an energy balance has been carried out with the following assumptions: (1) The only reactions taken into account in the solids are sulfidations of dolomite (where only CaO reacts with H_2S to form CaS[42]) and the Ni catalyst. (2) Because of the lack of data, carbon deposition and CaO carbonation have not been taken into account. (3) Only C_2H_4 and naphthalene have been considered for C_2H_n and tar, because they are the major compounds.

As seen in Table 5, the enthalpy needed in the dolomite bed (546.8 kJ/kg daf) is 8.1% of the final gas LHV. This value decreases to 6.0% if a Ni bed is used, because of the additional increase in LHV after this treatment. Combining both cleaning steps at 800 °C (dolomite + Ni) would consume 9.0% of the

Reprinted with permission from Desulfurization and catalytic gas cleaning in fluidized bed co-gasification of sewage sludge-coal blends, G.García, A. Monzon, F. Bimbela, J. L. Sanchez, and J. Abrego, Energy Fuels, DOI: 10.1021/ef400259g , Publication Date (Web): 18 Apr 2013). Copyright (2013) American Chemical Society

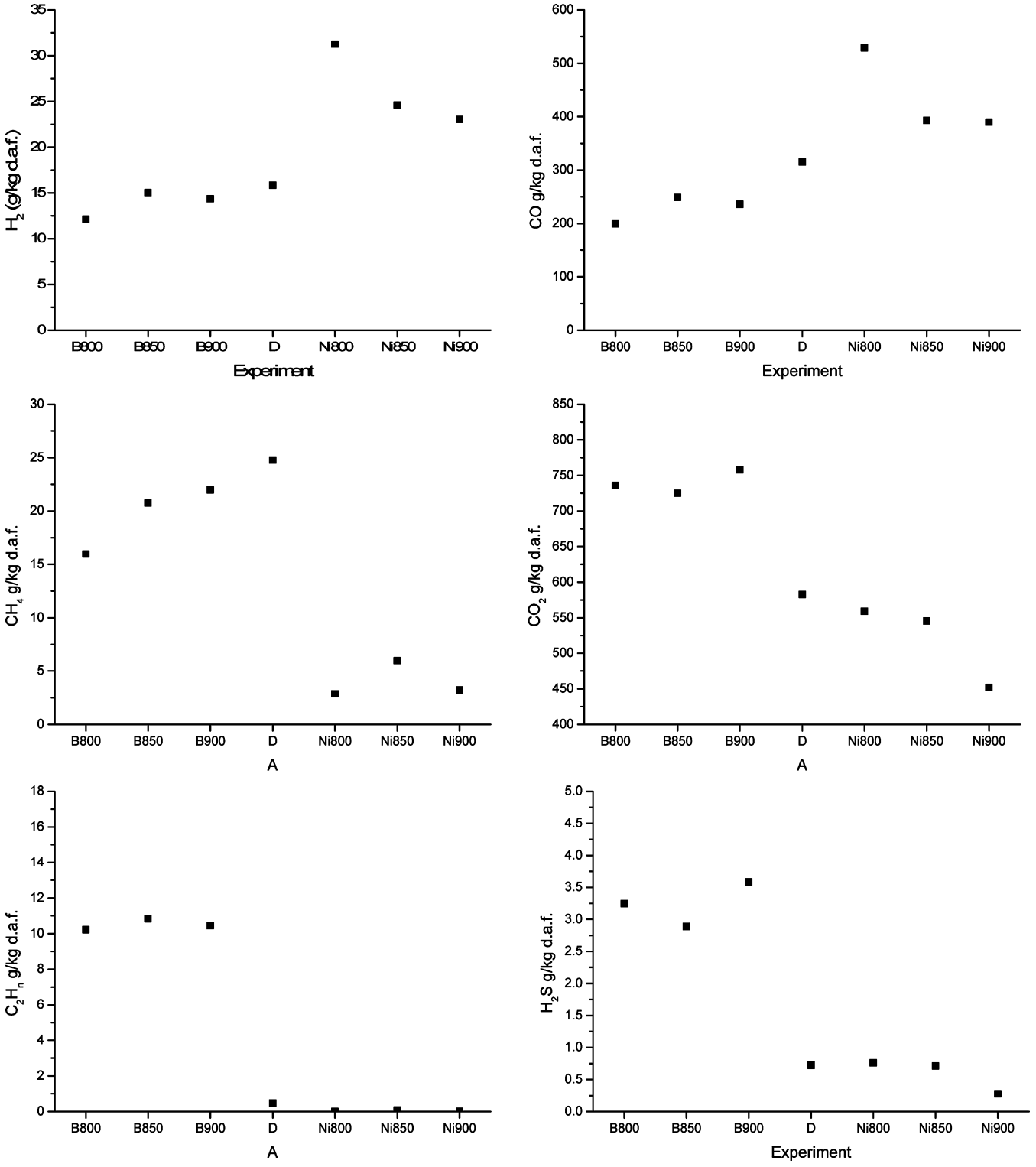

Figure 11. Yields (g/kg of sewage sludge daf) of each individual component of the product gas.

gas LHV, whereas an increase in the Ni bed temperature to 850 and 900 °C would increase the energy requirements to 19.1 and 26.3%, respectively. Thus, from the energy point of view, working at 800 °C in both beds is the most advisable option.

3.3.5. Tar Content of the Gas. The effect of the secondary treatments on the tar content of the gas is depicted in Figure 13. Note the significant tar reduction in experiment B900 (if compared to B800 and B850) because of the thermal cracking of some of the tars exiting the gasifier.[21] A possible consequence of this observed fact is the increase in the CH_4 yield given in Figure 11. The dolomite bed was able to reduce tars below 0.21 g/m^3 STD. Finally, under any tested temperature, the Ni catalyst bed produced a complete destruction of the tars. Further gas chromatography/mass spectrometry (GC/MS) analyses of the liquids confirmed that the typical predominant compounds from gasification tars, such

Reprinted with permission from Desulfurization and catalytic gas cleaning in fluidized bed co-gasification of sewage sludge-coal blends, G.García, A. Monzon, F. Bimbela, J. L. Sanchez, and J. Abrego, Energy Fuels, DOI: 10.1021/ef400259g , Publication Date (Web): 18 Apr 2013). Copyright (2013) American Chemical Society

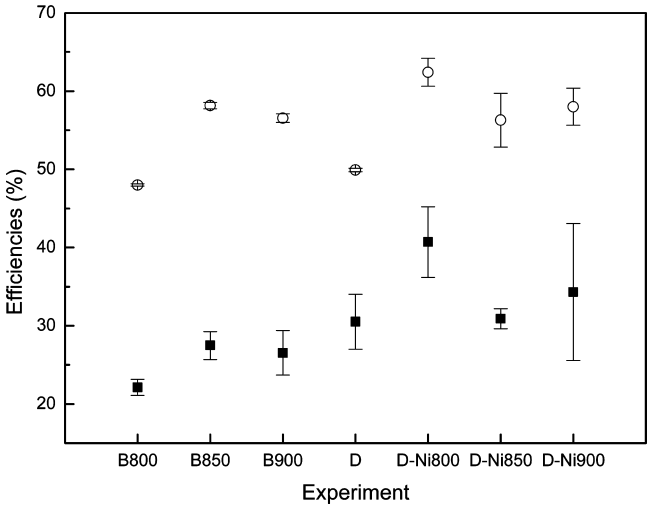

Figure 12. Cold gas efficiency (η_{gas}, ■) and carbon−gas efficiency (η_C, ○).

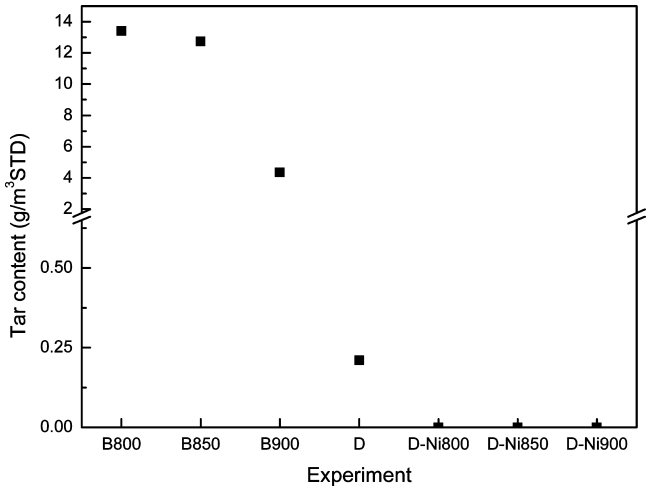

Figure 13. Tar content of the product gas.

as naphthalene, indene, and toluene,[43,44] were below 2 mg/m^3 STP. Similarly, the total destruction of gasification tars by a Ni catalyst was also observed by Pinto and co-workers for co-gasification of coal and wastes.[45] Despite the previously explained deactivation effect observed on the catalyst bed, the presence of a sufficiently large catalyst bed is able to overcome these drawbacks and produce complete tar elimination throughout the experiment.

4. CONCLUSION

In this work, the catalytic upgrading of gas from the co-gasification of sewage sludge and two types of coal has been studied by the combined use of two consecutive fixed beds of dolomite and a commercial Ni catalyst, respectively. The tar content of the gas was reduced from around 14 g/m^3 STP at 800 °C to 0.2 g/m^3 STP after passing through the dolomite bed and to undetectable levels with the use of the Ni catalyst at all of the three temperatures tested (800, 850, and 900 °C). The dolomite bed produced a sharp decrease in the H_2S concentration, from about 0.1 vol % (dry gas basis) to less than 0.01 vol %. Further reduction of the H_2S concentrations through the second fixed bed indicated sulfur poisoning of the Ni catalyst. Within the experimental conditions tested in this work, operating both fixed beds at 800 °C produced the best results in terms of gas LHV, which increased from 2000 to 2800 kJ/m^3 STP after the dolomite bed and to 3300 kJ/m^3 STP after the Ni catalyst, cold gas and carbon−gas efficiencies, and gas production (2.4−2.7 m^3 STP/kg daf), as well as for the energy needed in the cleaning process. Complete destruction of tars was achieved in all cases, but deactivation of the Ni catalyst could also be observed, probably because of coke deposition as a consequence of tar and hydrocarbon cracking reactions and also S poisoning.

AUTHOR INFORMATION

Corresponding Author

*Telephone: +34976762962. Fax: +34976761879. E-mail: abrego@unizar.es.

Notes

The authors declare no competing financial interest.

ACKNOWLEDGMENTS

The authors express their gratitude to the Research Programme of the Research Fund for Coal and Steel for funding the CO.CACO.R.K. Project (RFCR-CT-2005-00008), the Spanish Ministry of Science and Technology for financial support (Research Projects CTQ2007-66885PPQ and CTQ2010-2013), and the Aragón Government and the European Social Fund for providing funding support for the GREG and TPG research groups. Dr. Silvia Irusta from the Instituto de Nanociencia de Aragón (Universidad Zaragoza) is acknowledged for conducting the XPS measurements. Dr. Concepción Sánchez from the Servicio General de Apoyo a la Investigación (Universidad Zaragoza) is also acknowledged for supplying the standard diffraction patterns.

REFERENCES

(1) Manara, P.; Zabaniotou, A. *Renewable Sustainable Energy Rev.* **2012**, *16*, 2566−2582.

Table 5. Enthalpy Balance of the Gas-Cleaning Steps

step	T (°C), outlet of each stage	H[a] (kJ/kg of gas)	mass flow[b] (kg of gas/kg daf)	ΔH[c] (kJ/kg daf)	ΔH dolomite (%)[d]	ΔH Ni (%)[d]
gasifier	850	−2374	2.9			
dolomite bed	800	−2205	2.9	546.8	8.1	
Ni bed	800	−2041	3.0	270.1	6.0	3.0
	850	−2011	2.8	763.0	8.0	11.1
	900	−1767	2.8	1446.2	7.2	19.1

[a]Enthalpy of the product gas after each stage. [b]Mass of gas produced (per kilogram of daf solid fed) after each stage, including water and tar. [c]Enthalpy needed in each stage of the gas cleaning, per kilogram of daf solid fed. [d]Percentage of LHV (of the final product gas) needed for each cleaning stage.

Reprinted with permission from Desulfurization and catalytic gas cleaning in fluidized bed co-gasification of sewage sludge-coal blends, G.García, A. Monzon, F. Bimbela, J. L. Sanchez, and J. Abrego, Energy Fuels, DOI: 10.1021/ef400259g , Publication Date (Web): 18 Apr 2013). Copyright (2013) American Chemical Society

(2) Wang, X.; Xiao, Y. *Proceedings of the ASME Turbo Expo 2004: Power for Land, Sea, and Air*; Vienna Austria, June 14−17, 2004; pp 131−139.
(3) Pinto, F.; Lopes, H.; André, R. N.; Dias, M.; Gulyurtlu, I.; Cabrita, I. *Energy Fuels* **2007**, *21*, 2737−2745.
(4) Simell, P. A.; Bredenberg, J. B. *Fuel* **1990**, *69*, 1219−1225.
(5) Corella, J.; Aznar, M. P.; Gil, J.; Caballero, M. A. *Energy Fuels* **1999**, *13*, 1122−1127.
(6) Aznar, M. P.; Corella, J.; Delgado, J.; Lahoz, J. *Ind. Eng. Chem. Res.* **1993**, *32*, 1−10.
(7) Taralas, G. *Ind. Eng. Chem. Res.* **1996**, *35*, 2121−2126.
(8) Devi, L.; Ptasinski, K.; Janssen, F. *Fuel Proc. Technol.* **2005**, *86*, 707−730.
(9) Arauzo, J.; Radlein, D.; Piskorz, J.; Scott, D. S. *Energy Fuels* **1994**, *8*, 1192−1196.
(10) Bangala, D. N.; Abatzoglou, N.; Martin, J.-P.; Chornet, E. *Ind. Eng. Chem. Res.* **1997**, *36*, 4184−4192.
(11) Rapagná, S.; Provendier, H.; Petit, C.; Kiennemann, A.; Foscolo, P. U. *Biomass Bioenergy* **2002**, *22*, 377−388.
(12) Martínez, R.; Romero, E.; Garcia, L.; Bilbao, R. *Fuel Proc. Technol.* **2004**, *85*, 201−214.
(13) Hepola, J. *VTT Publ.* **2000**, *425*, 54.
(14) Jazbec, M.; Sendt, K.; Haynes, B. S. *Fuel* **2004**, *83*, 2133−2138.
(15) Cheah, S.; Carpenter, D. L.; Magrini-Bair, K. *Energy Fuels* **2009**, *23*, 5291−5307.
(16) Álvarez-Rodríguez, R.; Clemente-Jul, C. *Fuel* **2008**, *87*, 3513−3521.
(17) Adánez, J.; Abad, A.; García-Labiano, F.; de Diego, L. F.; Gayán, P. *Fuel* **2005**, *84*, 533−542.
(18) Meng, X.; de Jong, W.; Pal, R.; Verkooijen, A. H. M. *Fuel Proc. Technol.* **2010**, *91*, 964−981.
(19) García, G.; Cascarosa, E.; Ábrego, J.; Gonzalo, A.; Sánchez, J. L. *Chem. Eng. J.* **2011**, *174*, 644−651.
(20) Simell, P. A.; Hakala, N. A. K.; Haario, H. E.; Krause, A.O. I. *Ind. Eng. Chem. Res.* **1997**, *36*, 42−51.
(21) Han, J.; Kim, H. *Renewable Sustainable Energy Rev.* **2008**, *12*, 397−416.
(22) Zhang, R.; Brown, R. C.; Suby, A.; Cummer, K. *Energy Convers. Manage.* **2004**, *45*, 995−1014.
(23) García, G.; Arauzo, J.; Gonzalo, A.; Sánchez, J. L.; Ábrego, J. *Chem. Eng. J.* **2013**, *222*, 345−352.
(24) Giroudière, F.; Ambrosino, J. L.; Fischer, B.; Pavone, D.; Sanz-Garcia, E.; Le Gall, A.; Soutif, E.; Vleeming, H. *Oil Gas Sci. Technol.* **2010**, *65*, 673−688.
(25) García, L.; French, R.; Czernik, S.; Chornet, E. *Appl. Catal., A* **2000**, *201*, 225−239.
(26) Hou, Z. *Appl. Catal., A* **2003**, *253*, 381−387.
(27) Requies, J.; Cabrero, M. A.; Barrio, V. L.; Cambra, J. F.; Güemez, M. B.; Arias, P. L.; La Parola, V.; Peña, M. A.; Fierro, J. L. G. *Catal. Today* **2006**, *116*, 304−312.
(28) Li, C.; Chen, Y.-W. *Thermochim. Acta* **1995**, *256*, 457−465.
(29) Medrano, J. A.; Oliva, M.; Ruiz, J.; García, L.; Arauzo, J. *J. Anal. Appl. Pyrolysis* **2009**, *85*, 214−225.
(30) Sánchez-Sánchez, M.; Navarro, R.; Fierro, J. *Catal. Today* **2007**, *129*, 336−345.
(31) Salagre, P.; Fierro, J. L. G.; Medina, F.; Sueiras, J. E. *J. Mol. Catal. A: Chem.* **1996**, *106*, 125−134.
(32) Bimbela, F.; Chen, D.; Ruiz, J.; García, L.; Arauzo, J. *Appl. Catal., B* **2012**, *119*−*120*, 1−12.
(33) Devi, L. *Biomass Bioenergy* **2003**, *24*, 125−140.
(34) de Andrés, J. M.; Narros, A.; Rodríguez, M. E. *Fuel* **2011**, *90*, 521−527.
(35) Pérez, P.; Aznar, M. P.; Caballero, M. A.; Gil, J.; Martí, J. A.; Corella, J. *Energy Fuels* **1997**, *11*, 1194−1203.
(36) Corella, J.; Toledo, J. M.; Aznar, M. P. *Ind. Eng. Chem. Res.* **2002**, *41*, 3351−3356.
(37) Heesink, A. B. M.; van Swaaij, W. P. M. *Chem. Eng. Sci.* **1995**, *50*, 2983−2996.
(38) Czernik, S.; Evans, R.; French, R. *Catal. Today* **2007**, *129*, 265−268.
(39) Bartholomew, C. H. *Appl. Catal., A* **2001**, *212*, 17−60.
(40) Prabhawalkar, P.; Raole, P.; Kothari, D.; Nair, M. *Vacuum* **1986**, *36*, 817−820.
(41) Hepola, J.; McCarty, J.; Krishnan, G.; Wong, V. *Appl. Catal., B* **1999**, *20*, 191−203.
(42) Adánez, J.; de Diego, L. F.; Garcia-Labiano, F.; Abad, A. *Energy Fuels* **1998**, *12*, 617−625.
(43) Aznar, M.; Manyà, J. J.; García, G.; Sánchez, J. L.; Murillo, M. B. *Energy Fuels* **2008**, *22*, 2840−2850.
(44) Brage, C.; Yu, Q.; Chen, G.; Sjöström, K. *Biomass Bioenergy* **2000**, *18*, 87−91.
(45) Pinto, F.; André, R. N.; Franco, C.; Lopes, H.; Gulyurtlu, I.; Cabrita, I. *Fuel* **2009**, *88*, 2392−2402.

Reprinted with permission from Gas Catalytic Upgrading In A Two Zone Fluidized Bed Reactor Coupled To A Co-Gasification Plant, G. García, E. Campos, I. Fonts, J. L. Sanchez, and J. Herguido, Energy Fuels, DOI: 10.1021/ ef400227z , Publication Date (Web): 18 Apr 2013). Copyright (2013) American Chemical Society

energy&fuels Article
pubs.acs.org/EF

Gas Catalytic Upgrading in a Two-Zone Fluidized Bed Reactor Coupled to a Cogasification Plant

G. García,[†,‡] E. Campos,[†] I. Fonts,[†,§,*] J. L. Sánchez,[†] and J. Herguido[∥]

[†]Thermo-chemical Processes Group, Aragón Institute of Engineering Research (I3A), I+D building, Universidad de Zaragoza, C/Mariano Esquillor s/n, E-50018, Zaragoza, Spain

[‡]Aema Servicios, Pol. Ind. El Pilar, C/Fitero 9, E-26540 Alfaro (Logroño), Spain

[§]Centro Universitario de la Defensa, Ctra. Huesca s/n, E-50090 Zaragoza, Spain

[∥]Catalysis, Molecular Separations, and Reactor Engineering Group (CREG), Aragón Institute of Engineering Research (I3A), I+D building, Universidad de Zaragoza, C/Mariano Esquillor s/n, E-50018, Zaragoza, Spain

ABSTRACT: An integrated system has been designed and started up for sewage sludge and coal cogasification + desulfurization + gas reforming in a two-zone fluidized bed reactor (TZFBR). The system is capable of reforming tar compounds to nondetectable levels and improving gasification gas quality in terms of higher H_2 and CO concentrations. The use of a TZFBR enables both the catalytic upgrading of the gasification gas and the regeneration of the catalyst deactivated by coke deposition in a single vessel. Both an increase of 37% of gas LHV and a reduction of tar compounds to nondetectable levels are achieved in the best conditions used, with a 2 vol % of oxygen in the regeneration flow. Dolomite was used in the desulfurization unit at 800 °C, allowing the reduction of the H_2S content in the produced gas from 1100 ppm to less than 300 ppm, and a tar reduction from 15 g/m^3(STP) to 0.2 g/m^3(STP). With this novel integrated system, the catalytic cracking and reforming of a real gasification gas stream produced in the cogasification of sewage sludge and coal has been achieved, operating in a stable mode.

1. INTRODUCTION

Sewage sludge (SS) is the residual fraction produced during the purification of water at wastewater treatment plants. This biological residue is included in the European List of Residues (CER code 190805). Sewage sludge treatment and/or disposal is quite problematic due to the high content of potentially dangerous materials such as heavy metals, pathogens, or persistent organic pollutants. Moreover, SS production has increased dramatically during recent years due to very restrictive European legislation (Directive 91/271/EEC),[1] which promotes the installation of new sewage treatment plants. Specifically, in the EU more than 10 million tons (dry solids) of sewage sludge are produced annually.[2] The confluence between the increasing production and the limitations of current SS disposal methods (landfill, incineration, agricultural use) makes it necessary to establish new technologies to manage this waste.[3] In this context, the treatment of this residue by alternative thermochemical processes, such as pyrolysis and gasification, has been under investigation in recent years.[3−5]

Gasification is a thermochemical process carried out at high temperatures (700−1000 °C) and in a reducing atmosphere. The combination of SS with some other materials such as coal, in a practice known as cogasification, has been studied for some years,[6−12] since it can improve the global effectiveness of the process. Cogasification improves the technical viability of the process as well as the energetic yield, thanks to the stabilization effect of the use of coal on the feedstock quality.[6,9,11] Moreover, by cofeeding, the size of an industrial installation can be increased. Given the economy of scale, this is advantageous from an economic point of view.

One of the main drawbacks of gasification is the high tar content of the gas product, which is a potential source of equipment corrosion and obstruction.[13,14] For this reason, there has been extensive research into tar removal. It must be taken into account that the final use of the produced gas defines the degree of gas purity required. Heating purposes normally require less strict limits. However, when power is to be produced in a gas engine or the gas is to be used for chemical synthesis, very low contents of tar and other contaminants must be attained to avoid tar deposition problems or catalyst poisoning. There are two different ways of removing tars from gas: "separation" techniques and "elimination" techniques. The separation techniques involve the separation of tars through mainly physical processes, such as scrubbers or condensers, at the price of lowering the gas temperature and creating new waste products such as contaminated water streams.[13,15] On the other hand, the elimination techniques, such as thermal or catalytic cracking, are based on molecule breaking at high temperatures and/or the presence of a catalyst.[15,16] The latter offer some advantages over the separation techniques because they can achieve higher tar removal efficiencies, higher gas yields, and higher energetic yields (the gasification gas temperature is not lowered). However, the implementation of these techniques is more complicated and requires specific study.

Many authors have studied the elimination of tars by means of catalytic cracking. Several of these studies are based on the utilization of model compounds.[17−19] This has the disadvantage

Received: February 6, 2013
Revised: April 17, 2013

 © XXXX American Chemical Society

Reprinted with permission from Gas Catalytic Upgrading In A Two Zone Fluidized Bed Reactor Coupled To A Co-Gasification Plant, G. García, E. Campos, I. Fonts, J. L. Sanchez, and J. Herguido, Energy Fuels, DOI: 10.1021/ ef400227z , Publication Date (Web): 18 Apr 2013). Copyright (2013) American Chemical Society

that it does not take into account the possible interference between the tar compounds and other compounds present in the gas such as ammonia or hydrogen sulfide. However, there are also many interesting research works in which the catalytic removal of tar compounds contained in a real gasification gas has been studied.[20−28]

Metals from the VIII group of the periodic table act as very effective catalysts in tar cracking and gas reforming.[29,30] Nickel is the most commonly used.[18,19,31−36] In such processes, nickel catalyst may be deactivated mainly as a result of two deactivation mechanisms: poisoning by sulfur chemisorption[20,27,28,31,37−39] and fouling by carbon deposition.[40] The deactivation by sulfur poisoning is usually avoided by means of a guard bed.[23] The deactivation due to coke deposition is especially worrying when working on high scale facilities or long duration processes.[40] The most commonly accepted solution in industry requires two parallel catalyst beds: in one bed the reaction takes place, while in the other bed the deactivated catalyst is regenerated by coke combustion. In order to avoid the necessity of using two different catalytic beds, the use of a two-zone fluidized bed reactor (TZFBR)[41] is proposed in this work.

The configuration of this reactor enables the catalytic reaction (carried out in the upper zone of the bed) and the catalyst regeneration (carried out in the lower zone of the bed) to be combined in only one vessel. The operation of this reactor is based on the generation of these two different reaction zones defined by separated gas inlets for each of the two gaseous reactant streams: the entrance of the gasification gas to be reformed (somewhere in the middle of the bed) and the entrance of the gas with the precise amount of oxygen required to burn the coke deposited on the surface of the catalyst (from the bottom of the reactor). The TZFBR operation has been successfully tested in several dehydrogenation reactions (e.g., propane and butane dehydrogenation), as well as in ethanol reforming and methane aromatization using different catalysts.[42−46] To the best of the authors' knowledge, this kind of reactor has never been studied for gas upgrading from a real gasification or cogasification reaction.

The main objective of this work is to achieve a stable cogasification gas flow free of contaminants (H_2S and tar) and with a composition rich in H_2 and CO by means of the utilization of a guard bed and a TZFBR. Furthermore, the flow of O_2 required to regenerate the catalyst continuously is also investigated.

2. MATERIAL AND METHODS

2.1. Materials. The gasification feedstock used was a mechanical mixture composed of $^1/_3$ wt south African coal, $^1/_3$ wt local lignite coal of low quality (low HHV and high sulfur content), and $^1/_3$ wt dried sewage sludge blend by weight (all materials crushed and sieved, using a fraction of 250 to 500 μm). South African bituminous coal (BC) and local lignite coal (LC) were supplied by a coal power plant. Anaerobically digested and thermally dried sewage sludge (SS) was supplied by an urban wastewater treatment plant. Feedstock analyses were carried out employing standard methods: moisture according to ISO-589-1981, ash according to ISO-1171-1976, volatiles according to ISO-5623-1974, elemental analysis CHNS using a Carlo Erba 1108, and higher heating value (HHV) according to ISO-1928-89 (for the DSS) and ASTM D-3286-96 (for the coals) by means of a IKA C-2000 calorimeter (see Table 1).

Due to the high sulfur content of lignite coal, H_2S will be present in the cogasification product gas. In order to avoid deactivation problems when using an active metal such as Ni in the catalyst, its concentration must be reduced. Based on previous experiments carried out with a synthetic gas of a similar composition to the gasification gas,[47,48] a fixed bed of calcined dolomite was used in the experimental setup in order to reduce the amount of H_2S in the gas. Dolomite also has significant catalytic activity toward tar cracking, which is also beneficial for the purpose of this work.[49−51]

Table 1. Proximate, Ultimate, and Heating Value Analyses of the Raw Materials As Received

	BC	LC	SS
moisture (%)	6.9	19.2	6.5
ash (%)	14.3	26.3	41.3
volatiles (%)	25.2	26.0	46.9
fixed carbon (%)	53.6	28.5	5.4
carbon (%)	65.3	37.6	27.8
hydrogen (%)	4.1	4.1	4.4
nitrogen (%)	1.8	0.5	4.0
sulfur (%)	0.7	6.1	0.8
HHV (MJ/kg)	25.4	14.6	11.4
LHV (MJ/kg)	24.32	13.25	10.87

γ-Alumina (γ-Al_2O_3, Puralox NWa-155 from Sasol, Germany) was used as catalyst support and the catalyst (Ni/γ-Al_2O_3) was prepared by incipient wet impregnation using $Ni(NO_3)\cdot 6H_2O$ (Panreac, 99% purity) as the nickel source. An ICP-OES analysis confirmed a 4.8 wt % of nickel. Superficial properties of the catalyst, support, and calcined dolomite were determined by BET/BJH and mercury porosimetry and can be found in Table 2. XRD showed that γ-Al_2O_3 was the only crystal compound found in the support, and that Ni was incorporated on the support in spinel form (nickel aluminate). Nickel dispersion over the support surface was determined by SEM-EDX (Figure 1), and the Ni/Al ratio obtained by this technique had a similar value, around 0.28, irrespective of the zone considered on the solid sample surface.

Table 2. BET-BJH[a] Analyses for Calcined Dolomite and Alumina

	calcined dolomite	alumina
BET surface area(m^2/g)	118	142
micropore area (m^2/g)	1.6	
micropore vol. (cm^3/g)	6×10^{-4}	
mesopore average diam. (nm)	20	10.5
mesopore vol. (BJH analysis) (cm^3/g)	0.08	0.42

[a]Brunauer−Emmett−Teller-Barrett−Joyner−Halenda.

2.2. Catalytic Activity Tests. The catalytic activities of the Ni/γ-Al_2O_3 catalyst and the γ-Al_2O_3 support were tested in a small fixed bed facility based on a 1 cm i.d. and 40 cm in length quartz tubular reactor. The experimental setup is described elsewhere.[47,48] For each experiment, 1 g of alumina or Ni/alumina sample was placed in the fixed bed and subsequently reduced in a H_2 stream (vol 5% in N_2) at 800 °C (temperature selected according to Temperature programmed reduction (TPR)). A synthetic gas, SG-1, composed of H_2, CO, CO_2, CH_4, C_2H_6, C_2H_4, C_2H_2, and N_2 (with neither H_2S, steam nor tar compounds) (see Table 3) was used to test the activity and differences between the active catalyst and the support. Similarly, a new series of experiments was carried out using a different synthetic gas stream SG-2 (Table 3) including H_2S as a minor component (0.5 vol %) in order to study the extent and characteristics of its deactivating behavior.

2.3. Experimental Setup. This study was carried out at a laboratory scale plant, which includes a cogasification fluidized bed reactor (capacity 0.1−0.3 kg/h), a fixed bed desulfurization reactor, and a reforming two-zone fluidized bed reactor (TZFBR). In this last unit, only a slip stream of the product gas is processed. In order to simultaneously analyze the two gas streams (reformed in the TZFBR and nonreformed after the desulfurization bed), two condensing systems and two micro-gas chromatographs were used (see Figure 2).

Reprinted with permission from Gas Catalytic Upgrading In A Two Zone Fluidized Bed Reactor Coupled To A Co-Gasification Plant, G. García, E. Campos, I. Fonts, J. L. Sanchez, and J. Herguido, Energy Fuels, DOI: 10.1021/ ef400227z , Publication Date (Web): 18 Apr 2013). Copyright (2013) American Chemical Society

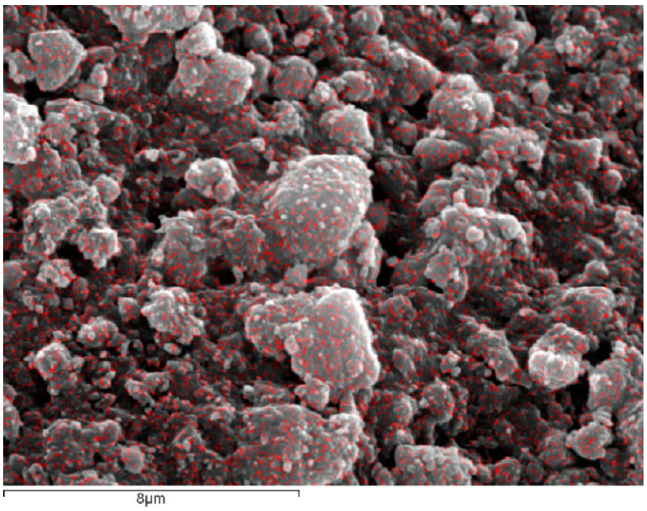

Figure 1. SEM-EDX scan of a Ni-γ-Al_2O_3 catalyst sample.

Table 3. Composition of Gas Mixtures Used in Fixed Bed Catalytic Tests

	SG-1	SG-2
H_2 (vol %)	9.00	10.00
CO (vol %)	15.00	10.00
CO_2 (vol %)	11.00	15.00
CH_4 (vol %)	4.00	4.00
C_2H_2 (vol %)	0.75	0.20
C_2H_4 (vol %)	0.75	1.50
C_2H_6 (vol %)	0.75	0.20
H_2S (vol %)		0.50
N_2 (vol %)	58.75	58.60

In the following sections, the different parts of the experimental setup are explained in detail.

2.3.1. Cogasification Section. The cogasification fluidized bed reactor is made of refractory steel (AISI 310), with an inner diameter of 40 mm in the bed zone and 70 mm in the freeboard. The maximum bed height was kept at 310 mm by means of a lateral pipe, which enabled the continuous removal of ash and char. The feedstock blend was continuously fed into the bed at about 10 mm over the distributor plate through a sloped pipe externally cooled by air. The air flow rate was 2.81 dm^3(STP)/min (standard temperature and pressure (STP): 0 °C and 1 atm). The feeding rate was set at 2.3 g/min (to obtain a stoichiometric ratio of 30%), but slight variations caused the stoichiometric ratio to range between 28.8 and 32.2% depending on the experiment. Both bed and freeboard temperatures were set at 850 °C by means of an electric oven. The initial bed was composed of 300 g of silica sand, with a particle diameter range of 250−350 μm. The product gas exited the reactor through a cyclone and a hot filter, which were kept at 450 °C. The total experiment took 90 min after starting the feeding.

2.3.2. Desulfurization Section. The desulfurization section is composed of the desulfurization reactor and the first gas cleaning and gas analysis system. Gasification gas, as produced, was led to the fixed bed desulfurization reactor through a steel pipe heated at 450 °C to prevent tar condensation. This reactor is also made of refractory steel, with an inner diameter of 35.5 mm and a total height of 990 mm. Calcined dolomite (135 g) was placed as bed material inside the reactor in order to retain the hydrogen sulfide. An electrical oven kept the bed at 800 °C.

2.3.3. Reforming, Gas Cleaning, and Analysis Sections. After the secondary reactor, the gas is divided into two streams. The highest fraction of the gas ("non-reformed flow", about 3 dm^3(STP)/min) exits the experimental installation through the first condensation and gas cleaning system. The rest of the gas ("reformed flow", 0.3 dm^3(STP)/min) is introduced inside the reforming reactor where a bed of Ni/γ-Al_2O_3 catalyst (42 g) is placed. As explained in the Introduction, the reforming reactor chosen is a TZFBR (Figure 3). It was designed in order to combine in only one vessel the two typical phases of catalytic processes: catalytic reaction and catalyst regeneration. This reactor is made of quartz and has a total height of 510 mm. The regeneration zone is 18 mm in diameter, whereas the reaction zone is 28 mm in diameter. The gas to be reformed enters the reactor from the top through a quartz tube, which directs it to the lower part of the reaction zone. The regeneration gas enters through the bottom of the reactor, as can be observed in Figure 3.

Reforming reactions take place in the upper part of the bed, while regeneration reactions (coke combustion) occur in the lower fraction of the bed by means an oxygen flow introduced from the bottom of the reactor.

An important parameter for the performance of this reactor is the u/u_{mf} ratio (actual gas superficial velocity/minimum fluidization superficial velocity) in the two sections of the bed.[52] In the experiments carried out, in order to achieve the appropriate fluidization conditions, the oxygen stream was fed diluted in nitrogen, with a total flow of 0.3 dm^3(STP)/min in the regeneration zone (u/u_{mf} = 2.5). Nitrogen was chosen for the sake of experimental simplicity, but it must be borne in mind that the reformed gas is subsequently diluted in nitrogen. This dilution effect has been removed by subtracting the nitrogen flow in order to show the effect of the catalyst by comparing the nonreformed gas composition with the reformed one. In an actual operation, either a TZFBR with different dimensions, which enables the fluidization of the catalyst in the regeneration zone of the TZBFR using non diluted oxygen, or oxygen and steam as regeneration agents should be used. In the latter case, steam may easily be removed as water when cooling the reformed gas. The gas flow rate from the desulfurization section entering the regeneration zone of the TZBFR was approximately 0.3 dm^3(STP)/min, which represents a u/u_{mf} = 3.4 (taking into account both the larger diameter of this section and the gas streamflow rate coming from the regeneration zone).

Because of the continuous circulation of the catalyst between the two zones, coke deposited over its surface during the catalytic reforming and cracking reactions is burned in the regeneration zone. Before the start of the experiment, the catalyst was reduced in a H_2 stream (vol 5% in N_2) at 800 °C, in the same way as in the catalyst activity tests. The operational temperature of the TZFBR for the experiments was also set at 800 °C. This temperature was chosen in order to promote CH_4 reforming and tar cracking.

2.3.4. Double Gas Cleaning and Analysis System. The "non-reformed flow" was cleaned with two ice-cooled condensers and a cotton filter (first condensation system) in order to remove water and tar from the gas. Once cleaned, the total gas volume was measured and its composition analyzed with a micro-gas chromatograph (MicroGC1, Agilent 3000A). The "reformed flow" was cleaned with a second condensation system, and its flow rate was measured. Another micro-gas chromatograph (MicroGC2, Agilent 3000A) was used to analyze the composition of this "reformed gas flow". For both gas flows, the nonreformed and the reformed, H_2, CO, CO_2, CH_4, C_2H_2, C_2H_4, C_2H_6, and H_2S concentrations were determined. The gas lower heating value (LHV) of both streams was calculated by means of the determined gas compositions. The tar content of the condensed liquid was analyzed by weight difference between the total liquid condensed and the water content determined through Karl Fischer titration (Mettler Toledo V-20). The tar components were analyzed by gas chromatography with simultaneous mass spectrometry and flame ionization detectors (GC/MS-FID) using an Agilent chromatograph model 7890A, in a similar mode as in previous works.[53,54] GC-FID analyses were used to find out the relative proportion of each compound in the sample by calculating the area percentage. The quantification method by FID area percentage considers the response factors of all the compounds to be similar. This method has been widely used by other authors because when the compounds belong to the same families the response factors do not change significantly.[55]

Reprinted with permission from Gas Catalytic Upgrading In A Two Zone Fluidized Bed Reactor Coupled To A Co-Gasification Plant, G. García, E. Campos, I. Fonts, J. L. Sanchez, and J. Herguido, Energy Fuels, DOI: 10.1021/ef400227z , Publication Date (Web): 18 Apr 2013). Copyright (2013) American Chemical Society

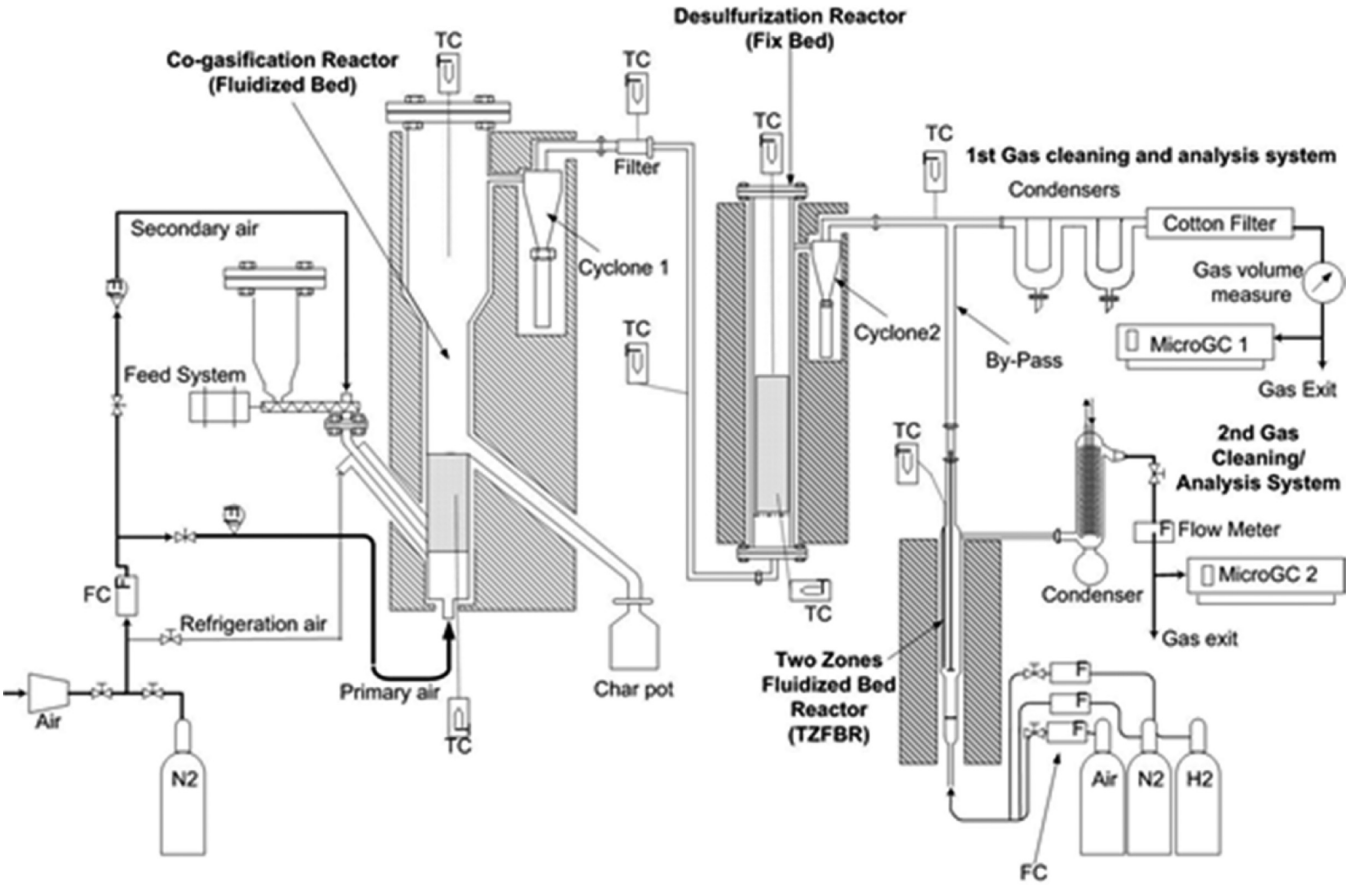

Figure 2. Experimental plant diagram (TC: temperature controller. FC: flow controller).

The double gas cleaning and gas analysis system enabled both the tar of the reformed and nonreformed flow and also the reformed and the nonreformed gas composition in each experiment to be determined. This double system was aimed to facilitate the comparison and comprehension of the effect of the TZFBR catalytic processing.

2.4. Experimental Planning. Apart from the catalytic activity tests in the fixed bed reactor, the experiments carried out in this work were gathered in two sets: first, the experiments designed to study separately the effect of each part of the installation (cogasification, desulfurization and gas reforming units) and, second, those experiments focused on finding the oxygen flow necessary to regenerate online the catalyst in the reforming unit, achieving a steady state operation.

2.4.1. Experiments Designed to Study Separately Each Part of the Installation. The first experimental set included some experiments to determine the original response of the cogasification system before any amendment was made to it. The desulfurization reactor with dolomite was then added to the installation and experimentally studied. The last experiments in this series included the addition of the TZFBR with an alumina bed, as a blank study to test the catalytic effect of the catalyst support.

Furthermore, several experiments were run under the same operating conditions. The results obtained showed that there is practically no difference between them, confirming the good repeatability of the experiments as can be observed in some of the figures shown in the Results section (Figures 5, 7, and 9).

2.4.2. Oxygen Optimization Experiments. The regeneration oxygen flow was optimized in order to achieve, in the TZFBR regeneration zone, the continuous combustion of the coke deposited on the catalyst surface. This will be achieved but oxygen should not reach the reaction zone. If that happened, the combustible components of the gas in that zone would react with the remaining oxygen after the regeneration, leading to a lowering of the gas quality. The relative oxygen percentages tested were 0 vol % (reference), 1 vol %, 2 vol %, 6 vol %, and 10 vol %. The correct oxygen percentage was determined by trial and error.

In the two series of experiments (experiments focused on studying each part of the installation and experiments focused on finding out the oxygen flow required in the TZFBR), the response variables studied were tar production and composition, gas composition, and lower heating value (LHV). The operational conditions used in the two series are shown in Table 4 and were mostly scheduled according to the optimum values obtained in previous works.[25,47,48,56−58]

2.5. Characterization of the Used Catalyst. The samples of the catalysts used in the different runs were characterized by controlled thermogravimetric oxidation (30−900 °C, 10 °C/min, 30 cm^3(STP)/min air) using a STA 449 F3 Jupiter (Netzsch) and the CO_2 present in the gas exiting from the TG equipment was analyzed online using a Pfeiffer mass spectrometer model Omnistar Prisma.

3. RESULTS AND DISCUSSION

3.1. Catalyst Activity. As stated previously, catalytic activity tests were carried out in a fixed bed reactor loaded with alumina or Ni/alumina and with one or other of the synthetic gas streams SG-1 or SG-2. In all the runs carried out with the SG-1 gas, i.e., without H_2S as a constituent, steady state was approximately attained in about 10 min and continued until the end of the experiment (150 min). However, in the runs carried out with Ni/alumina catalyst and using the SG-2 gas (i.e., with H_2S as a constituent), the steady state was never reached during the testing time. This is consistent with the deactivating effect of H_2S found by several authors working with Ni-based catalysts or with oxide catalysts in gas reforming processes,[31,38] and even in gas coming from gasification

dx.doi.org/10.1021/ef400227z | Energy Fuels XXXX, XXX, XXX−XXX

Reprinted with permission from Gas Catalytic Upgrading In A Two Zone Fluidized Bed Reactor Coupled To A Co-Gasification Plant, G. García, E. Campos, I. Fonts, J. L. Sanchez, and J. Herguido, Energy Fuels, DOI: 10.1021/ef400227z , Publication Date (Web): 18 Apr 2013). Copyright (2013) American Chemical Society

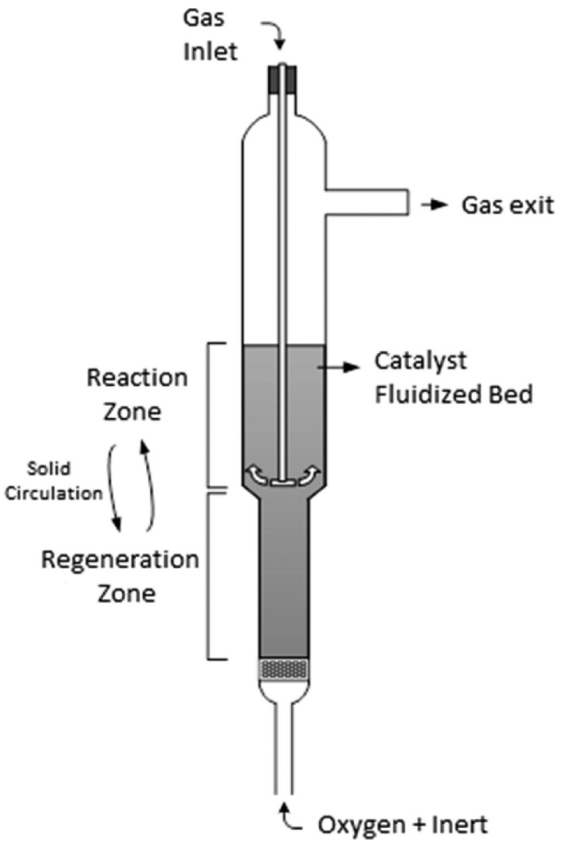

Figure 3. Scheme of the TZFBR.

Table 4. Operational Conditions for Each Plant Section

cogasifier	bed temp.	850 °C
	freeboard temp.	850 °C
	cogasification air	2.82 dm^3(STP)/min
	coal + DSS feeding rate	2.3 g/min
	initial sand bed	300 g
	stoichiometric ratio	30%
desulfurization reactor	bed temp.	800 °C
	dolomite bed (prior to calcination)	250 g
	calcined dolomite bed	135 g
	calcination conditions	800 °C, air, >2 h
TZFBR	bed temp.	800 °C
	catalyst in reaction zone	25 g
	catalyst in regeneration zone	17 g
	gas entering reaction zone	≈ 0.3 dm^3(STP)/min
	O_2 + N_2 regeneration flow	0.3 dm^3(STP)/min

upgrading processes[37,39,59] similar to the current one. Figure 4 shows the changes for each one of the gas species (in vol %) when SG-1 or SG-2 are subjected to the activity tests. The outlet gas composition (vol %) considered was the steady state when working with the SG-1 gas, and the average for last 30 min in the case of working with the SG-2 gas.

As can be observed in Figure 4, broadly speaking, methane, carbon dioxide, and C_2 hydrocarbons act as reactants while hydrogen and carbon monoxide are produced in the process. This behavior is mainly due to the dry reforming of both methane ($CH_4 + CO_2 \leftrightarrow 2\ CO + 2\ H_2$) and C_2 hydrocarbons ($C_2H_n + 2\ CO_2 \leftrightarrow 4\ CO + {}^n/_2\ H_2$).

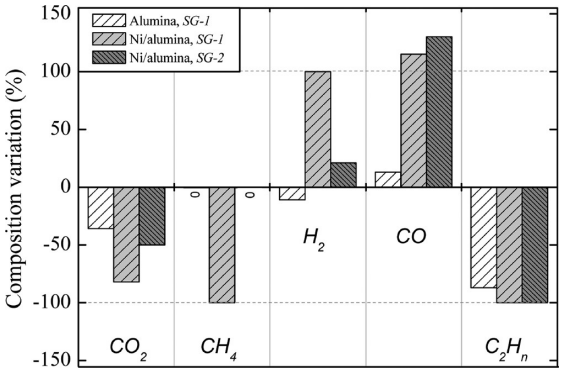

Figure 4. Gas composition variation (vol %) in catalytic tests in fixed bed reactor.

However, the extent of these reactions depends on the solid used as catalytic bed and also on the presence of hydrogen sulfide in the synthetic gas stream. Thus, when only catalyst support (i.e., γ-Al_2O_3) is used, apparently there is no methane reforming but almost complete C_2 hydrocarbon reforming. Indeed, taking into account the inlet gas composition, the stoichiometry of the C_2 reforming reaction and the degree of disappearance of C_2 (87.5%), a carbon dioxide decrease of 35.6% would be expected, which roughly corresponds with what was observed (Figure 4).

Conversely, Ni/γ-Al_2O_3 appears to be able to reform both methane and C_2 hydrocarbons in the gas, which should theoretically cause a 77.3% decrease in CO_2, while experimentally an 82% reduction was determined. This resulted in a significant increase in the volumetric percentage of hydrogen and carbon monoxide in the gas mixture. As the synthetic gas used in these runs was the same, SG-1, it can be said that the catalytic activity of alumina in the reforming of methane and the production of carbon monoxide and hydrogen is much smaller than that showed in the presence of Ni.

When H_2S is present in the gas (SG-2), as would be expected[31,37−39,59] the Ni/γ-Al_2O_3 no longer reforms methane due to the poisoning of the Ni active sites, but it maintains a good activity in C_2 hydrocarbons reforming. This corroborates the fact that Ni/γ-Al_2O_3 reforms both methane and light hydrocarbons, but if Ni is poisoned by the sulfur then only light hydrocarbons are reformed by the effect of γ-Al_2O_3 due to the selective deactivation mainly affecting the ability of catalytic methane dry reforming. Thus, the removal of H_2S is a necessary task in order to carry outgas upgrading with this Ni/γ-Al_2O_3 catalyst in a stationary mode.

3.2. Cogasification and Desulfurization. Before extracting results from the experimental plant, some previous experiments were carried out in order to know how the gas quality changes when the different units are added to the cogasification plant. These previous experiments comprised a cogasification process with a single fluidized bed and cogasification with a subsequent desulfurization process using a downstream fixed bed of dolomite.

The gas produced in the cogasification process had, on average, the composition and heating value shown in Table 5. As far as tar production is concerned, the gas had around 15 g/m^3(STP) when leaving the gasifier. Table 6 shows the main compounds identified, as well as their FID area percentages, which are about 90% in FID area of the total peaks detected. As can be observed, naphthalene is the major compound, with all the compounds detected having a marked aromatic character.

Reprinted with permission from Gas Catalytic Upgrading In A Two Zone Fluidized Bed Reactor Coupled To A Co-Gasification Plant, G. García, E. Campos, I. Fonts, J. L. Sanchez, and J. Herguido, Energy Fuels, DOI: 10.1021/ef400227z , Publication Date (Web): 18 Apr 2013). Copyright (2013) American Chemical Society

Table 5. Main Properties of Cogasification Outlet Stream

avg. gas composition (vol %)	
H_2	7.9 ± 0.2
CO	9.1 ± 0.1
CO_2	14.5 ± 0.3
CH_4	1.2 ± 0.1
C_2H_n	0.31 ± 0.05
H_2S	0.11 ± 0.02
tar amount in gas (g/m^3(STP))	15
LHV (kJ/m^3(STP))	2590 ± 120

Table 6. Tar Compounds Identified by GC/MS-FID

cmpd	FID area (%)
naphthalene	58.3
acenaphthylene	7.1
phenanthrene	3.8
benzo[b]thiophene	3.7
benzonitrile	2.0
quinoline	2.0
dibenzofuran	1.4
fluorene	1.4
biphenyl	1.2
indene	1.1
naphthalene, 2-methyl-	1.0
fluoranthene	1.0
pyrene	0.8
naphthalene-2-carbonitrile	0.6
anthracene	0.5
naphthalene, 1-methyl-	0.5
dibenzothiophene	0.4
4H-cyclopenta[def]phenanthrene	0.2
1,8-anthracenediamine	0.2

On the other hand, the gas as produced in the gasifier contained 1100 ± 200 ppm of H_2S (Table 5). In order to reduce the presence of this gas, noxious for the Ni catalyst as previously established, the produced gas was fed into the secondary fixed bed reactor with dolomite, at 800 °C. After the secondary reactor with dolomite, in the experiment made exclusively with this guard bed, the H_2S concentration in the gas fell to 140 ± 10 ppm. The concentration of tar in the gas flow after the dolomite guard bed was 0.21 g/m^3(STP). This represents 98.7% tar reduction by the introduction of the dolomite bed. This tar reduction is slightly higher than those obtained in other works[22] (around 90%), although the ratio of kg dolomite/kg biomass (daf)/h used in this work (1.52) was also greater than that utilized by these authors (0.85 at most). The hydrocarbon cracking effect of dolomite was also evidenced in the dramatic decrease of C_2 hydrocarbons (C_2H_2 + C_2H_4 + C_2H_6) in the gas, which was 0.31 ± 0.05 vol % after the cogasifier and diminished to 20 ppm after the dolomite bed.

3.3. Catalytic Gas Upgrading with the TZFBR. As explained in the Materials and Methods section, a slip stream of the product gas exiting the desulfurization reactor was fed into the TZFBR. First, to distinguish between the effect of the support (γ-alumina) and the catalyst (Ni/γ-alumina), an alumina bed was placed in the TZFBR instead of the catalyst, and the reactor was operated as a conventional fluidized bed (no regeneration oxygen flow was used). The operation conditions were those as previously described (Table 4). Subsequently, catalytic experiments were carried out with the prepared Ni/γ-alumina catalyst and a regenerating stream with different oxygen percentages in order to allow burning of the coke deposited on the catalyst, without burning the reformed gas components.

Regarding the condensed liquids remaining after the gas passed through the TZFBR, no tar species were detected by GC/MS-FID in any of the experiments performed using this reactor. The effects of using the TZFBR on the gas compositions are discussed and compared with those previously obtained (i.e., after cogasification and desulfurization units).

The volumetric percentage of each gas species in the nonreformed gas stream (gas stream that does not pass through the TZFBR) should be similar in all the experiments and also analogous to that determined in the experiment carried out only with the dolomite guard bed. However, as will be observed in Figures 5, 7, and 9, some differences have been found in these concentrations. These alterations could be related to the different stoichiometric ratios, which varied between 28.8 and 32.2%, in the case of the major species (H_2, CO, CO_2, CH_4) and also to the difficulties in the quantification of species with low concentrations in the case of C_2H_n and H_2S.

Considering H_2 and CO as representative products in the reforming process (as previously stated in relation to the catalytic activity tests carried out with synthetic gases), their evolution with the different experimental configurations used is shown in Figure 5. In order to make this comparison, the average percentage of each individual gas has been calculated using the last values of the time-on-stream for each run (the last 30 min in 90 min experiments). The confidence interval for

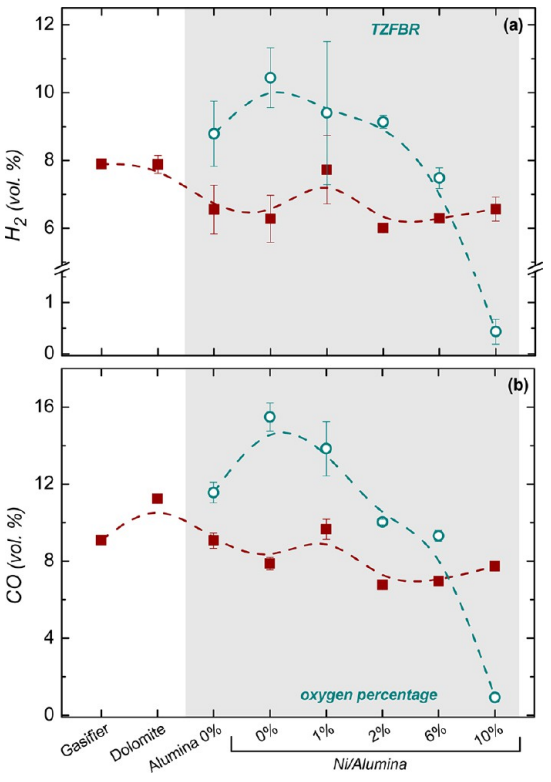

Figure 5. Hydrogen (a) and carbon monoxide (b) content in nonreformed gas (■) and in reformed gas (○) for different reaction configurations, including several oxygen contents (0−10%) in regenerating gas fed to the TZFBR. (Lines for visual help.)

dx.doi.org/10.1021/ef400227z | Energy Fuels XXXX, XXX, XXX−XXX

Reprinted with permission from Gas Catalytic Upgrading In A Two Zone Fluidized Bed Reactor Coupled To A Co-Gasification Plant, G. García, E. Campos, I. Fonts, J. L. Sanchez, and J. Herguido, Energy Fuels, DOI: 10.1021/ef400227z , Publication Date (Web): 18 Apr 2013). Copyright (2013) American Chemical Society

these average values, taking into account the Student's t-distribution and standard deviation of the data, has also been calculated and is shown in Figures 5, 7, and 9. In these comparisons, there is one value for the experiments done without the TZFBR and two values for those experiments carried out using the TZFBR: nonreformed and reformed gas.

The use of dolomite in the secondary reactor does not affect the H_2 content in the gas, remaining at around 8% (Figure 5a). Nevertheless, the proportions of CO and CH_4 slightly increase (from 9 to 11% and from 1.1 to 1.4%, respectively), while CO_2, C_2H_n, and H_2S decrease significantly (Figures 5, 7, and 9). The trends found in CO and CO_2 could be due to the enhancement by the dolomite bed of both the reverse water−gas shift reaction and the tar reforming reactions.

Alumina in the TZFBR increases H_2 and CO, and the use of Ni/γ-alumina catalyst also has a major positive effect on their concentrations. The maximum contents in these products are obtained with this catalyst and without oxygen or with only 1% of oxygen diluted in the regenerating stream entering the TZFBR. However, in these experimental conditions, a non-stable system is found, as is manifested by the prolonged 95% confidence interval bars. If the oxygen percentage in the regenerating gas increases, the system stabilizes (shorter confidence interval bars), although this decreases the CO and H_2 concentration in the resulting gas. When 10% of oxygen is used, these CO and H_2 concentrations fall to values lower than those found in the nonreformed gas. This oxygen percentage is therefore too high, and the excess oxygen reaches the upper zone of the TZFBR, allowing oxidation reactions of the fuel compounds in the gasification gas.

Therefore, an optimal oxygen percentage must be selected so that both process stability and gas quality improvement are preserved. For the experimental series shown in Figure 5, a percentage of 2% of O_2 represents this optimal value taking into account that it is the minimum oxygen content in regenerating gas that allows a stable operation in steady state. In fact, analyzing the time evolution of the CO content in the reformed gas, considering it as a representative specie of the gas composition, it can be seen (Figure 6) that 2% is the lowest oxygen percentage leading to a stable behavior. Working with 2% O_2 in the TZFBR, during the first 40 min the gas composition changes but for the rest of the experiment the gas composition is very stable. Furthermore, comparing the data of both reformed and nonreformed flows, it can be observed (Figure 5) that the catalyst has a positive effect on the gas composition because the percentages of H_2 and CO of the reformed gas flow are significantly greater than those of the nonreformed flow. Higher oxygen percentages lead to stable states but lower quality gas. Lower oxygen percentages lead to unstable states, even in long-term experiments (e.g., for 0% and 1% oxygen as shown in Figure 6).

In summary, 2% of O_2 was selected as the most suitable percentage to be used in the regeneration agent gas introduced in the TZFBR due to both the lack of repeatability (or stability) among consecutive measurements of CO and the operation in nonsteady state produced with 0 and 1% of O_2. On the other hand, percentages of O_2 higher than 2% lead to the combustion not only of the coke deposited over the catalyst but also of part of the gasification gas entering the TZFBR.

The evolution of the CH_4, CO_2, and C_2H_n concentrations, the gas components expected to act as reactants (i.e., decreasing their content) in the reforming process, is shown in Figure 7 for the different experimental configurations. It can be observed that for percentages of oxygen lower than 2%, the CO_2 tendency in the nonreformed and the reformed gas is opposite

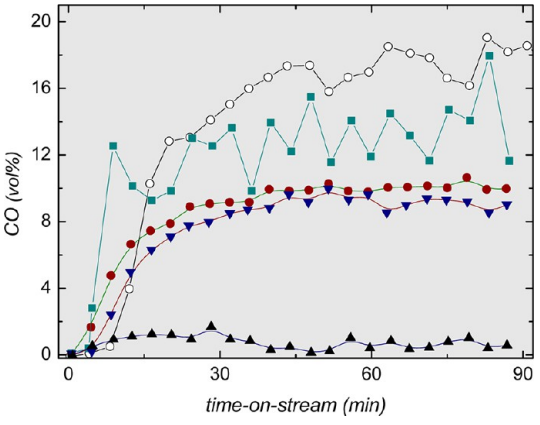

Figure 6. Time evolution of CO content in reformed gas (with Ni/γ-Al_2O_3 catalyst) for different oxygen percentages (○ 0% O_2, (■) 1% O_2, (●) 2% O_2, ▼ 6% O_2 and ▲ 10% O_2) in the TZFBR regenerating gas stream. (Lines for visual help.)

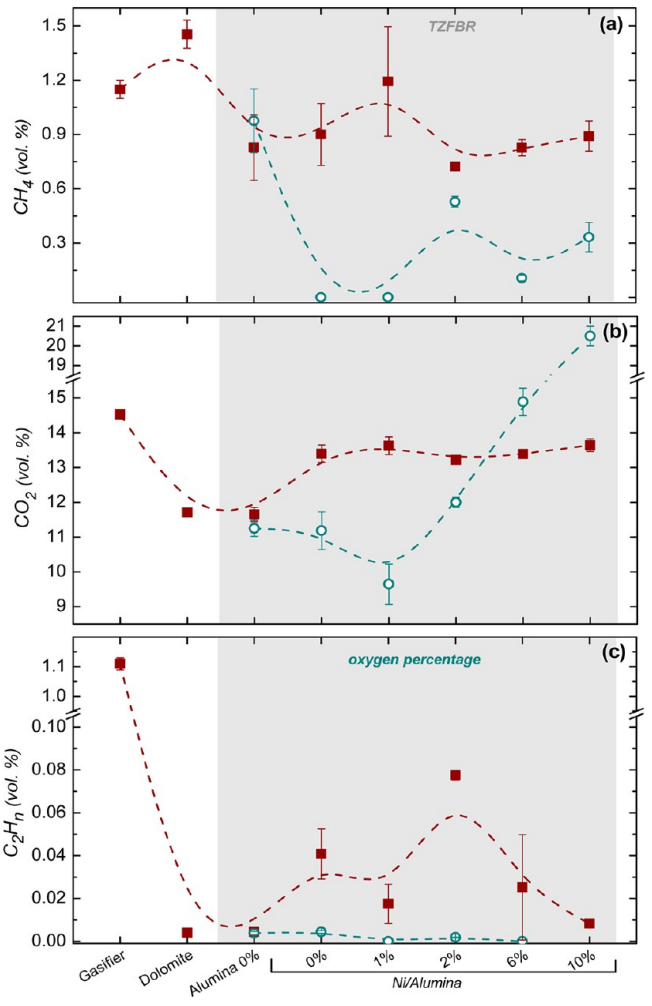

Figure 7. Methane (a), carbon dioxide (b), and C_2 hydrocarbons (c) content in nonreformed gas (■) and in reformed gas (○) for different reaction configurations, including several oxygen contents (0−10%) in regenerating gas fed to the TZFBR. (Lines for visual help.)

dx.doi.org/10.1021/ef400227z | Energy Fuels XXXX, XXX, XXX−XXX

Reprinted with permission from Gas Catalytic Upgrading In A Two Zone Fluidized Bed Reactor Coupled To A Co-Gasification Plant, G. García, E. Campos, I. Fonts, J. L. Sanchez, and J. Herguido, Energy Fuels, DOI: 10.1021/ef400227z , Publication Date (Web): 18 Apr 2013). Copyright (2013) American Chemical Society

to that shown in Figure 5 for CO and H_2. This trend may be expected as a result of reforming reactions. The decrease in CO_2, CH_4 and C_2H_n, and the significant increase in the proportion of CO would evidence that the mass of C entering the TZFBR remains stable and therefore no coke is formed.

The CO_2 and C_2H_n content decreases in the gas stream exiting from the dolomite bed outlet, and the presence of ethane + ethylene + acetylene is reduced to very low levels (lower than 0.018%, being around 1.1% after passing through the gasifier). On the other hand, the presence of CH_4 and CO increases significantly. These results are consistent with the recognized behavior of dolomite as a suitable catalyst for cracking and reforming heavy hydrocarbons.[49]

As expected, according to the catalytic tests (Figure 4) the use of alumina in the TZFBR has no significant effect on the depletion of CO_2 and CH_4, although in this case the presence of steam in the processed stream is likely promoting water−gas shift and other gasification and reforming reactions. However, C_2 hydrocarbons are almost completely removed with this configuration. As commented on previously, the differences between the percentages of CH_4 obtained in the experiment carried out only with dolomite and in the nonreformed stream of the experiments performed with the TZFBR could be caused by the deviations of the stoichiometric ratios, which varied between 28.8 and 32.3%.

The use of Ni/γ-Al_2O_3 catalyst reduces the presence of CH_4, CO_2, and C_2H_n in the gas. On the one hand, the gas content in C_2 hydrocarbons is null, irrespective of the oxygen percentage used in the regenerating gas. On the other hand, its content in CH_4 and CO_2 reaches minimal values in the experiments carried out with 0 and 1% oxygen (e.g., CH_4 was not detected by GC during the experiment) but in experiments using 2, 6, and 10% oxygen in the gas, the CH_4 and CO_2 proportions increased. Thus, up to 2% O_2, the CO_2 percentage in the gas is smaller than in the nonreformed gas, so no net gas oxidation occurs, and probably only coke is removed. Although this also leads to CO_2 formation, the increase in other compounds due to the catalytic reforming compensates for this. When 6 or 10% O_2 in the regenerating gas is used, the CO_2 in the reformed gas is higher than in the nonreformed stream due to the oxidation of the fuel species such as C_2H_n, CH_4, and CO.

The overall effect of all the tested experimental conditions on the quality of outgoing gas from the process can be analyzed in terms of gas LHV (see Figure 8). As CH_4 and CO increase while CO_2 decreases when dolomite is used, its heating value increases from 2590 kJ/m^3(STP) (Table 5) to around 2800 kJ/m^3(STP), that is to say around 8%. In order to assess the effect of the catalytic treatment carried out in the TZFBR, the LHV of the gases upgraded in this reactor has been compared with the heating value of the nonreformed gas streams obtained in the same experiments since, as mentioned previously, the different stoichiometric ratios may cause a variation in the gas composition entering the TZFBR. Once the gas has undergone the dolomite treatment, alumina in the TZFBR causes a 28% increase in the LHV over the nonreformed stream, as can be seen in Figure 8. This increase is caused by the enrichment in CO and H_2, as a consequence of the reforming reactions. The configuration with Ni/γ-Al_2O_3 catalyst in the TZFBR also provokes a growth in the gas LHV when using 0 or 1% O_2 in the regenerating gas, but this entails working in a nonstationary state (Figure 6). Further increases in the oxygen supply above 2% cause the LHV to diminish, there being a sharp drop at 10% O_2. The composition of the gas is downgraded since there is increasing gas combustion in the TZFBR, with a consequent decrease in CO and H_2 percentages in the gas products (Figure 5). An optimal condition is achieved working with 2% O_2, as both stability and LHV upgrading over the nonreformed gas are achieved.

Summing up, small percentages of O_2 (2% in this case) cause a slight increase in the CO_2 but also favor the cracking of heavier compounds, leading to a slight improvement in the gas heating value (see Figure 8). Using 2% of O_2 also ensures a stable operating process and aids the autothermicity of the process.

Lastly, in order to apply this upgrading process in a full scale unit, it should be taken into account that pure (or high purity) oxygen should be used, mixed with a carrier agent that may be easily removed as steam that can be condensed prior to the final use of the produced gas. Moreover, the presence of a higher concentration of steam, which is a reforming agent, can be advantageous as the reforming reactions and hydrogen formation would be enhanced.

3.4. H_2S Abatement using TZFBR. Regarding the H_2S content in the produced gas (Figure 9), the use of dolomite allows its removal with an efficiency of 80 to 90%, depending on the experiment considered. There are differences in the H_2S

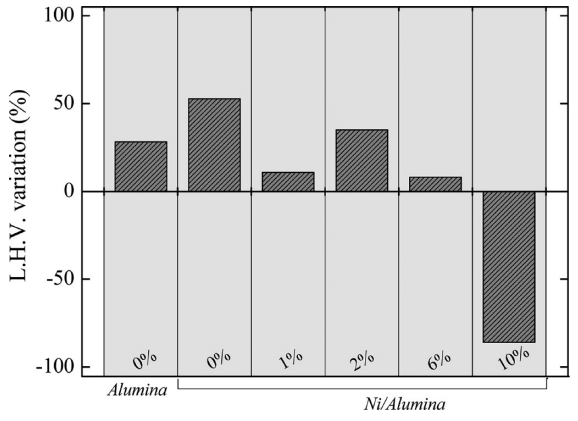

Figure 8. LHV percent increase percentage in TZFBR reformed gas regarding the nonreformed one, working with different solids (alumina and Ni/γ-Al_2O_3 catalyst) and oxygen percentages (0−10%).

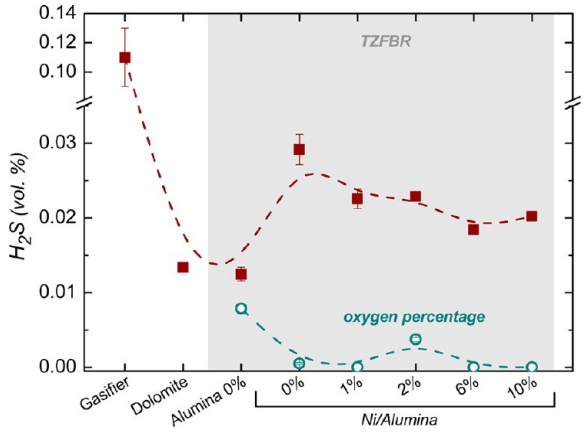

Figure 9. H_2S content in nonreformed gas and in reformed one in nonreformed gas (■) and in reformed one (○) for different reaction configurations, including several oxygen percentages (0−10%) in regenerating gas fed to the TZFBR. (Lines for visual help.)

dx.doi.org/10.1021/ef400227z | Energy Fuels XXXX, XXX, XXX−XXX

Reprinted with permission from Gas Catalytic Upgrading In A Two Zone Fluidized Bed Reactor Coupled To A Co-Gasification Plant, G. García, E. Campos, I. Fonts, J. L. Sanchez, and J. Herguido, Energy Fuels, DOI: 10.1021/ef400227z , Publication Date (Web): 18 Apr 2013). Copyright (2013) American Chemical Society

percentage in the gas for experiments carried out with alumina in the TZFBR and for the rest carried out with Ni/γ-Al_2O_3 catalyst in this reactor. The H_2S concentration for the nonreformed stream is between 200 and 300 ppm. The H_2S leaving the dolomite bed is retained by the Ni/γ-Al_2O_3 catalyst, resulting in its almost complete elimination. However, the total amount retained on the catalyst surface was not large enough to deactivate it in the runs carried out in an experimental series (e.g., those runs included in Figures 5−9), since all the runs were performed with the same sample of catalyst. In fact, taking into account the mass of catalyst placed in the TZFBR (42 g) and its Ni load (4.8 wt %), 1.16 g of H_2S could be retained by the catalyst in the form of NiS. Moreover, if the gas flow fed to the TZFBR (0.3 dm^3(STP)/min) contains at the most 300 ppm of H_2S, the catalyst deactivation by sulfur poisoning will take place after around 8500 min of operation.

In order to analyze more in depth the effects of H_2S on catalyst deactivation and the subsequent outgoing gas composition, a final experimental configuration was adopted using Ni/γ-Al_2O_3 catalyst in the TZFBR. In this new arrangement, the dolomite guard bed was omitted with the aim of exposing the catalyst to higher tar content in the gasification gas (avoiding the cracking effect of the dolomite). During a standard 90-min experiment, the system was stable and capable of cracking tars, attaining nondetectable tar content in the reformed gas as against 15 g tar/m^3 (STP) in the nonreformed gas. The variation in the composition of the TZFBR reformed gas compared with the nonreformed gas both including and not including dolomite bed is shown in Figure 10.

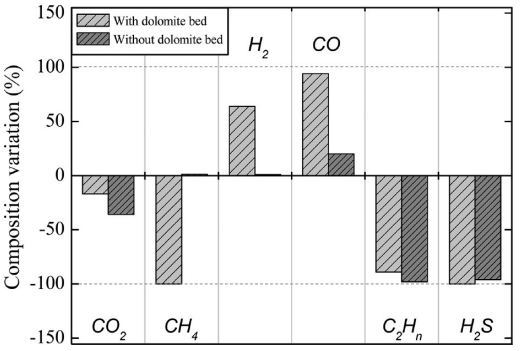

Figure 10. Composition variations in TZFBR reformed gas regarding the nonreformed one for both including and not including dolomite bed.

As can be observed, in the configuration without the dolomite bed the H_2S was still fully removed from the gas stream. This involves its removal for more than 90 min time-on-stream (i.e., more than 0.23 H_2S mol/Ni mol in catalyst), consistent with the high selectivity of Ni catalyst found for hydrogen sulfide chemisorption.[27] Although a large amount of sulfur was adsorbed by the sites, the catalyst bed was still capable of maintaining its reforming activity of light hydrocarbons such as C_2H_n, as occurred in the catalytic activity tests made with alumina only and described in section 3.1. However, methane was not reformed as a result of nickel poisoning with hydrogen sulfide (not retained by the dolomite this time). This behavior agrees with that observed previously corresponding to an active alumina support not deactivated by sulfur (Figure 4). As a consequence, a decrease in CO_2, consumed in cracking reactions, and an increase in H_2 and CO, produced in reforming reactions, is perceived. Thus, the variation in the gas composition induced by the Ni/γ-Al_2O_3 catalyst when no dolomite bed is used in the experimental arrangement is very similar to that resulting from the alumina activity test (Figure 4).

3.5. Characterization of the Used Catalyst. Figure 11 shows the results of the thermogravimetric oxidation analyses

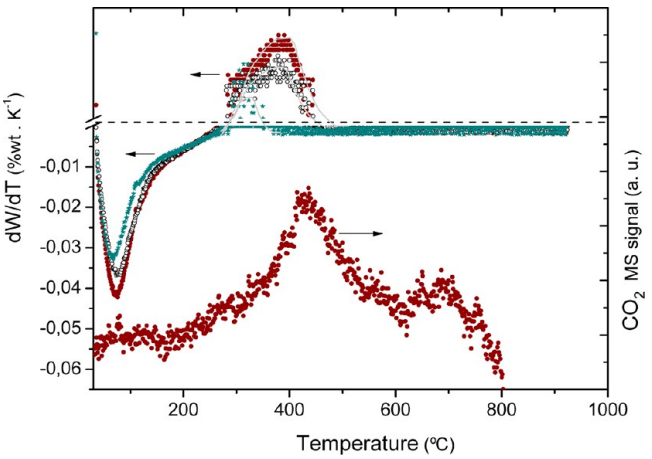

Figure 11. Weight change and CO_2 mass spectra evolution of exhaust gases during the oxidation with air in temperature ramp of catalysts samples after experiments carried out with (●) % O_2, (○) 1% O_2, and (☆) 6% O_2 in the regenerating gas fed to the TZFBR.

carried out on samples of the catalysts used in the runs using 0%, 1% and 6% of O_2. As can be observed, the samples underwent a weight reduction in the temperature interval from 30 to 300 °C. The higher the oxygen percentage fed to the TZFBR in the previous experiment, the lower was the weight loss. In any case, this weight loss was not due to coke combustion, as evidenced by the fact that no CO_2 was detected by online mass spectrometry in the exhaust gas exiting from the TG equipment. Indeed, this can be observed in the MS signal (mass 44 Da) shown in Figure 11, corresponding to the catalyst from the 0% oxygen run in the TZFBR. In the range from 300 to 500 °C, a weight increase is perceived for all the solid samples. The higher the oxygen percentage fed to the TZFBR in the previous experiment, the lower was the weight gain. This behavior is related to nickel oxidation (Ni to NiO) and evidence the likely lower oxidation state of the solid when low oxygen percentages are used in the TZFBR. The original blue color of the solid samples corresponding to lower oxygen percentages (0% and 1%) turned to black at the end of the experiment. Moreover, in TG oxidation analysis, a peak of CO_2 was detected by MS in the temperature range from 300 to 600 °C, evidencing the existence of coke depositions over the catalyst surface. For the 0% O_2 sample, this peak corresponds to a carbon content of approximately 0.03 mg C/gram of catalyst (see Figure 11).

4. CONCLUSIONS

The main aim of this study is to upgrade the gasification gas obtained by the cogasification of sewage sludge, bituminous coal, and lignite. In the experimental study, a slip stream of the gas produced at lab scale was fed into a new catalytic reactor, the two-zone fluid bed reactor, which allows both the catalytic upgrading of the gas with Ni/γ-alumina catalyst and the in situ

dx.doi.org/10.1021/ef400227z | Energy Fuels XXXX, XXX, XXX−XXX

regeneration of the catalyst deactivated by coke deposition. The use of this system enables a stable gasification gas stream to be achieved free of tars and H_2S, one of the main contaminants in raw cogasification gas.

The experiments included in this work started with a simple cogasification process, to which two other processes (desulfurization and gas reforming in TZFBR) were subsequently added. Each of these stages resulted in an added value to the technical features of the process under study.

With the cogasification unit alone, a gas was obtained with relative low contents of H_2 and CO (7.9% and 9.1% respectively, volume basis), a LHV of 2.6 MJ/m^3(STP) and high tar (15 g tar/m^3(STP)) and H_2S (1100 ppm) contents.

When the desulfurization step (with dolomite) was added, the H_2S content was reduced to less than 300 ppm, and the C_2H_n and tars were to a large extent reformed and cracked. For example, the amount of naphthalene, the major compound in the produced tar and the only peak present in the chromatograms, in the gas generated after the gas passes through the dolomite guard bed, was smaller than 2 mg/m^3(STP).

Lastly, the complete system (cogasification + desulfurization + TZFBR) designed and started up in this work was capable of (1) removing almost the totality of hydrogen sulfide from the gas flow, (2) reducing tars in the gasification gas down to nondetection limits by GC-MS, with even the disappearance of the naphthalene peak, (3) reforming the gasification gas, improving its quality as a combustible gas, in terms of higher H_2 and CO content, (4) increasing by 37% the LHV of the product gas, and (5) operating in a stable manner during continuous operation with a real gasification gas, while adjusting the relative oxygen flow necessary to regenerate the catalyst, the optimum oxygen percentage in the regeneration gas flow being around 2%.

AUTHOR INFORMATION

Corresponding Author

*E-mail: isabelfo@unizar.es.

Notes

The authors declare no competing financial interest.

ACKNOWLEDGMENTS

The authors express their gratitude to the Spanish Ministry of Science and Technology for financial support (Research Project CTQ2007-66885PPQ and CTQ2010-2013).

REFERENCES

(1) Directive 91/271/EEC of 21 May 1991 concerning urban waste water treatment.

(2) Laturnus, F.; von Arnold, K.; Gron, C. *Environ. Sci. Pollut. Res.* **2007**, *14*, 53−60.

(3) Fonts, I.; Gea, G.; Azuara, M.; Ábrego, J.; Arauzo, J. *Renewable Sustainable Energy Rev.* **2012**, *16*, 2781−2805.

(4) Werther, J.; Ogada, T. *Prog. Energy Combust. Sci.* **1999**, *25*, 55−116.

(5) Manara, P.; Zabaniotou, A. *Renewable Sustainable Energy Rev.* **2012**, *16*, 2566−2582.

(6) Cousins, A.; Zhuo, Y.; George, A.; Paterson, N.; Dugwell, D. R.; Kandiyoti, R. *Energy Fuels* **2008**, *22*, 2491−2503.

(7) Paterson, N.; Reed, G. P.; Dugwell, D. R.; Kandiyoti, R. Gasification Tests With Sewage Sludge and Coal/Sewage Sludge Mixtures in a Pilot Scale, Air Blown, Spouted Bed Gasifier. In *ASME Turbo Expo 2002: Power for Land, Sea, and Air*; ASME: Amsterdam, 2002; pp 197−202.

(8) Paterson, N.; Zhuo, Y.; Dugwell, D.; Kandiyoti, R. *Energy Fuels* **2005**, *19*, 1016−1022.

(9) Pinto, F.; Lopes, H.; Andre, R. N.; Dias, M.; Gulyurtlu, I.; Cabrita, I. *Energy Fuels* **2007**, *21*, 2737−2745.

(10) Reed, G. P.; Dugwell, D. R.; Kandiyoti, R. *Energy Fuels* **2001**, *15*, 794−800.

(11) Wang, X.; Xiao, Y. Analysis of Sludge and Coal Cogasification Power Plant. In *ASME Turbo Expo 2004: Power for Land, Sea, and Air*; ASME: Vienna, 2004; pp 131−139.

(12) Zhang, Q.; Liu, H.; Li, W.; Xu, J.; Liang, Q. *Energy Fuels* **2012**, *26*, 2830−2836.

(13) Boerrigter, H.; van Paasen, S. V. B.; Bergman, P. C. A.; Könemann, J. W.; Emmen, R.; Wijnands, A. *Report ECN-C-05-009*; Energy Research Centre of the Netherlands (ECN): Petten, Holanda, 2005.

(14) Milne, T. A.; Evans, R. J.; Abatzoglou, N. *NREL/TP-570-25357*; National Renewable Energy Laboratory: Golden, CO, 1998.

(15) Anis, S.; Zainal, Z. A. *Renewable Sustainable Energy Rev.* **2011**, *15*, 2355−2377.

(16) Han, J.; Kim, H. *Renewable Sustainable Energy Rev.* **2008**, *12*, 397−416.

(17) Virginie, M.; Courson, C.; Niznansky, D.; Chaoui, N.; Kiennemann, A. *Appl. Catal. B* **2010**, *101*, 90−100.

(18) Furusawa, T.; Saito, K.; Kori, Y.; Miura, Y.; Sato, M.; Suzuki, N. *Fuel* **2013**, *103*, 111−121.

(19) Kong, M.; Yang, Q.; Fei, J.; Zheng, X. *Int. J. Hydrogen Energy* **2012**, *37*, 13355−13364.

(20) Arauzo, J.; Radlein, D.; Piskorz, J.; Scott, D. S. *Energy Fuels* **1994**, *8*, 1192−1196.

(21) Caballero, M. A.; Corella, J.; Aznar, M.-P.; Gil, J. *Ind. Eng. Chem. Res.* **2000**, *39*, 1143−1154.

(22) Corella, J.; Aznar, M.-P.; Gil, J.; Caballero, M. A. *Energy Fuels* **1999**, *13*, 1122−1127.

(23) Corella, J.; Narvaez, I.; Orio, A. *Advanced Gasification of Biomass with Downstream Commercial Steam Reforming Catalysts for Hot Flue Gas Cleaning. Comparison of Different Catalysts with Their Apparent Kinetic Constants for Tar Conversion* **1996**, 368.

(24) Corella, J.; Toledo, J. M.; Molina, G. *Fuel Process. Technol.* **2006**, *87*, 841−846.

(25) Corella, J.; Toledo, J. M.; Molina, G. *Bioresour. Technol.* **2008**, *99*, 7539−7544.

(26) Corella, J.; Toledo, J. M.; Padilla, R. *Ind. Eng. Chem. Res.* **2004**, *43*, 2433−2445.

(27) Hepola, J.; Simell, P. *Appl. Catal. B* **1997**, *14*, 287−303.

(28) Hepola, J.; Simell, P. *Appl. Catal. B* **1997**, *14*, 305−321.

(29) Juutilainen, S. J.; Simell, P. A.; Krause, A. O. I. *Appl. Catal. B* **2006**, *62*, 86−92.

(30) Ronkkonen, H.; Simell, P.; Niemela, M.; Krause, O. *Fuel Process. Technol.* **2011**, *92*, 1881−1889.

(31) Bartholomew, C. H.; Weatherbee, G. D.; Jarvi, G. A. *J. Catal.* **1979**, *60*, 257−269.

(32) Di Felice, L.; Courson, C.; Foscolo, P. U.; Kiennemann, A. *Int. J. Hydrogen Energy* **2011**, *36*, 5296−5310.

(33) Guan, G.; Chen, G.; Kasai, Y.; Lim, E. W. C.; Hao, X.; Kaewpanha, M.; Abuliti, A.; Fushimi, C.; Tsutsumi, A. *Appl. Catal. B* **2012**, *115*, 159−168.

(34) Li, D.; Wang, L.; Koike, M.; Nakagawa, Y.; Tomishige, K. *Appl. Catal. B-Environ.* **2011**, *102*, 528−538.

(35) Liu, H.; Chen, T.; Chang, D.; Chen, D.; Kong, D.; Zou, X.; Frost, R. L. *Chem. Eng. J.* **2012**, *188*, 108−112.

(36) Kinoshita, C. M.; Wang, Y.; Zhou, J. *Ind. Eng. Chem. Res.* **1995**, *34*, 2949−2954.

(37) Czekaj, I.; Struis, R.; Wambach, J.; Biollaz, S. *Catal. Today* **2011**, *176*, 429−432.

(38) Gallego, J.; Batiot-Dupeyrat, C.; Barrault, J.; Mondragon, F. *Energy Fuels* **2009**, *23*, 4883−4886.

(39) Sato, K.; FujiMoto, K. *Catal. Commun.* **2007**, *8*, 1697−1701.

(40) Bartholomew, C. H. *Appl. Catal. A* **2001**, *212*, 17−60.

(41) Menéndez, M.; Herguido, J.; Tellez, C.; Soler, J.; Gimeno, M. P. Two zone fluidized bed reactor. Spanish Patent Application P200801857, 2008.
(42) Soler, J.; Tellez, C.; Herguido, J.; Men
Powder Technol. **2001**, *120*, 88−96.
(43) Gimeno, M. P.; Soler, J.; Herguido, J.; Menendez, M. *Ind. Eng. Chem. Res.* **2010**, *49*, 996−1000.
(44) Herguido, J.; Menendez, M.; Santamaria, J. *Catal. Today* **2005**, *100*, 181−189.
(45) Lobera, M. P.; Tellez, C.; Herguido, J.; Menendez, M. *Ind. Eng. Chem. Res.* **2008**, *47*, 9314−9320.
(46) Perez-Moreno, L.; Soler, J.; Herguido, J.; Menendez, M. *Ind. Eng. Chem. Res.* **2012**, *51*, 8840−8848.
(47) Cascarosa, E.; Ortiz de Zarate, M. C.; Sanchez, J. L.; Gea, G.; Arauzo, J. *Biomass Bioenergy* **2012**, *40*, 190−193.
(48) García, G.; Cascarosa, E.; Ábrego, J.; Gonzalo, A.; Sánchez, J. L. *Chem. Eng. J.* **2011**, *174*, 644−651.
(49) Gonzalez, J. F.; Roman, S.; Engo, G.; Encinar, J. M.; Martinez, G. *Biomass Bioenergy* **2011**, *35*, 4324−4330.
(50) Seshadri, K. S.; Shamsi, A. *Ind. Eng. Chem. Res.* **1998**, *37*, 3830−3837.
(51) Yu, Q. Z.; Brage, C.; Nordgreen, T.; Sjostrom, K. *Fuel* **2009**, *88*, 1922−1926.
(52) Gascon, J.; Tellez, C.; Herguido, J.; Jakobsen, H. A.; Menendez, M. *AlChE J.* **2006**, *52*, 3911−3923.
(53) Aznar, M.; Manya, J. J.; Garcia, G.; Sánchez, J. L.; Murillo, M. B. *Energy Fuels* **2008**, *22*, 2840−2850.
(54) Aznar, M.; San Anselmo, M.; Manya, J. J.; Benita Murillo, M. *Energy Fuels* **2009**, *23*, 3236−3245.
(55) Kallai, M.; Veres, Z.; Balla, J. *Chromatographia* **2001**, *54*, 511−517.
(56) García, G.; Cascarosa, E.; Sánchez, J. L. Analysis of catalytic cogasification of two types of coal with sewage sludge and olive bagasse. In *Proceedings of the 17th European Biomass Conference and Exhibition*, June 29−July 3, 2009; pp 721−724.
(57) Sutton, D.; Kelleher, B.; Doyle, A.; Ross, J. R. H. *Bioresour. Technol.* **2001**, *80*, 111−116.
(58) Abu El-Rub, Z.; Bramer, E. A.; Brem, G. *Ind. Eng. Chem. Res.* **2004**, *43*, 6911−6919.
(59) Tomishige, K.; Miyazawa, T.; Kimura, T.; Kunimori, K.; Koizumi, N.; Yamada, M. *Appl. Catal. B* **2005**, *60*, 299−307.

Reprinted with permission from Gas Catalytic Upgrading In A Two Zone Fluidized Bed Reactor Coupled To A Co-Gasification Plant, G. García, E. Campos, I. Fonts, J. L. Sanchez, and J. Herguido, Energy Fuels, DOI: 10.1021/ef400227z , Publication Date (Web): 18 Apr 2013). Copyright (2013) American Chemical Society